



universität  
wien

# DIPLOMARBEIT

Titel der Diplomarbeit

## Gabor Frames and the Fractional Fourier Transform

Verfasser

Andreas Missbauer

angestrebter akademischer Grad

Magister der Naturwissenschaften (Mag. rer.  
nat.)

Wien, 2012

Studienkennzahl lt. Studienblatt: A405

Studienrichtung lt. Studienblatt: Mathematik

Betreuer: Univ.-Prof. Dr. Hans Georg Feichtinger

# Contents

<b>Introduction</b>	<b>2</b>
<b>1 Fourier Analysis</b>	<b>4</b>
1.1 The Fourier transform . . . . .	4
1.2 Basic operators . . . . .	5
1.3 The short-time Fourier transform . . . . .	8
1.4 The discrete Fourier transform . . . . .	11
1.5 Gaussians . . . . .	12
1.6 The Hermite functions . . . . .	14
<b>2 Frames</b>	<b>15</b>
2.1 Basic concepts . . . . .	15
2.2 Perturbation of frames . . . . .	20
<b>3 Gabor Analysis</b>	<b>22</b>
3.1 Gabor frames . . . . .	22
3.2 Finite-dimensional Gabor analysis . . . . .	24
<b>4 The Fractional Fourier Transform</b>	<b>26</b>
4.1 Definition and properties . . . . .	26
4.2 Spectral decomposition of the FrFT . . . . .	33
4.3 Implementation of the FrFT . . . . .	35
<b>5 Experiments on Rotated Gabor-like Systems</b>	<b>46</b>
5.1 The Gabor case . . . . .	46
5.2 Some special cases . . . . .	53
5.3 The random case . . . . .	57
5.4 Conclusion . . . . .	60
<b>6 Stability Results for Rotated Gabor-like Systems</b>	<b>63</b>
6.1 Wiener amalgam spaces . . . . .	63
6.2 Stability results . . . . .	64
<b>Appendix</b>	<b>72</b>
<b>Abstract in English</b>	<b>81</b>
<b>Deutsches Abstract</b>	<b>82</b>
<b>Author's curriculum vitae</b>	<b>83</b>

# Introduction

Aside from the general perturbation theory for frames (see [4]) there are many results concerning the stability of Gabor systems under perturbations such as distortions of the lattice or the window (see for example [10], [22]).

In this thesis we want to consider another type of stability: For  $g$  a Gaussian and lattice parameters  $a, b > 0$  consider the system  $\{g_{m,n}\}_{m,n \in \mathbb{Z}}$  where

$$g_{m,n}(t) = e^{2\pi i n b t} g_{\alpha_{m,n}}(t - ma)$$

and  $g_{\alpha_{m,n}}$  is obtained from rotating  $g$  by an angle  $\alpha_{m,n}$  in the time-frequency plane. This rotation is realized by applying a fractional power of the Fourier transform, also simply known as a fractional Fourier transform (FrFT). Geometrically one can think of the system  $\{g_{m,n}\}$  as a collection of rotated ellipses, which are positioned along the lattice  $a\mathbb{Z} \times b\mathbb{Z}$  in the time-frequency plane. We will refer to such systems as rotated Gabor-like systems. In general they are not Gabor systems and we want to investigate the influence of the rotation parameters on the frame bounds.

In chapter 1 we briefly recall many of the basic concepts from Fourier Analysis including the Fourier transform (FT), the short-time Fourier transform (STFT) and Hermite functions, which are important when dealing with the FrFT. Chapters 2 and 3 contain the fundamental notions from frame theory and Gabor analysis that we are going to use.

Chapter 4 is dedicated to the fractional Fourier transform and especially its implementation on a computer. After discussing the definition and basic properties we compare two algorithms for computing discrete Hermite functions, which we then use to construct discrete analogs of the FrFT. One of these algorithms, which was developed by Feichtinger, focuses on the rotation aspect mentioned above and we will use it to simulate the systems  $\{g_{m,n}\}$  numerically.

In chapter 5 we describe the results of such simulations for various choices of the  $\alpha_{m,n}$ . We start with the case  $\alpha_{m,n} = \alpha \forall m, n$  which yields a Gabor system. We will see that in this case the behavior of the frame bounds is easily understood, yet not unsurprising. Then we will look at some special choices of the rotation parameters as well as the randomized case.

Chapter 6 finally contains results concerning the stability of the frame bounds for the systems at hand. We show that if the width of the Gaussian  $g$  is sufficiently close to 1, any choice of the  $\alpha_{m,n}$  will yield a frame, as long as the lattice allows it. Furthermore if  $\{g_{m,n}\}$  is a frame then a small, uniformly bounded perturbation

of the  $\alpha_{m,n}$  does not change this fact.

The numerous experiments throughout the paper have been performed in MATLAB 7.9 with heavy use of the tools developed at NuHAG, which are available from <http://nuhag.eu>. There one can also find a color version of this thesis.

# 1 Fourier Analysis

In this section we give a brief overview over the concepts from Fourier Analysis that will be used later on and cover the basic definitions. For more detailed information including proofs we refer to [11], [12] and [13].

## 1.1 The Fourier transform

**Definition 1.1.** Let  $f \in L^1(\mathbb{R}^d)$ , we define the Fourier transform of  $f$  by

$$\mathcal{F}f(\omega) = \hat{f}(\omega) := \int_{\mathbb{R}^d} f(x)e^{-2\pi i x \cdot \omega} dx, \omega \in \mathbb{R}^d \quad (1.1)$$

**Theorem 1.1.** (Riemann-Lebesgue) The Fourier transform of an  $L^1$ -function is uniformly continuous and vanishes at infinity, i.e.

$$\mathcal{F} : L^1(\mathbb{R}^d) \rightarrow C_0(\mathbb{R}^d)$$

**Theorem 1.2.** (Inversion Formula) Take  $f \in L^1(\mathbb{R}^d)$ , if  $\hat{f} \in L^1(\mathbb{R}^d)$  then

$$f(x) = \int_{\mathbb{R}^d} \hat{f}(\omega)e^{2\pi i x \cdot \omega} d\omega \quad (1.2)$$

at all points  $x$  where  $f$  is continuous.

**Theorem 1.3.** (Plancherel) For  $f \in L^1(\mathbb{R}^d) \cap L^2(\mathbb{R}^d)$

$$\|f\|_2 = \|\hat{f}\|_2$$

For  $f \in L^2(\mathbb{R}^d)$  we can choose  $f_n \in L^1(\mathbb{R}^d) \cap L^2(\mathbb{R}^d)$  s.t  $\|f - f_n\|_2 \rightarrow 0$  (e.g.  $f_n = f \cdot \chi_{[-n,n]^d}$ ). Then by Theorem 1.3:  $\|\hat{f}_n - \hat{f}\|_2 = \|f_n - f\|_2$  and we define  $\hat{f} := \lim \hat{f}_n$ . It turns out that extends  $\mathcal{F}$  to a unitary operator on  $L^2(\mathbb{R}^d)$  (therefore  $\langle f, g \rangle = \langle \hat{f}, \hat{g} \rangle$  for  $f, g \in L^2$  and sometimes we refer to this statement as Plancherel's theorem). Keep in mind though, that the integral (1.1) might not exist for  $f \in L^2$ , but by the above we can still approximate  $\hat{f}$  by integrals, because

$$\hat{f}(\omega) = \lim_{n \rightarrow \infty} \int_{[-n,n]^d} f(x)e^{-2\pi i x \cdot \omega} dx, a.e.$$

*Remark 1.1.* The integral kernel in (1.1) consists of the functions  $x \mapsto e^{2\pi i x \cdot \omega}$ ,  $\omega \in \mathbb{R}^d$ , so-called pure frequencies. For  $d = 1$  they move along the unit circle in the complex plane with frequency  $|\omega|$ . So, if we interpret  $f(t)$  as a signal varying in time,  $\hat{f}(\omega)$  can be seen as its decomposition into frequencies (we often use  $\omega$  for 'frequency-variables'). This shift of perspective allows for new insights and ways to manipulate a signal, making the Fourier transform one of the basic and most important tools for signal processing.

## 1.2 Basic operators

**Definition 1.2.** (*Translation and modulation*) Let  $x, \omega \in \mathbb{R}^d$

(i) We define the translation operator (or time shift)  $T_x : L^2(\mathbb{R}^d) \rightarrow L^2(\mathbb{R}^d)$  by

$$T_x f(t) := f(t - x).$$

(ii) The modulation operator  $M_\omega : L^2(\mathbb{R}^d) \rightarrow L^2(\mathbb{R}^d)$  is defined by

$$M_\omega f(t) := e^{2\pi i t \cdot \omega} f(t).$$

( $M_\omega$  is also called frequency shift. This name will be clear in light of Theorem 1.4(iv).)

**Theorem 1.4.** For  $x, \omega, x_1, x_2, \omega_1, \omega_2 \in \mathbb{R}^d$  and  $f \in L^2(\mathbb{R}^d)$

(i)  $T_x$  and  $M_\omega$  are unitary operators on  $L^2(\mathbb{R}^d)$ .  $T_x^{-1} = T_x^* = T_{-x}$  and  $M_\omega^{-1} = M_\omega^* = M_{-\omega}$ .

(ii)  $T_0 = M_0 = Id$

(iii)  $T_{x_2} \circ T_{x_1} = T_{x_1+x_2}$  and  $M_{\omega_2} \circ M_{\omega_1} = M_{\omega_1+\omega_2}$ .

(iv)  $\mathcal{F} \circ T_x = M_{-x} \circ \mathcal{F}$  and  $\mathcal{F} \circ M_\omega = T_\omega \circ \mathcal{F}$

(v)  $T_x M_\omega f = e^{-2\pi i x \cdot \omega} M_\omega T_x f$

*Proof.* Straightforward. □

Note that by Theorem 1.4 (ii), (iii) the mappings  $(x, f) \mapsto T_x f$  and  $(\omega, f) \mapsto M_\omega f$  define actions of  $(\mathbb{R}^d, +)$  on  $L^2(\mathbb{R}^d)$ . Combining translations and modulations yields time-frequency shifts, the key operators for time-frequency analysis:

**Definition 1.3.** For  $\lambda = (x, \omega) \in \mathbb{R}^d \times \widehat{\mathbb{R}^d} = \mathbb{R}^{2d}$  we define the time-frequency shift  $\pi(\lambda) : L^2(\mathbb{R}^d) \rightarrow L^2(\mathbb{R}^d)$

$$\pi(\lambda) := M_\omega \circ T_x.$$

As a composition of unitary operators  $\pi(\lambda)$  is unitary and thus

$$\pi(\lambda)^{-1} = \pi(\lambda)^* = T_x^* M_\omega^* = T_{-x} M_{-\omega} = e^{-2\pi i x \cdot \omega} M_{-\omega} T_{-x} = e^{-2\pi i x \cdot \omega} \pi(-\lambda)$$

and more general

$$\pi(\lambda_2) \circ \pi(\lambda_1) = e^{-2\pi i x_2 \omega_1} \pi(\lambda_1 + \lambda_2) \quad (1.3)$$

**Definition 1.4.** (Dilation) For  $A \in GL(d, \mathbb{R})$  we define the dilation operator  $D_A : L^2(\mathbb{R}^d) \rightarrow L^2(\mathbb{R}^d)$  by

$$D_A f(t) := |\det A|^{-1/2} f(A^{-1}t) \quad (1.4)$$

We will mostly consider the case  $d = 1$ ,  $A = s > 0$ , then (1.4) becomes

$$D_s f(t) = |s|^{-1/2} f\left(\frac{t}{s}\right)$$

**Theorem 1.5.** For  $A, B \in GL(d, \mathbb{R})$ ,  $x, \omega \in \mathbb{R}^d$ :

- (i)  $D_A$  is unitary on  $L^2(\mathbb{R}^d)$ .
- (ii)  $D_{Id} = Id$ .
- (iii)  $D_B \circ D_A = D_{BA}$ .
- (iv)  $\mathcal{F} \circ D_A = D_{A^{-T}} \circ \mathcal{F}$ .
- (v)  $T_x \circ D_A = D_A \circ T_{A^{-1}x}$ .
- (vi)  $M_\omega \circ D_A = D_A \circ M_{A^T \omega}$ .

*Proof.* Straightforward. □

**Definition 1.5.** (Involution, reflection) Given a function  $f : \mathbb{R}^d \rightarrow \mathbb{C}$  we define the involution operator  $*$  by

$$f^*(x) := \overline{f(-x)}$$

and the reflection operator  $\mathcal{I}$  by

$$\mathcal{I}f(x) := f(-x)$$

One easily checks

$$\mathcal{F}f^* = \overline{\mathcal{F}f} \text{ and } \mathcal{F}\mathcal{I}f = \mathcal{I}\mathcal{F}f$$

**Definition 1.6.** (Convolution) For two suitable functions  $f, g : \mathbb{R}^d \rightarrow \mathbb{C}$  the function defined by

$$(f * g)(x) := \int_{\mathbb{R}^d} f(y)g(t - y)dy, x \in \mathbb{R}^d$$

is called the convolution of  $f$  and  $g$ .

**Theorem 1.6.** (Young's Inequality) For  $1 \leq p, q, r \leq \infty$ ,  $\frac{1}{p} + \frac{1}{q} = 1 + \frac{1}{r}$  and  $f \in L^p(\mathbb{R}^d), g \in L^q(\mathbb{R}^d)$

$$\|f * g\|_r \leq \|f\|_p \|g\|_q < \infty$$

Note that Young's inequality implies that  $(L^1(\mathbb{R}^d), *)$  is a Banach algebra. Of fundamental importance is the following relation between the Fourier transform and convolutions.

**Theorem 1.7.** (Convolution Theorem) For  $f, g \in L^1(\mathbb{R}^d)$

$$\mathcal{F}(f * g) = (\mathcal{F}f) \cdot (\mathcal{F}g)$$

or:  $\mathcal{F} : (L^1(\mathbb{R}^d), *) \rightarrow (C_0(\mathbb{R}^d), \cdot)$  is a homomorphism of Banach algebras.

*Remark 1.2.* The Convolution Theorem is also true for  $f, g \in L^2(\mathbb{R}^d)$  in which case we have  $f * g \in L^\infty \cap C_0$  (see [11], p.203). Furthermore the convolution (as well as the FT) can be extended to certain distributions, see [11] for a thorough treatment. We mention only one case, which we will need in chapter 6: Given a measure  $\mu \in M(\mathbb{R}) = C'_0(\mathbb{R})$  and  $f \in C_0(\mathbb{R})$  we define

$$(\mu * f)(x) := \mu(T_x \mathcal{I}f), x \in \mathbb{R}$$

and it turns out that  $(\mu * f) \in C_0(\mathbb{R})$ .

A function  $t \mapsto e^{i\pi qt^2}$  is called a chirp. We can think of it as the line  $\omega = -qx$  in the TF-plane. We define two operators based on chirps which we will encounter when we dealing with the fractional Fourier transform.



**Definition 1.7.** (*Chirp multiplication and chirp convolution*) For  $q, c \in \mathbb{R}$  we define the chirp multiplication  $\mathcal{Q}_q : L^2(\mathbb{R}) \rightarrow L^2(\mathbb{R})$  by

$$(\mathcal{Q}_q f)(t) := e^{-i\pi q t^2} f(t)$$

and the chirp convolution  $\mathcal{C}_c : L^2(\mathbb{R}) \rightarrow L^2(\mathbb{R})$  by

$$(\mathcal{C}_c f)(t) := e^{-i\pi/4} \sqrt{\frac{1}{c}} (f * e^{i\pi u^2/c})$$

**Theorem 1.8.**  $\mathcal{Q}_q$  and  $\mathcal{C}_c$  are unitary operators on  $L^2(\mathbb{R})$  and

$$\mathcal{F} \circ \mathcal{Q}_q = \mathcal{C}_q \circ \mathcal{F}$$

### 1.3 The short-time Fourier transform

So while for a suitable signal  $f$  all information is contained in its time representation  $f$  as well as in its frequency representation  $\hat{f}$ , we do not yet have a representation uniting both aspects. Except for simple special cases we will not gain much frequency information by looking at  $f$  only, since cancellation and superposition often make it impossible to recognize the presence of specific frequencies. On the other hand  $\hat{f}$  provides information about which frequencies are active in our signal, but not about at which time they occur.

The idea now is to localize  $f$  in time at a point  $x$  by multiplying with a suitable window function  $g$  centered at  $x$  and then perform a Fourier transform, hoping to obtain information about the frequency content near  $x$ . While this idea is easily distilled into the definition of the short-time Fourier transform (or STFT) there are fundamental obstacles, we refer to them as uncertainty principles, which limit the quality of the resulting time-frequency picture. [13] contains an excellent introduction to the STFT and we will give a short summary. With minor exceptions the rest of the chapter is taken from [13] and we also refer to it for omitted proofs.

**Definition 1.8.** (*Short-Time Fourier Transform*) Given  $g \in L^2(\mathbb{R}^d)$  we define the short-time Fourier transform of  $f \in L^2(\mathbb{R}^d)$  with window  $g$  by

$$V_g f(x, \omega) := \mathcal{F}(f \cdot T_x \bar{g})(\omega) = \int_{\mathbb{R}^d} f(t) \overline{g(t-x)} e^{-2\pi i t \cdot \omega} dt \quad (1.5)$$

**Lemma 1.1.** For  $f, g \in L^2(\mathbb{R}^d)$  the function  $V_g f : \mathbb{R}^{2d} \mapsto \mathbb{R}$  is uniformly continuous and can be written as

$$V_g f(x, \omega) = \langle f, M_\omega T_x g \rangle \quad (1.6)$$

The following theorem gives the analog of Plancherel's formula for the STFT:

**Theorem 1.9.** (*Orthogonality Relations for the STFT*) For  $f_1, f_2, g_1, g_2 \in L^2(\mathbb{R}^d)$  we have that  $V_{g_i} f_i \in L^2(\mathbb{R}^{2d})$ ,  $i = 1, 2$  and furthermore

$$\langle V_{g_1} f_1, V_{g_2} f_2 \rangle_{L^2(\mathbb{R}^{2d})} = \langle f_1, f_2 \rangle \langle g_1, g_2 \rangle \quad (1.7)$$

So if  $\|g\|_2 = 1$  the mapping  $V_g : L^2(\mathbb{R}^d) \mapsto \mathcal{R}(V_g) \subseteq L^2(\mathbb{R}^{2d})$  is unitary. Since

$$\langle H, V_g h \rangle_{L^2(\mathbb{R}^{2d})} = \iint_{\mathbb{R}^{2d}} H(x, \omega) \langle M_\omega T_x g, h \rangle dx d\omega \quad (1.8)$$

the adjoint operator  $V_g^*$  is given by  $F \mapsto \iint_{\mathbb{R}^{2d}} F(x, \omega) M_\omega T_x g dx d\omega$ , where the integral is interpreted in the weak sense (see [13], p.43). Therefore

$$f = V_g^* V_g f = \iint_{\mathbb{R}^{2d}} V_g f(x, \omega) M_\omega T_x g dx d\omega \quad (1.9)$$

Remarkably, a much stronger inversion formula for the STFT formula holds:

**Theorem 1.10.** (*Inversion Formula for the STFT*) Take  $g, \gamma \in L^2(\mathbb{R}^d)$  with  $\langle g, \gamma \rangle \neq 0$ , then  $\forall f \in L^2(\mathbb{R}^d)$

$$f = \frac{1}{\langle g, \gamma \rangle} \iint_{\mathbb{R}^{2d}} V_g f(x, \omega) M_\omega T_x \gamma dx d\omega \quad (1.10)$$

or

$$\frac{1}{\langle g, \gamma \rangle} V_\gamma^* V_g = Id. \quad (1.11)$$

Now that we are equipped with the basic facts about the STFT we come back to the limitations mentioned above. Ideally we would like  $V_g f(x, \omega)$  to measure the presence of the frequency  $\omega$  at time  $x$ . Unfortunately this is not possible in a perfect way because of so-called uncertainty principles which limit the combined quality of the time and frequency resolution of the STFT. We will only state one fundamental result in this direction and refer once again to [13] for more detailed information.

**Theorem 1.11.** (*Heisenberg-Pauli-Weyl Inequality*) For  $f \in L^2(\mathbb{R})$  and  $a, b \in \mathbb{R}$

$$\left( \int_{\mathbb{R}} (x-a)^2 |f(x)|^2 dx \right)^{1/2} \left( \int_{\mathbb{R}} (\omega-b)^2 |\hat{f}(\omega)|^2 d\omega \right)^{1/2} \geq \frac{1}{4\pi} \|f\|_2^2, \quad (1.12)$$

with equality iff  $f$  is a multiple of  $T_a M_b \varphi_c(x)$ , where  $\varphi_c(x) = (2/c)^{d/4} e^{-\pi x^2/c}$ .

The first factor on the left side of (1.12) measures the size of the essential support of  $f$ , while the second term gives the essential bandwidth. Theorem 1.11 basically says that a function can not be well concentrated in both, time and frequency. If we apply this to our window function  $g$  we see that we cannot have arbitrarily good time- and frequency resolution for the STFT and that increased time resolution (by a narrow window) implies worse frequency resolution and vice versa.

We state a few more observations we will need later.

**Lemma 1.2.**

$$V_g \hat{f}(x, \omega) = e^{-2\pi i y \tau} V_g f(-\omega, x) \quad (1.13)$$

**Lemma 1.3.**

$$(V_g M_\tau T_y f)(x, \omega) = e^{2\pi i(\tau-\omega)y} V_g f(x-y, \omega-\tau) \quad (1.14)$$

*Proof.* An easy computation using the commutation relation for time-frequency shifts.  $\square$

**Lemma 1.4.** Given  $A \in GL(d, \mathbb{R})$

$$V_{D_A g} D_A f = D_{\tilde{A}} V_g f \quad (1.15)$$

where  $\tilde{A} = \begin{pmatrix} A & 0 \\ 0 & A^{-T} \end{pmatrix} \in SL(2d, \mathbb{R})$ .

*Proof.* By Theorem 1.5

$$\begin{aligned} V_{D_A g} D_A f(x, \omega) &= \langle D_A f, M_\omega T_x D_A g \rangle \\ &= \langle D_A f, D_A M_{A^T \omega} T_{A^{-1} x} g \rangle \\ &= \langle f, M_{A^T \omega} T_{A^{-1} x} g \rangle \\ &= V_g f(A^{-1} x, A^T \omega) \end{aligned}$$

and the claim follows since  $\det \tilde{A} = \det A \frac{1}{\det A} = 1$ .  $\square$

**Lemma 1.5.** For  $q \in \mathbb{R}$ ,  $f, g \in L^2(\mathbb{R})$

$$V_{\mathcal{Q}_{qg}} \mathcal{Q}_q f(x, \omega) = e^{i\pi q x^2} V_g f(x, \omega + qx)$$

*Proof.* Straightforward  $\square$

## 1.4 The discrete Fourier transform

When working with digital signals we have to do Fourier analysis on sequences and vectors. We will give analogs to many of the above concepts for  $\mathbb{C}^L$  which allow direct implementation on a computer.

**Definition 1.9.** For  $L \in \mathbb{N}$  we define the discrete Fourier transform (DFT)  $F : \mathbb{C}^L \rightarrow \mathbb{C}^L$  via

$$(Ff)_k := \frac{1}{\sqrt{L}} \sum_{n=0}^{L-1} f_n e^{-2\pi i kn/L}, \text{ for } k = 0, \dots, L-1 \quad (1.16)$$

where  $f = (f_0, \dots, f_{L-1})$ .

We will also use  $F$  to denote the matrix corresponding to the DFT, i.e.  $(F)_{m,n} = \frac{1}{\sqrt{L}} e^{-2\pi i mn/L}$ . It's not difficult to see that  $F$  is unitary and thus

$$f_n = \frac{1}{\sqrt{L}} \sum_{k=0}^{L-1} (Ff)_k e^{2\pi i kn/L}, \text{ for } n = 0, \dots, L-1 \quad (1.17)$$

*Remark 1.3.* The usual definition of the discrete Fourier transform is without the factor  $\frac{1}{\sqrt{L}}$ , making it non-unitary. For us it is more convenient to work directly with the normalized version.

We also want to define discrete analogs of translation, modulation and convolution (see [9], Chapter 8). From now on we do all arithmetic on vector indices in  $\mathbb{Z}_L$ .

**Definition 1.10.** Given  $f = (f_0, \dots, f_{L-1}) \in \mathbb{C}^L$ ,  $x, \omega \in \mathbb{Z}$  we define

$$\begin{aligned} (T_x f)_k &:= f_{k-x} \\ (M_\omega f)_k &:= e^{2\pi i \omega k/L} f_k \\ (f * g)_k &:= \sum_{n=0}^{L-1} f_n g_{k-n} \end{aligned}$$

**Theorem 1.12.**

- (i)  $FT_x = M_{-x}F$  and  $FM_\omega = T_\omega F$ .
- (ii)  $(F(f * g))_n = (Ff)_n \cdot (Fg)_n$ .

*Remark 1.4.* One of the main reasons for the importance of Fourier Analysis for applications is the existence of the fast Fourier transform (FFT), an algorithm implementing the DFT with complexity  $O(L \log L)$ , while a direct implementation would require  $O(L^2)$  operations. The FFT can also be used to efficiently compute discrete convolutions in the DFT-domain and thus carry out multiplications of polynomials or very high integers.

## 1.5 Gaussians

**Definition 1.11.** Given  $c > 0$  define the normalized  $d$ -dimensional Gaussian of width  $c$  by

$$\varphi_c(t) = (2/c)^{d/4} e^{-\pi t^2/c}$$

and we often write  $\varphi$  for  $\varphi_1$ . Observe that  $\varphi_c = D_{\sqrt{c}} \varphi$ .

Gaussians are the minimizers of (1.12) and they also behave nicely under the Fourier transform:

$$\mathcal{F}\varphi_c = \varphi_{1/c}. \quad (1.18)$$

and in particular  $\mathcal{F}\varphi = \varphi$ . This makes  $g = \varphi$  a canonical choice for the STFT window function and it is the most commonly used one.

The STFT of a Gaussian can be computed explicitly:

**Lemma 1.6.** (*STFT of a Gaussian*) For  $x, \omega \in \mathbb{R}^d$ ,  $a > 0$

$$V_\varphi \varphi_c(x, \omega) = \varphi_{c+1}(x) \varphi_{\frac{c+1}{c}}(\omega) e^{-2\pi i \frac{c}{c+1} x \omega}. \quad (1.19)$$

*Proof.* A variation of the proof of Lemma 1.5.2 in [13]:

$$\begin{aligned} V_\varphi \varphi_c(x, \omega) &= 2^{d/2} c^{-d/4} \int_{\mathbb{R}^d} e^{-\pi t^2/c} e^{-\pi(t-x)^2} e^{-2\pi i t \cdot \omega} dt \\ &= 2^{d/2} c^{-d/4} \int_{\mathbb{R}^d} e^{-\pi((\sqrt{1+1/c} t - \frac{1}{\sqrt{1+1/c}} x)^2 + (1 - \frac{1}{1+1/c}) x^2)} e^{-2\pi i t \cdot \omega} dt \\ &= 2^{d/2} c^{-d/4} \int_{\mathbb{R}^d} e^{-\pi \frac{1}{c+1} x^2} e^{-\pi \frac{c+1}{c} (t - \frac{c}{c+1} x)^2} e^{-2\pi i t \cdot \omega} dt \\ &= \varphi_{c+1}(x) (\mathcal{T}_{\frac{c}{c+1}} x \varphi_{\frac{c}{c+1}})^\wedge(\omega) \\ &= \varphi_{c+1}(x) \varphi_{\frac{c+1}{c}}(\omega) e^{-2\pi i \frac{c}{c+1} x \omega} \end{aligned}$$

□

*Remark 1.5.* From Lemma 1.6 it's easy to see that the level-set of  $|V_\varphi\varphi_c|$  at level  $L \in (0, K]$ , where  $K := (\frac{4c}{(c+1)^2})^{d/4}$  is the solution set of

$$x^2 + c\omega^2 = -\frac{(c+1)}{\pi} \log \frac{L}{K} \quad (1.20)$$

and thus, for  $d=1$ , an ellipse in first canonical position for  $c > 1$  and second canonical position for  $c < 1$ . For  $c = 1$  we get a circle in the TF-plane.

In Chapter 5 we make heavy use of discrete Gaussians in numerical experiments. They are obtained by sampling and periodization of the continuous functions (see [14] for more on this general principle). For signal length  $L$  the vector  $\Phi_c \in \mathbb{C}^L$ , defined by

$$\Phi_c(n) := L^{1/4} \sum_{j=-\infty}^{\infty} \varphi_c(n/\sqrt{L} + j\sqrt{L}), \quad n = 0, \dots, L-1. \quad (1.21)$$

is used instead of  $\varphi_c$ . It behaves nicely under the DFT:

**Theorem 1.13.**

$$F\Phi_c = \Phi_{1/c}.$$

*Proof.* Since the Poisson summation formula holds pointwise for the Schwartz function  $\varphi_c$  (see [11], p.347) we get

$$\begin{aligned} \Phi_c(n) &= L^{1/4} \sum_{j=-\infty}^{\infty} \varphi_c(n/\sqrt{L} + j\sqrt{L}) \\ &= L^{-1/4} \sum_{j=-\infty}^{\infty} \widehat{\varphi}_c(j/\sqrt{L}) e^{2\pi i j n / L} \\ &= L^{-1/4} \sum_{j=-\infty}^{\infty} \varphi_{1/c}(j/\sqrt{L}) e^{2\pi i j n / L}. \end{aligned}$$

Because the series converges absolutely we can change the order of summation and writing  $j = kL + m$  we get

$$\Phi_c(n) = L^{-1/4} \sum_{m=0}^{L-1} \left( \sum_{k=-\infty}^{\infty} \varphi_{1/c}\left(\frac{kL+m}{\sqrt{L}}\right) \right) e^{2\pi i n m / L}$$

and thus

$$\begin{aligned}
(F\Phi_c)(m) &= L^{-1/4} \sum_{k=-\infty}^{\infty} \varphi_{1/c}(m/\sqrt{L} + k\sqrt{L}) \\
&= \Phi_{1/c}(m)
\end{aligned}$$

□

## 1.6 The Hermite functions

Since  $\mathcal{F}$  is unitary and  $\mathcal{F}^4 = Id$  the only possible eigenvalues for  $\mathcal{F}$  are  $1, i, -1, -i$  and we cannot expect the corresponding eigenfunctions to be unique. However there exists a particularly nice set of eigenfunctions of  $\mathcal{F}$ , called the Hermite functions (or Hermite-Gaussian functions). They are defined via the Hermite polynomials:

**Definition 1.12.** For  $n \in \mathbb{N}$  the  $n$ -th Hermite polynomial  $H_n$  is defined as

$$H_n(x) := (-1)^n e^{x^2/2} \frac{d}{dx^n} e^{-x^2/2} \quad (1.22)$$

The Hermite polynomials satisfy an easy recursion ([17]) allowing for fast computation:

$$H_0(x) = 1, H_1(x) = 2x, H_{n+1}(x) = 2xH_n(x) - 2nH_{n-1}(x) \quad (1.23)$$

Now the Hermite functions are just normalized Hermite polynomials multiplied with a Gaussian weight:

**Definition 1.13.** For  $n \in \mathbb{N}$  the  $n$ -th Hermite function  $\psi_n$  is defined as

$$\psi_n(x) := \frac{2^{1/4}}{\sqrt{2^n n!}} H_n(\sqrt{2\pi}x) e^{-\pi x^2} \quad (1.24)$$

**Theorem 1.14.** The Hermite functions satisfy ([17])

- (i)  $\{\psi_n\}_{n \in \mathbb{N}}$  is an orthonormal basis for  $L^2(\mathbb{R})$ .
- (ii)  $\mathcal{F}\psi_n = e^{-in\pi/2}\psi_n$ .
- (iii)  $\frac{d^2}{dx^2}\psi_n + 4\pi^2\left(\frac{2n+1}{2\pi} - x^2\right)\psi_n = 0$ .
- (iv)  $\psi_n$  is even if  $n$  is even and odd otherwise.
- (v)  $\psi_0 = \varphi$ .

## 2 Frames

In modern signal processing it is customary to work within the concept of frames. Unlike bases they are usually linearly dependent and thus more robust against noise or data loss. We give a short introduction to the topic, following mainly [4], which is a perfect introduction to the topic.

### 2.1 Basic concepts

**Definition 2.1.** A sequence  $(g_k)_{k=1}^{\infty}$  of elements of a Hilbert space  $\mathcal{H}$  is called a frame for  $\mathcal{H}$  if there exist constants  $A, B > 0$  s.t.

$$A \|f\|^2 \leq \sum_{k=1}^{\infty} |\langle f, g_k \rangle|^2 \leq B \|f\|^2, \forall f \in \mathcal{H} \quad (2.1)$$

We refer to  $A$  and  $B$  as upper and lower frame bound. The largest (resp. smallest) number  $A$  (resp.  $B$ ) satisfying (2.1) is called the optimal lower (upper) frame bound and denoted by  $A_{opt}$  ( $B_{opt}$ ). If  $A_{opt} = B_{opt}$  we call  $\{g_k\}_{k=1}^{\infty}$  a tight frame.

If there exists at least  $B > 0$  satisfying the right hand-side of (2.1) we call  $\{g_k\}_{k=1}^{\infty}$  a Bessel sequence.

*Remark 2.1.* Notice that any an orthonormal basis  $\{e_k\}_{k=1}^{\infty}$  for  $\mathcal{H}$  is a (tight) frame with bound 1. The system  $\{e_1, e_1, e_2, e_3, \dots\}$  is a frame with bound 1 and 2, whereas  $\{e_2, e_3, \dots\}$  is only a Bessel sequence. It is clear from a definition that any frame for  $\mathcal{H}$  is complete in  $\mathcal{H}$ .

Given a Bessel sequence  $\{g_k\}_{k=1}^{\infty}$  we can define the bounded operator

$$T : l^2(\mathbb{N}) \mapsto \mathcal{H}, Tc = \sum_{k=1}^{\infty} c_k g_k \quad (2.2)$$

called the pre-frame operator (or synthesis operator). Its adjoint  $T^*$  is called the analysis operator and given by

$$T^* : \mathcal{H} \mapsto l^2(\mathbb{N}), T^* f = (\langle f, g_k \rangle)_{k=1}^{\infty}. \quad (2.3)$$

A central role is now taken by the frame operator  $S$  defined by

$$S : \mathcal{H} \mapsto \mathcal{H}, Sf = TT^* f = \sum_{k=1}^{\infty} \langle f, g_k \rangle g_k \quad (2.4)$$



**Theorem 2.1.** *Given a frame  $\{g_k\}_{k=1}^\infty$  with bounds  $A, B$  and frame operator  $S$  we have*

- (i)  *$S$  is bounded, invertible, self-adjoint and positive definite.*
- (ii)  *$\{S^{-1}g_k\}_{k=1}^\infty$  is a frame with bounds  $\frac{1}{B}$  and  $\frac{1}{A}$  and frame operator  $S^{-1}$ . We call it the canonical dual frame for  $\{g_k\}_{k=1}^\infty$  and , denote the corresponding operators by  $T_D$  and  $S_D$ .*
- (iii)  *$\{S^{-1/2}g_k\}_{k=1}^\infty$  is a tight frame with bounds equal to 1, whose frame operator is the identity. We call it the canonical tight frame for  $\{g_k\}_{k=1}^\infty$ .*

*Proof.* See [4], Lemma 5.1.5. and Theorem 5.3.4. □

**Theorem 2.2.** *With the above notation we set  $h_k = S^{-1}g_k$ , then we have for all  $f \in \mathcal{H}$*

$$T_D T^* = Id = T T_D^* \quad (2.5)$$

or

$$f = \sum_{k=1}^{\infty} \langle f, h_k \rangle g_k \text{ and } f = \sum_{k=1}^{\infty} \langle f, g_k \rangle h_k \quad (2.6)$$

and both series converge unconditionally in  $\mathcal{H}$ .

*Proof.* By Theorem 2.1

$$f = S S^{-1} f = \sum_{k=1}^{\infty} \langle S^{-1} f, g_k \rangle g_k = \sum_{k=1}^{\infty} \langle f, S^{-1} g_k \rangle g_k \quad (2.7)$$

and the second statement in (2.6) follows similarly. The convergence statement follows from [4], Corollary 3.2.5. □

Any frame  $\{h_k\}_{k=1}^\infty$  satisfying the left side of (2.6) is called a dual frame for  $\{g_k\}_{k=1}^\infty$ . The canonical dual is special in the sense that among all dual frames the frame coefficients obtained from the canonical dual have minimal  $l^2$ -norm.

**Theorem 2.3.** *For a frame  $\{g_k\}_{k=1}^\infty$  denote the largest and smallest eigenvalues of its frame operator  $S$  by  $\lambda_{min}$  and  $\lambda_{max}$ . Then the optimal frame bounds are given by*

$$A_{opt} = \|S^{-1}\|^{-1} = \lambda_{min} = \|T^\dagger\|^2 \text{ and } B_{opt} = \|S\| = \lambda_{max} = \|T\|^2 \quad (2.8)$$

*Proof.* Since  $S$  is self-adjoint

$$\|S\| = \sup_{\|f\|=1} \langle Sf, f \rangle = \sup_{\|f\|=1} \sum_{k=1}^{\infty} \langle f, g_k \rangle \langle g_k, f \rangle = \sup_{\|f\|=1} \sum_{k=1}^{\infty} |\langle f, g_k \rangle|^2 = B_{opt}$$

By Theorem 2.1 the canonical dual frame has frame operator  $S^{-1}$  and optimal upper bound  $\frac{1}{A_{opt}}$ , so by the above argument it follows that  $\|S^{-1}\| = \frac{1}{A_{opt}}$ . For the statements concerning  $T$  see [4], Proposition 5.4.4.  $\square$

*Remark 2.2.* A measure of a frame's quality is its condition number, given by the expression

$$\frac{B_{opt}}{A_{opt}} = \|S\| \|S^{-1}\| = \text{cond}(S)$$

For a tight frame (e.g. an orthonormal basis) this is equal to one, and since  $\text{cond}(S_D) = \text{cond}(S^{-1}) = \text{cond}(S)$  the canonical dual frame has the same condition number.

A special class of frames are the so-called Riesz basis, which have many desirable properties we know from finite-dimensional basis. We summarize the main facts from [4]:

**Definition 2.2.** A Riesz basis for a Hilbert space  $\mathcal{H}$  is a family of the form  $\{Ue_k\}_{k=1}^{\infty}$  where  $\{e_k\}_{k=1}^{\infty}$  is an orthonormal basis for  $\mathcal{H}$  and  $U$  is a bounded bijective operator from  $\mathcal{H}$  to  $\mathcal{H}$ .

**Lemma 2.1.** For family  $\{f_k\}_{k=1}^{\infty}$  the following are equivalent

- (i)  $\{f_k\}$  is a Riesz basis.
- (ii)  $\{f_k\}$  is an unconditional basis and satisfies  $0 < \inf \|f_k\| \leq \sup \|f_k\| < \infty$ .
- (iii)  $\{f_k\}$  is complete and there exist  $A, B > 0$ , s.t. for every finite scalar sequence  $(c_k)$  one has

$$A \sum |c_k|^2 \leq \left\| \sum c_k f_k \right\|^2 \leq B \sum |c_k|^2$$

**Theorem 2.4.** For a frame  $\{f_k\}_{k=1}^{\infty}$  the following are equivalent

- (i)  $\{f_k\}$  is a Riesz basis.

(ii)  $\{f_k\}$  is minimal.

(iii)  $\{f_k\}$  and  $\{S^{-1}f_k\}$  are biorthogonal.

(iv) If  $\sum_k c_k f_k = 0$  for  $(c_k) \in l^2(\mathbb{N})$  then  $c_k = 0, \forall k \in \mathbb{N}$ .

(v)  $\{f_k\}$  is a basis.

We now want get an intuitive idea of the above concepts by looking at a very simple finite-dimensional example:

**Example 2.1.** In  $\mathbb{R}^n$  the notion of frames reduces to that of finite generating systems. For  $n = 2$  we consider the system  $\{g_k\}_{k=1}^3$  given by

$$g_1 = (2, 0)^T, g_2 = (-1, 0.1)^T, g_3 = (-2, -0.1)^T$$

and we easily compute

$$T = \begin{pmatrix} 2 & -1 & -2 \\ 0 & 0.1 & -0.1 \end{pmatrix}, S = TT^* = \begin{pmatrix} 9 & 0.1 \\ 0.1 & 0.02 \end{pmatrix}.$$

The eigenvalue-decomposition of  $S$  is given by

$$S = \begin{pmatrix} -0.9999 & 0.0111 \\ -0.0111 & -0.9999 \end{pmatrix} \cdot \begin{pmatrix} 9.0011 & 0 \\ 0 & 0.0198 \end{pmatrix} \cdot \begin{pmatrix} -0.9999 & 0.0111 \\ -0.0111 & -0.9999 \end{pmatrix}^T$$

and it follows  $A_{opt} = 0.0198$  and  $B_{opt} = 9.0011$ . We get the canonical dual frame  $\{h_k\}_{k=1}^3$  from

$$(h_1 | h_2 | h_3) = S^{-1}T = \begin{pmatrix} 0.2353 & -0.1765 & -0.1765 \\ -1.1765 & 5.8824 & -4.117 \end{pmatrix}$$

and the canonical tight frame  $\{t_k\}_{k=1}^3$  from

$$(t_1 | t_2 | t_3) = S^{-1/2}T = \begin{pmatrix} 0.6683 & -0.3419 & -0.6606 \\ -0.1546 & 0.8049 & -0.5730 \end{pmatrix}$$

In Figure 1 all three systems are displayed as arrows. Let us first look at  $\{g_k\}_{k=1}^3$ . The frame bounds indicate a systems of very poor quality and looking at eigenvectors of  $S$  we see that they tell us about areas of low or high concentration: The eigenvector corresponding to  $B_{opt}$  points along the x-axis where we have very high concentration of the  $g_k$  whereas the eigenvector for  $A_{opt}$  points along the y-axis, where the frame has very low concentration. This seems to be exactly reversed

for the dual frame, and it's not surprising:

Assume for an arbitrary frame  $\{f_k\}_{k=1}^{\infty}$  for  $\mathcal{H}$  with dual frame  $\{d_k\}_{k=1}^{\infty}$  that there is  $f \in \mathcal{H}$ ,  $\|f\| = 1$  s.t.  $|\langle f, f_k \rangle| < \epsilon$ ,  $\forall k$ . Then

$$\begin{aligned} 1 = \langle f, f \rangle &= \left\langle f, \sum \langle f, d_k \rangle f_k \right\rangle \leq \epsilon \sum |\langle f, d_k \rangle| \\ &\Rightarrow \sum |\langle f, d_k \rangle| \geq \frac{1}{\epsilon} \end{aligned}$$

So a dual frame is always highly concentrated in areas where the primal frame has low concentration.

Returning to our example we also see that the canonical tight frame balances the primal and dual frame, yielding a uniform distribution across the plane.

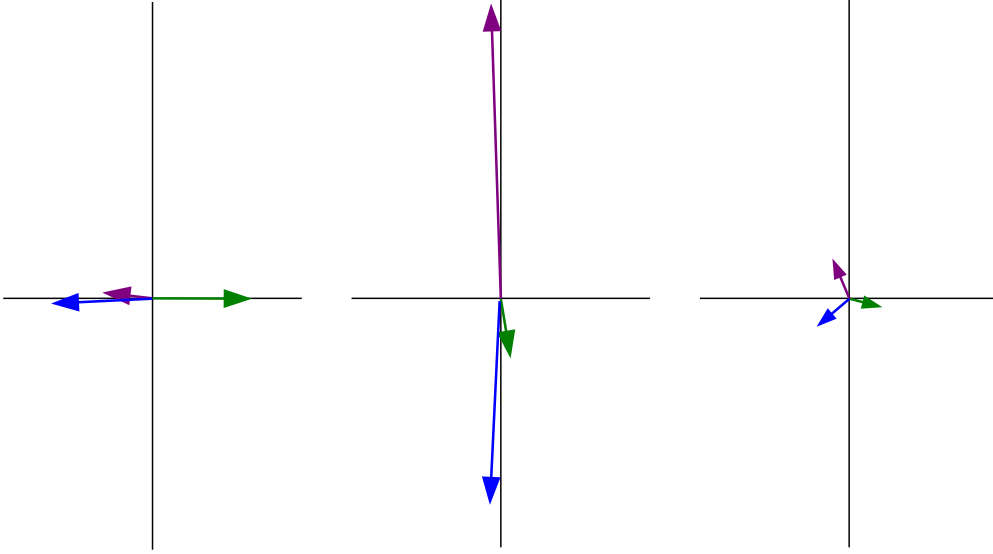


Figure 1: From left to right: primal, canonical dual and canonical tight frame for Example 2.1

*Remark 2.3.* Frames are a useful tool for signal processing: Given a signal  $f \in \mathcal{H}$  with  $\|f\| = 1$ , a frame  $\{g_k\}_{k=1}^{\infty}$  with bounds  $A$  and  $B$  and a corresponding dual frame  $\{h_k\}_{k=1}^{\infty}$  and the corresponding operators  $T, S, T_D, S_D$  we can use (2.6) to analyze the signal. First we compute the frame coefficients  $\{\langle f, g_k \rangle\}_{k=1}^{\infty}$  (by

applying  $T^*$ , also called the analysis step). These we can store, transmit or manipulate and afterwards we perform the synthesis step (i.e. apply  $T_D$ ) and recover (a manipulated version of)  $f$ . Where do the frame bounds come in?

Assume that the frame coefficients are corrupted a noise term  $n \in l^2(\mathbb{N})$ . The signal we reconstruct from the noisy coefficients is given by

$$f_{rec} = T_D(T^*f + n) = f + T_Dn$$

and thus

$$\|f - f_{rec}\| \leq \|T_D\| \|n\| = \frac{1}{\sqrt{A_{opt}}} \|n\|$$

So we see that a high lower frame bound increases the robustness of the analysis-synthesis procedure against noise on the coefficients. On the other hand a high upper frame bound increases the stability against noise on  $f$ . It might also indicate that one could remove elements from the frame (and thus save time and space when doing analysis or synthesis) without significantly reducing its quality.

## 2.2 Perturbation of frames

The following theorem concerns stability of the frame property against perturbations of the frame elements. We will make use of it in chapter 6.

**Theorem 2.5** (Paley-Wiener Theorem for frames). *Let  $\{f_k\}_{k \in \mathbb{N}}$  be a frame for a Hilbert space  $\mathcal{H}$  with bounds  $A, B$ . Let  $\{g_k\}_{k \in \mathbb{N}}$  be a sequence in  $\mathcal{H}$  and assume that there exist constants  $\lambda, \mu \geq 0$  such that  $\lambda + \frac{\mu}{\sqrt{A}} < 1$  and*

$$\left\| \sum c_k (f_k - g_k) \right\| < \lambda \left\| \sum c_k f_k \right\| + \mu \left( \sum |c_k|^2 \right)^{1/2}$$

for all finite scalar sequences  $(c_k)$ . Then  $\{g_k\}_{k \in \mathbb{N}}$  is a frame for  $H$  with bounds

$$A \left( 1 - \left( \lambda + \frac{\mu}{\sqrt{A}} \right) \right)^2, B \left( 1 + \lambda + \frac{\mu}{\sqrt{B}} \right)^2$$

Moreover, if  $\{f_k\}$  is a Riesz basis, then so is  $\{g_k\}$ .

*Proof.* See [4], Theorem 15.1.1 □

**Corollary 2.1.** *Take  $\{f_k\}_{k \in \mathbb{N}}, \{g_k\}_{k \in \mathbb{N}}$  as above. If the perturbation operator*

$$P : l^2(\mathbb{Z}) \rightarrow H, (c_k) \mapsto \sum c_k(f_k - g_k)$$

*is bounded with  $\|P\| < \sqrt{A}$ , then  $\{g_k\}_{k \in \mathbb{N}}$  is a frame with bounds*

$$A \left(1 - \frac{\|P\|}{\sqrt{A}}\right)^2, B \left(1 + \frac{\|P\|}{\sqrt{B}}\right)^2.$$

### 3 Gabor Analysis

While the STFT is an elegant tool for describing the time-frequency behavior of a function  $f$ , representing  $f$  as  $V_g f$  is clearly highly redundant. The idea behind Gabor analysis is to consider only samples of the STFT, respectively to discretize the TF-plane. Of course a main question is how such a discretization can be done in order to get a well-behaved and invertible transform. We summarize some important results and briefly describe the construction of finite-dimensional Gabor systems. Our main references are [13] and [8].

#### 3.1 Gabor frames

**Definition 3.1.** (*Lattice*) A subgroup  $\Lambda$  of  $(\mathbb{R}^{2d}, +)$  is called a lattice if there exists  $A \in GL(2d, \mathbb{R})$  s.t.  $\Lambda = AZ^{2d}$ . If  $A$  is diagonal the lattice is called separable. The redundancy of  $\Lambda$  is defined as  $|\Lambda| := \frac{1}{|\det(A)|}$ .

**Definition 3.2.** Given a lattice  $\Lambda$  and a window function  $g \in L^2(\mathbb{R}^d)$  the family

$$\mathcal{G}(g, \Lambda) := \{\pi(\lambda)g : \lambda \in \Lambda\} \quad (3.1)$$

is called a Gabor system. If it is a frame we call it a Gabor frame and denote the frame operator by  $S_{g, \Lambda}$ . If  $\Lambda = a\mathbb{Z} \times b\mathbb{Z}$  we also write  $\mathcal{G}(g, a, b)$ .

*Remark 3.1.* A warning to the reader: Often (e.g. in [13]) time-frequency shifts are defined as

$$\tilde{\pi}(x, \omega) := T_x M_\omega = e^{-2\pi i x \cdot \omega} \pi(x, \omega).$$

This alternative definition is motivated by the connections to the Heisenberg group, while ours is natural when starting from the STFT. One easily checks that the resulting frame operators are equal, and therefore this difference is not important for us.

One of the main reasons for the usefulness of Gabor analysis is that the dual frame of a Gabor frame is again a Gabor frame:

**Theorem 3.1.** If  $\mathcal{G}(g, \Lambda)$  is a frame then there exists a dual window  $\gamma = S_{g, \Lambda}^{-1}g \in L^2(\mathbb{R}^d)$  s.t the dual frame of  $\mathcal{G}(g, \Lambda)$  is given by  $\mathcal{G}(\gamma, \Lambda)$ . Therefore every  $f \in L^2(\mathbb{R}^d)$  satisfies

$$\begin{aligned} f &= \sum_{\lambda \in \Lambda} \langle f, \pi(\lambda)g \rangle \pi(\lambda)\gamma \\ &= \sum_{\lambda \in \Lambda} V_g(\lambda) \pi(\lambda)\gamma \end{aligned} \quad (3.2)$$

with unconditional convergence in  $L^2(\mathbb{R}^d)$ .

*Proof.* It suffices to show that for  $\lambda' \in \Lambda$  we have  $S_{g,\Lambda}\pi(\lambda') = \pi(\lambda')S_{g,\Lambda}$  which is not difficult ([13], p.94). The rest follows from Theorems 2.1 and 2.2.  $\square$

So to compute (resp. store) the dual frame for  $\mathcal{G}_{g,\Lambda}$  it suffices to compute (store)  $\gamma$ . We call  $\gamma$  the canonical dual window.

A necessary condition on the lattice parameters  $a$  and  $b$  is given by the so-called density theorem. For an easily accessible proof we refer to [15].

**Theorem 3.2.** *If  $\mathcal{G}(g, a, b)$  is a frame, then  $ab \leq 1$ . If  $\mathcal{G}(g, a, b)$  is a Riesz basis then  $ab = 1$ .*

More is known for Gaussian windows (i.e.  $g = \varphi_c$ , for some  $c > 0$ ):  $\mathcal{G}(\varphi_c, a, b)$  is a frame if and only if  $ab < 1$ . Thus it is never a Riesz basis ([8]).

Given a lattice  $\Lambda \subseteq \mathbb{R}^{2d}$  we define

$$\Lambda^\circ := \{\lambda^\circ \in \mathbb{R}^{2d} : \pi(\lambda)\pi(\lambda^\circ) = \pi(\lambda^\circ)\pi(\lambda) \forall \lambda \in \Lambda\}$$

One easily checks that  $\Lambda^\circ$  is again a lattice and we call it the adjoint lattice of  $\Lambda$ . It appears in many of the fundamental results in Gabor analysis. The next theorem, which is taken from [8], summarizes some these results. Unfortunately for them to hold we need to restrict our window space. A well-suited candidate is Feichtinger's algebra  $S_0$ :

**Definition 3.3.**

$$S_0(\mathbb{R}^d) := \{f \in L^2(\mathbb{R}^d) : \|f\|_{S_0} = \|V_\varphi f\|_{L^1(\mathbb{R}^{2d})} < \infty\}$$

$S_0$  has numerous nice properties which make it a perfect candidate for a window space in Gabor analysis. We refer to [9] for a thorough treatment.

**Theorem 3.3.** *Given a lattice  $\Lambda \subseteq \mathbb{R}^{2d}$  and  $g, \gamma \in S_0(\mathbb{R}^d)$  we have*

(i) *(Fundamental Identity of Gabor Analysis)*

$$\sum_{\lambda \in \Lambda} \langle f, \pi(\lambda)\gamma \rangle \langle \pi(\lambda)g, h \rangle = |\Lambda| \sum_{\lambda^\circ \in \Lambda^\circ} \langle g, \pi(\lambda^\circ)\gamma \rangle \langle \pi(\lambda^\circ)f, h \rangle$$

for all  $f, h \in L^2$  and both sides converge absolutely.

(ii) *(Wexler-Raz Identity)*

$$S_{g,\gamma,\Lambda}f = |\Lambda| \cdot S_{f,\gamma,\Lambda^\circ}g$$

for all  $f \in L^2$ .



(iii) (Janssen Representation)

$$S_{g,\gamma,\Lambda} = |\Lambda| \sum_{\lambda^\circ \in \Lambda^\circ} (V_g \gamma)(\lambda^\circ) \pi(\lambda^\circ)$$

where the series converges unconditionally in the strong operator sense.

**Theorem 3.4.** (Ron-Shen Duality Principle) For  $g \in L^2(\mathbb{R}^d)$  the system  $\mathcal{G}(g, \Lambda)$  is a frame for  $L^2(\mathbb{R}^d)$  if and only if  $\mathcal{G}(g, \Lambda^\circ)$  is a Riesz basis for its closed linear span.

### 3.2 Finite-dimensional Gabor analysis

In section 1.6 we have already defined the translation and modulation operator on  $\mathbb{C}^L$  and we will now use them to build finite-dimensional Gabor system. We basically follow [20] and [8]. For  $L \in \mathbb{N}$ , two divisors  $a, b$  of  $L$  and a window  $g = (g(0), \dots, g(L-1))^T$  we define

$$g_{m,n}(t) := (M_{nb} T_{ma} g)(t) = e^{2\pi i n b t / L} g(t - ma), \quad t = 0, \dots, L-1$$

where the indices are again taken modulo  $L$ . Setting  $\tilde{a} := \frac{L}{a}, \tilde{b} := \frac{L}{b}$  we define the matrix  $G$  corresponding to the Gabor system as

$$G := \left( g_{0,0}, g_{1,0}, \dots, g_{\tilde{a}-1,0}, g_{0,1}, \dots, g_{\tilde{a}-1,1}, \dots, g_{0,\tilde{b}-1}, \dots, g_{\tilde{a}-1,\tilde{b}-1} \right) \in \mathbb{C}^{L, \tilde{a}\tilde{b}}$$

and the associated frame operator matrix as

$$S := GG^*.$$

Computing the elements in  $S$  and using the fact that  $\sum_{k=0}^{\tilde{a}-1} e^{2\pi i j b k / L} = 0$  if  $\tilde{b}$  does not divide  $j$  (this is a consequence of Poisson's summation formula) we get the so-called Walnut Representation of  $S$  ([20]):

**Theorem 3.5.**

$$(S)_{jl} = \begin{cases} \tilde{b} \sum_{m=0}^{\tilde{a}-1} g(j - am) \overline{g(l - am)} & \text{if } |j - l| \text{ is divided by } \tilde{b} \\ 0 & \text{otherwise} \end{cases}$$

From this it is easy to see that  $S$  is a block circulant matrix with block size  $a \times a$  and that only every  $\tilde{b}$ -th subdiagonal is non-zero.

Clearly we can obtain the canonical dual frame from the rows of  $G^\dagger = G^*(GG^*)^{-1} = G^*S^{-1}$ , the pseudoinverse of  $G$ . However, as in the continuous case, it is again a Gabor frame with window  $\gamma = S^{-1}g$ , so it suffices to solve  $S\gamma = g$ . Because of the highly structured form of  $S$  there exist several efficient algorithms that solve this problem, see for example [9].

For much more information on discrete Gabor analysis see also [21] and [14].

## 4 The Fractional Fourier Transform

The Fourier transform  $\mathcal{F} : L^2(\mathbb{R}) \mapsto L^2(\mathbb{R})$  can be interpreted as change of coordinates in the time-frequency plane: A function  $f$ , which we think of as being represented along the time axis, is mapped to  $\hat{f}$ , which is a function in the frequency variable. Theorem 1.2 further justifies interpreting the Fourier transform as a counterclockwise axis rotation in the time-frequency plane by an angle of  $\frac{\pi}{2}$ . This is consistent with

$$\mathcal{F}^2 f(x) = f(-x), \mathcal{F}^3 f(\omega) = \hat{f}(-\omega) \text{ and } \mathcal{F}^4 f(x) = f(x)$$

or in operator notation

$$\mathcal{F}^2 = \mathcal{I}, \mathcal{F}^3 = \mathcal{I}\mathcal{F} \text{ and } \mathcal{F}^4 = Id$$

Given an angle  $\alpha$  we now ask for an operator  $R^\alpha$ , which we can interpret as a counterclockwise axis rotation in the TF-plane by  $\alpha$ . So the family of operators  $\{R^\alpha | \alpha \in \mathbb{R}\}$  should satisfy

- (i)  $R^{\pi/2} = \mathcal{F}$
- (ii)  $R^0 = Id$
- (iii)  $R^\beta R^\alpha = R^{\alpha+\beta}$

Note that (ii) and (iii) imply that  $(\{R^\alpha\}, \circ)$  is an abelian group.

In addition we would like to have a connection between certain time-frequency representations of a function  $f$  and  $R^\alpha f$ , justifying the interpretation as a rotation in the TF-plane. For each  $\alpha \in \mathbb{R}$  such an operator  $R^\alpha$  exists and we call it the *fractional Fourier transform* (FrFT) with angle  $\alpha$ .

### 4.1 Definition and properties

We give a definition of the FrFT as a linear integral transform which is taken from [17].

**Definition 4.1.** For  $\alpha \in \mathbb{R}$ ,  $\alpha$  not an integer multiple of  $\pi$ , we define the fractional Fourier transform with angle  $\alpha$  of a function  $f \in L^2(\mathbb{R})$  by

$$R^\alpha f(u) = f_\alpha(u) := \sqrt{1 - i \cot \alpha} \int_{\mathbb{R}} f(v) e^{i\pi((u^2+v^2) \cot \alpha - 2uv \csc \alpha)} dv \quad (4.1)$$

where  $\csc(\alpha) = \sin(\alpha)^{-1}$  and the square root is defined s.t. the result's argument is in  $(-\frac{\pi}{2}, \frac{\pi}{2}]$ . Sometimes we will write  $f_\alpha$  instead of  $R^\alpha f$ .

For  $\alpha = 2k\pi$ ,  $k \in \mathbb{Z}$  we define  $R^\alpha f(u) := f(u)$ , and for  $\alpha = (2k+1)\pi$  set  $R^\alpha f(u) := f(-u)$

*Remark 4.1.* The FrFT is continuous in  $\alpha$  but this is not immediately clear from the above piecewise definition. See [17], p.120 for details.

*Remark 4.2.* We choose the notation  $R^\alpha$  to emphasize the interpretation of the FrFT as a rotation. Often it is denoted (as a power of the FT) by  $\mathcal{F}^a$ , where  $a = \frac{2\alpha}{\pi}$ .

*Remark 4.3.* Considering that for  $0 < |\alpha| < \pi$  we have ([17], p.119)

$$A_\alpha := \sqrt{1 - i \cot \alpha} = \frac{1}{\sqrt{|\sin \alpha|}} e^{i(\alpha/2 - \text{sgn}(\alpha)\pi/4)}$$

we can rewrite (4.1) as

$$\begin{aligned} R^\alpha f(u) &= A_\alpha e^{i\pi u^2 \cot \alpha} \int_{\mathbb{R}} f(v) e^{i\pi v^2 \cot \alpha} e^{-2\pi iuv \csc \alpha} dv \\ &= e^{i(\alpha/2 - \text{sgn}(\alpha)\pi/4)} (\mathcal{Q}_{-\cot \alpha} D_{\sin \alpha} \mathcal{F} \mathcal{Q}_{-\cot \alpha} f)(u) \end{aligned} \quad (4.2)$$

So  $R^\alpha$  is a composition of unitary operators on  $L^2(\mathbb{R})$  and therefore unitary. Also, since with the exception of  $\mathcal{F}$  all operators appearing in the above expression are 'harmless', the FrFT inherits numerous properties from the Fourier transform, e.g. the Riemann-Lebesgue Lemma is still valid (whenever  $\alpha$  is not a multiple of  $\pi$ ).

The above representation of  $R^\alpha$  immediately implies an inversion formula:

$$\begin{aligned} f(u) &= e^{-i(\alpha/2 - \text{sgn}(\alpha)\pi/4)} (\mathcal{Q}_{\cot \alpha} \mathcal{F}^{-1} D_{\csc \alpha} \mathcal{Q}_{\cot \alpha} f_\alpha)(u) \\ &= e^{-i(\alpha/2 - \text{sgn}(\alpha)\pi/4)} \sqrt{|\sin \alpha|} e^{-i\pi u^2 \cot \alpha} \\ &\quad \times \int_{\mathbb{R}} f_\alpha(v |\sin \alpha|) e^{-i\pi v^2 \sin^2 \alpha \cot \alpha} e^{2\pi iuv} dv \\ &= R^{-\alpha} f_\alpha(u) \end{aligned}$$

where the last equality follows easily from a change of variables  $v' = v |\sin \alpha|$ . So  $(R^\alpha)^{-1} = (R^\alpha)^* = R^{-\alpha}$ .

The next Theorem summarizes some basic properties of the FrFT.

**Theorem 4.1.** (*Properties of the FrFT*)

(i)  $R^0 = Id$

(ii)  $R^{\pi/2} = \mathcal{F}$

(iii)  $R^\beta \circ R^\alpha = R^{\alpha+\beta}$

(iv)  $R^\alpha : L^2(\mathbb{R}) \mapsto L^2(\mathbb{R})$  is unitary.

*Proof:* (i) and (ii) are obvious from the definition, for (iii) we refer to [17], for (iv) see the above remark.

*Remark 4.4.* Following [1] we can interpret the FrFT as a decomposition into chirps: Denote the integral kernel in (4.1) by

$$K_\alpha(u, v) := \sqrt{1 - i \cot \alpha} e^{i\pi((u^2+v^2) \cot \alpha - 2uv \csc \alpha)} \quad (4.3)$$

then we have

$$f(u) = \int_{\mathbb{R}} K_{-\alpha}(u, v) f_\alpha(v) dv. \quad (4.4)$$

Define for fixed  $v$  and  $\alpha$  the function  $c_{v,\alpha} : t \mapsto K_\alpha(t, v)$ , then  $f_\alpha$  can be seen as a decomposition of  $f$  into the system  $\{c_{v,\alpha} \mid v \in \mathbb{R}\}$ . It's easy to check that

$$c_{v,\alpha}(t) = e^{-i\pi v^2 \tan \alpha} c_{0,\alpha}(u - v \sec \alpha) \quad (4.5)$$

or

$$c_{v,\alpha} = e^{-i\pi v^2 \tan \alpha} T_{v \sec \alpha} c_{0,\alpha} \quad (4.6)$$

So, up to phase factors, the system  $\{c_{v,\alpha}\}$  consists of Translations of the chirp  $c_{0,\alpha}(t) = \sqrt{1 - i \cot \alpha} e^{i\pi t^2 \cot \alpha}$ . See Figure 2 for plots of  $c_{0,\alpha}$  for different values of  $\alpha$ .

We can understand the chirp- and translation parameters geometrically: For  $v \in \mathbb{R}$  consider the line in the TF-plane

$$\begin{pmatrix} x_0(\lambda) \\ \omega_0(\lambda) \end{pmatrix} := \begin{pmatrix} v \\ 0 \end{pmatrix} + \lambda \cdot \begin{pmatrix} 0 \\ 1 \end{pmatrix}$$

which can be interpreted as the TF-picture of  $\delta_v$ . If we apply a rotation by  $-\alpha$  the rotated line is given by

$$\begin{pmatrix} x_\alpha(\lambda) \\ \omega_\alpha(\lambda) \end{pmatrix} := \begin{pmatrix} v \cos \alpha \\ -v \sin \alpha \end{pmatrix} + \lambda \cdot \begin{pmatrix} \sin \alpha \\ \cos \alpha \end{pmatrix}$$

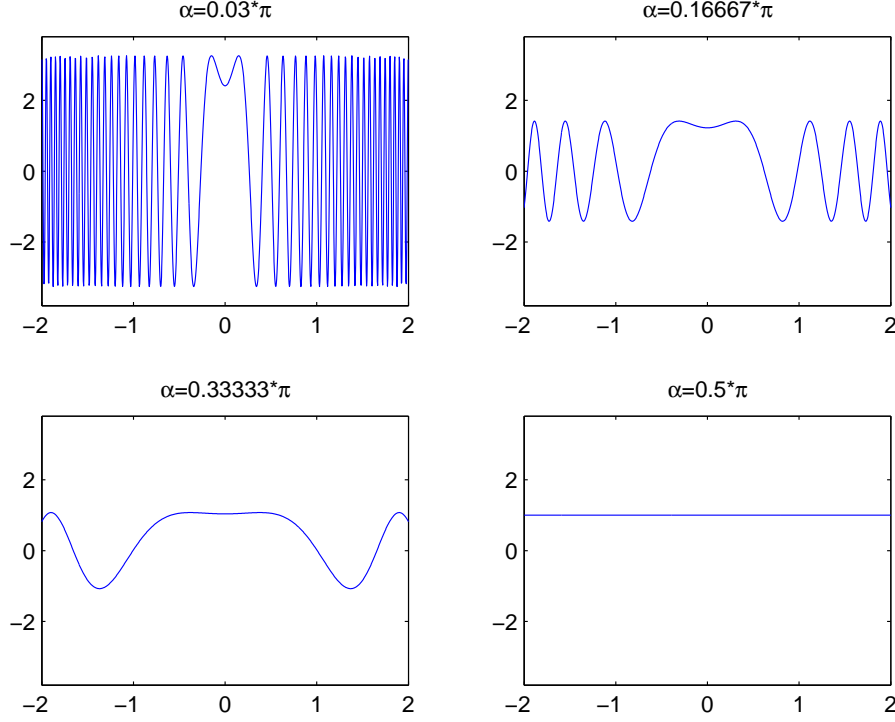


Figure 2: The real part of the chirp  $c_{0,\alpha}$  in the interval  $[-2, 2]$  for different values of  $\alpha$ .

and we get

$$\begin{aligned}
 \cot \alpha (x_\alpha(\lambda) - v \csc \alpha) &= \cot \alpha (v(\cos \alpha - \csc \alpha) + \lambda \sin \alpha) \\
 &= v \frac{\cos^2 \alpha - 1}{\sin \alpha} + \lambda \cos \alpha \\
 &= \omega_\alpha(\lambda)
 \end{aligned}$$

The parameters in the linear equation above correspond to the chirp- and translation parameters in (4.6). So the TF-picture of  $c_{v,\alpha}$  is a vertical line at  $x = v$  rotated clockwise by  $\alpha$ . For  $\alpha = \frac{\pi}{2}$  we get horizontal lines, which we can interpret as pure frequencies.

After these observation it's not surprising that the FrFT can indeed be interpreted as a rotation in the TF-plane. From now on we denote by

$$M_\alpha := \begin{pmatrix} \cos \alpha & -\sin \alpha \\ \sin \alpha & \cos \alpha \end{pmatrix} \quad (4.7)$$

the rotation matrix for an angle  $\alpha$  and for given  $(x, \omega)$  we write

$$\begin{pmatrix} y \\ \tau \end{pmatrix} := M_\alpha \cdot \begin{pmatrix} x \\ \omega \end{pmatrix} \quad (4.8)$$

for the rotated coordinates.

The following theorem gives the desired TF-rotation property. It is a generalization of Theorem 1 in [19], where it is proofed for Gaussian windows. We also give a somewhat more accessible proof, based on the decomposition in (4.2). Also note that the complex factor disappears if we replace the STFT by the Wigner transform.

**Theorem 4.2.** For  $f, g \in L^2(\mathbb{R})$ ,  $\alpha \in \mathbb{R}$

$$(V_{R^\alpha g} R^\alpha f)(x, \omega) = (V_g f)(y, \tau) e^{2\pi i((x^2 - \omega^2)(\sin 2\alpha/4) - x\omega \sin^2 \alpha)}.$$

*Proof.* Using (4.2) together with Lemmas 1.2, 1.4 and 1.5 we get

$$\begin{aligned} V_{R^\alpha g} R^\alpha f(x, \omega) &= V_{\mathcal{Q}_{-\cot \alpha} D_{\sin \alpha} \mathcal{F} \mathcal{Q}_{-\cot \alpha} g} \mathcal{Q}_{-\cot \alpha} D_{\sin \alpha} \mathcal{F} \mathcal{Q}_{-\cot \alpha} f(x, \omega) \\ &= V_{D_{\sin \alpha} \mathcal{F} \mathcal{Q}_{-\cot \alpha} g} D_{\sin \alpha} \mathcal{F} \mathcal{Q}_{-\cot \alpha} f(x, \omega - \cot \alpha x) \cdot e^{-i\pi x^2 \cot \alpha} \\ &= V_{\mathcal{F} \mathcal{Q}_{-\cot \alpha} g} \mathcal{F} \mathcal{Q}_{-\cot \alpha} f\left(\frac{x}{\sin \alpha}, -x \cos \alpha + \omega \sin \alpha\right) \cdot e^{-i\pi x^2 \cot \alpha} \\ &= V_{\mathcal{Q}_{-\cot \alpha} g} \mathcal{Q}_{-\cot \alpha} f\left(x \cos \alpha - \omega \sin \alpha, \frac{x}{\sin \alpha}\right) \\ &\quad \cdot e^{-i\pi x^2 \cot \alpha} \cdot e^{2\pi i(x^2 \cot \alpha - x\omega)} \\ &= V_g f\left(x \cos \alpha - \omega \sin \alpha, \frac{x}{\sin \alpha} - \cot \alpha(x \cos \alpha - \omega \sin \alpha)\right) \\ &\quad \cdot e^{i\pi(x^2 \cot \alpha - 2x\omega)} \cdot e^{i\pi \cot \alpha(x^2 \cos^2 \alpha - 2x\omega \sin \alpha \cos \alpha + \omega^2 \sin^2 \alpha)} \\ &= V_g f\left(x \cos \alpha - \omega \sin \alpha, x\left(\frac{1}{\sin \alpha} - \frac{\cos^2 \alpha}{\sin \alpha}\right) + \omega \cos \alpha\right) \\ &\quad \cdot e^{i\pi((x^2 - \omega^2) \sin \alpha \cos \alpha - 2x\omega \sin^2 \alpha)} \\ &= V_g f(y, \tau) e^{2\pi i((x^2 - \omega^2)(\sin 2\alpha/4) - x\omega \sin^2 \alpha)}. \end{aligned}$$

where the last equality follows from

$$\sin \alpha \cos \alpha = \frac{\sin 2\alpha}{2}.$$

□

*Remark 4.5.* As mentioned in [17], Theorem 4.2 is essentially based on the matrix decomposition

$$\begin{pmatrix} \cos \alpha & \sin \alpha \\ -\sin \alpha & \cos \alpha \end{pmatrix} = \begin{pmatrix} 1 & 0 \\ \cot \alpha & 1 \end{pmatrix} \begin{pmatrix} \sin \alpha & 0 \\ 0 & \frac{1}{\sin \alpha} \end{pmatrix} \begin{pmatrix} 0 & 1 \\ -1 & 0 \end{pmatrix} \begin{pmatrix} 1 & 0 \\ \cot \alpha & 1 \end{pmatrix} \quad (4.9)$$

The first and last matrix on the right side of (4.9) describe the effect of  $\mathcal{Q}_{-\cot \alpha}$  in the TF-plane which is a vertical shear. The other matrices describe a counter-clockwise rotation by  $\frac{\pi}{2}$  which corresponds to the Fourier transform and the effect of  $D_{\sin \alpha}$  - a stretch by  $\sin \alpha$  in time and  $\frac{1}{\sin \alpha}$  in frequency. Figure 3 illustrates how these operations result in a counter-clockwise rotation by  $\alpha$ .

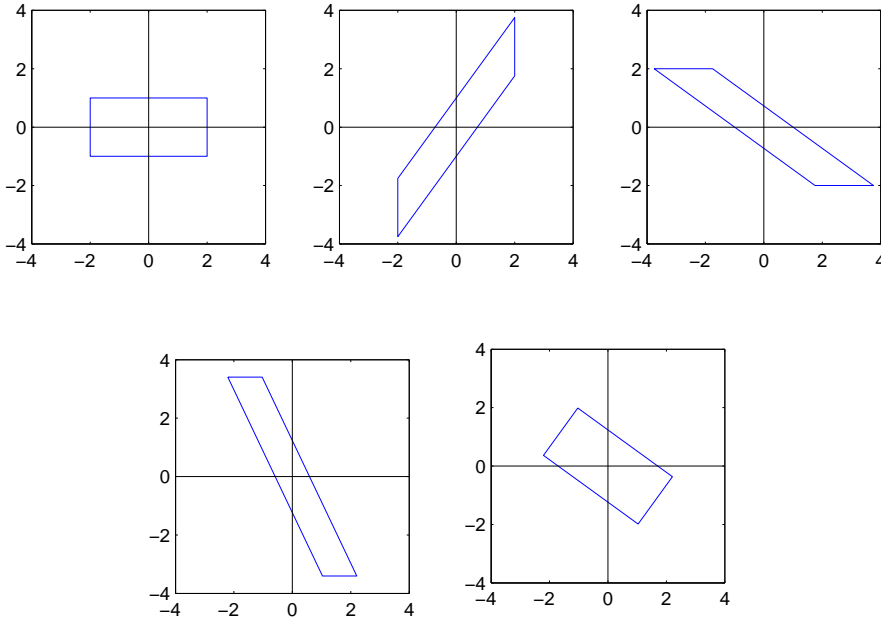


Figure 3: A rectangular area in the TF-plane (top left) after subsequent application of the matrices in (4.9) (for  $\alpha = \frac{\pi}{5}$ ).

From Theorem 4.2 follows easily a commutation relation for TF-shifts and the FrFT:

**Corollary 4.1.** *Take  $f \in L^2(\mathbb{R})$ ,  $x, \omega, \alpha \in \mathbb{R}$ , then we have*

$$M_\omega T_x F^\alpha f = e^{-2\pi i((x^2 - \omega^2)\sin(2\alpha)/4 - x\omega \sin^2 \alpha)} \cdot F^\alpha M_\tau T_y f.$$



*Proof.* Set  $c := e^{2\pi i((x^2 - \omega^2)\sin(2\alpha)/4 - x\omega\sin^2\alpha)}$ , then for any  $h \in L^2(\mathbb{R})$

$$\begin{aligned} \langle h, M_\omega T_x F^\alpha f \rangle &= V_{F^\alpha f} h(x, \omega) \\ &= c \cdot V_f F^{-\alpha} h(y, \tau) \\ &= c \cdot \langle \mathcal{F}^{-\alpha} h, M_\tau T_y f \rangle \\ &= \langle h, \bar{c} \cdot F^\alpha M_\tau T_y f \rangle. \end{aligned}$$

□

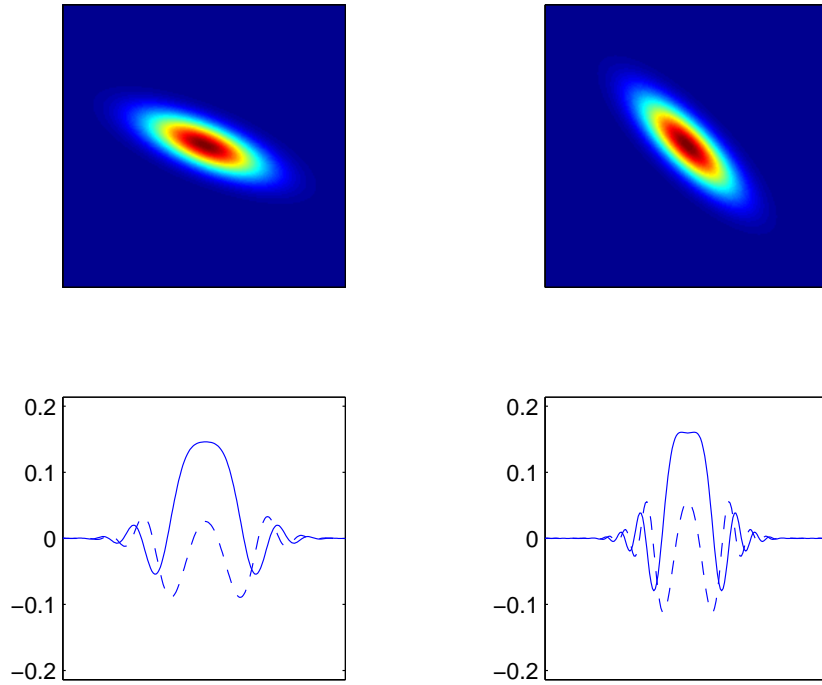


Figure 4: For  $\alpha = \frac{\pi}{8}$  (left) and  $\alpha = \frac{\pi}{4}$  (right) the time-frequency and time representations of  $R^\alpha D_3 \varphi$  (real part: solid, imaginary part: dashed).

The Gaussian is invariant under the FrFT:

**Lemma 4.1.** For  $a \in \mathbb{R}$

$$F^a \varphi = \varphi \tag{4.10}$$

*Proof.* Using Lemmas 1.6 and 4.2 we get

$$\begin{aligned}
(V_\varphi F^\alpha \varphi)(x, \omega) &= \varphi_2(y)\varphi_2(\tau) e^{-\pi i y \tau} e^{2\pi i((x^2-\omega^2)(\sin 2\alpha/4)-x\omega \sin^2 \alpha)} \\
&= e^{-\pi(y^2+\tau^2)/2} e^{\pi i x^2(-\sin 2\alpha/2+\cos \alpha \sin \alpha)} e^{\pi i \omega^2(\sin 2\alpha/2-\cos \alpha \sin \alpha)} \\
&\quad \times e^{-\pi i x \omega(-2\sin^2 \alpha-\cos^2 \alpha+\sin^2 \alpha)} \\
&= e^{-\pi(x^2+\omega^2)/2} e^{-\pi i x \omega} \\
&= (V_\varphi \varphi)(x, \omega)
\end{aligned}$$

and the claim follows from Theorem 1.9.  $\square$

**Theorem 4.3.** (*FrFT and Dilation*) Take  $\alpha \in \mathbb{R}, s > 0$  and choose  $\alpha'$  s.t.  $\tan \alpha' = \frac{1}{s^2} \tan \alpha$  and  $\alpha$  and  $\alpha'$  lie in the same quadrant. Then for  $f \in L^2(\mathbb{R}^d)$

$$R^\alpha D_s f = d \cdot \mathcal{Q}_{\cot \alpha(\cos^2 \alpha' / \cos^2 \alpha - 1)} D_{\frac{\sin \alpha}{s \sin \alpha'}} R^{\alpha'} f \quad (4.11)$$

for a unit magnitude constant  $d := s \cdot \sqrt{\frac{\sin \alpha - i \cos \alpha}{\sin \alpha' - i \cos \alpha'}}$ .

*Proof.* An adaption of [17], p.154, table 4.3, formula 2 to our notation and subsequent simplification. That  $|d| = 1$  follows from the unitarity of the involved operators.  $\square$

*Remark 4.6.* Following [17], p. 157 we can again state a matrix equality corresponding to Theorem 4.3: Set  $s' := \frac{\sin \alpha}{s \sin \alpha'}$  and  $q := \cot \alpha(\frac{\cos^2 \alpha'}{\cos^2 \alpha} - 1)$  then

$$\begin{pmatrix} \cos \alpha & \sin \alpha \\ -\sin \alpha & \cos \alpha \end{pmatrix} \begin{pmatrix} s & 0 \\ 0 & \frac{1}{s} \end{pmatrix} = \begin{pmatrix} 1 & 0 \\ -q & 1 \end{pmatrix} \begin{pmatrix} s' & 0 \\ 0 & \frac{1}{s'} \end{pmatrix} \begin{pmatrix} \cos \alpha' & \sin \alpha' \\ -\sin \alpha' & \cos \alpha' \end{pmatrix} \quad (4.12)$$

Figure 5 illustrates (4.12) for  $\alpha = \frac{\pi}{3}$  and  $s = 2$ .

## 4.2 Spectral decomposition of the FrFT

Since the Hermite functions provide a complete eigensystem for the Fourier transform we can use them to define an operator satisfying (i)-(iv) in Theorem 4.1. For  $n \in \mathbb{N}$ : The  $n$ -th order Hermite function  $\psi_n$  satisfies

$$\mathcal{F}\psi_n(\omega) = e^{-in\pi/2}\psi_n(\omega) \quad (4.13)$$

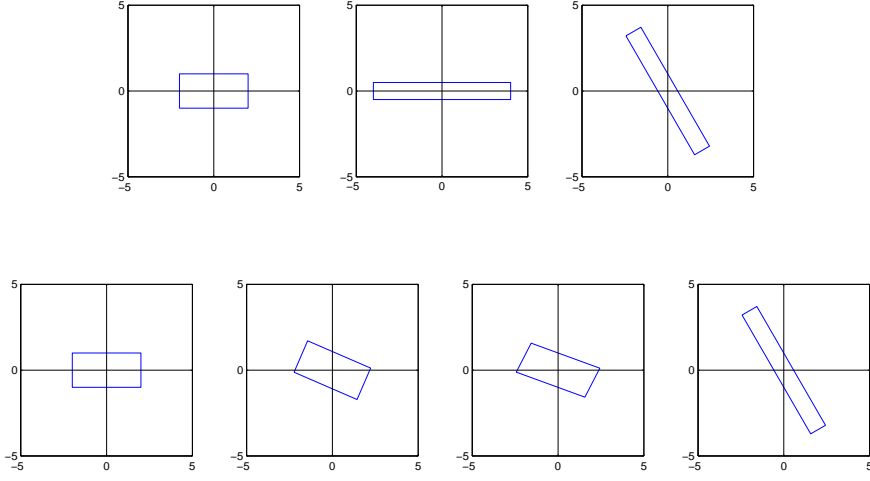


Figure 5: Illustration of (4.12) for  $\alpha = \frac{\pi}{3}$ : left side - top row, right side - bottom row.

and any linear operator  $T : L^2(\mathbb{R}) \mapsto L^2(\mathbb{R})$  that meets 4.13 with  $T$  instead of  $\mathcal{F}$  for all  $n$  is equal to the Fourier transform. So it suffices to find a sequence  $z = (z_n)_{n \in \mathbb{N}}$  of complex numbers s.t.  $z_n^{\pi/2} = e^{-in\pi/2}$  and define for  $\alpha \in \mathbb{R}$

$$T_z^\alpha f := \sum_{n \in \mathbb{N}} z_n^\alpha \langle f, \psi_n \rangle \psi_n.$$

Then  $T_z^\alpha$  satisfies (i)-(iv) in Theorem 4.1. For any integer-sequence  $(k_n)_{n \in \mathbb{N}}$

$$z_n := e^{-i(n+4k_n)}$$

meets the above requirement and different choices for  $(k_n)$  yield different operators  $T_z^\alpha$ . But they don't necessarily satisfy the rotation property of the FrFT (see Figure 6). It turns out that  $k_n = 0 \forall n$  gives the FrFT:

**Theorem 4.4.** For  $f \in L^2(\mathbb{R})$  we have

$$R^\alpha f = \sum_{n \in \mathbb{N}} e^{-in\alpha} \langle f, \psi_n \rangle \psi_n. \quad (4.14)$$

*Proof.* See [17], p.122. □

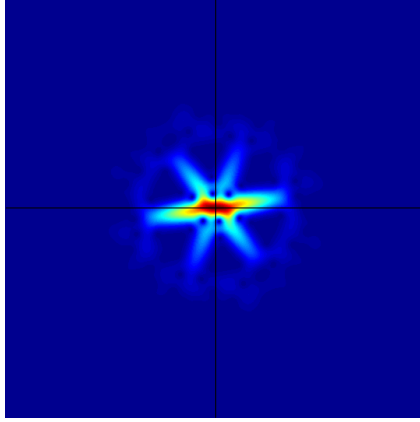


Figure 6:  $|V_\varphi T_z^\alpha D_6 \varphi|$ , for  $\alpha = \frac{7\pi}{5}$  and  $k_n = 2^k$ .

### 4.3 Implementation of the FrFT

In this section we describe various different ways of implementing the fractional Fourier transform. First we look at an algorithm approximating the FrFT as it is defined in Definition 4.1. Our main focus however will lie on comparing an implementation of the so-called discrete FrFT with an algorithm developed by Feichtinger.

#### 4.3.1 Computation of the continuous FrFT

We summarize an algorithm from [17] and [2] which maps samples of a function  $f \in L^2(\mathbb{R})$  to samples of an approximation of  $f_\alpha$ . The key idea is to rewrite (4.1) as a chirp multiplication followed by a chirp convolution and another chirp multiplication: Using  $\cot \alpha - \csc \alpha = \tan \frac{\alpha}{2}$  we have

$$(u^2 - v^2) \cot \alpha - 2uv \csc \alpha = -u^2 \tan \frac{\alpha}{2} + (u - v)^2 \csc \alpha - v^2 \tan \frac{\alpha}{2}$$

and (assuming w.l.o.g.  $0 < |\alpha| < \pi$ ) we can rewrite (4.1) as

$$\begin{aligned} f_\alpha(u) &= A_\alpha e^{-i\pi u^2 \tan \alpha/2} \int_{\mathbb{R}} f(v) e^{-i\pi v^2 \tan \alpha/2} e^{i\pi(u-v)^2 \csc \alpha} dv \\ &= B_\alpha (\mathcal{Q}_{\tan \alpha/2} \mathcal{C}_{\sin \alpha} \mathcal{Q}_{\tan \alpha/2} f)(u) \end{aligned} \quad (4.15)$$

where  $B_\alpha := e^{i(\alpha + \text{sgn}(\alpha)\pi)/2}$ .

The input for the algorithm is a vector  $F$  containing uniform samples of  $f$  (which is assumed to be essentially compactly supported and bandlimited). The chirp multiplication is easily computed, then the chirp convolution is computed in the FFT-domain and finally another chirp multiplication is applied. One has to take into account that chirp multiplication and convolution can increase the bandwidth. So in order to avoid aliasing  $F$  is upsampled at the begin of the algorithm (using sinc-interpolation) and in the end the result is downsampled to match the length of  $F$ . The resulting algorithm is FFT-based and therefore has complexity  $N \log N$ , where  $N$  is the length of  $F$ . For a detailed description of the implementation and the freely available Matlab-file we refer to [2].

### 4.3.2 The discrete fractional Fourier transform

The discrete fractional Fourier transform (DFrFT) was developed in [3]. For  $n \in \mathbb{N}$  the goal is to construct an orthonormal set  $\{E_i\}_{i=1,\dots,n}$  of eigenvectors of the DFT-matrix  $F$  of size  $n$ , that can be interpreted a discrete analog of the Hermite functions. Given  $\alpha \in \mathbb{R}$  the DFrFT is then defined as a Hermite-multiplier analogous to (4.14). From this definition the analog of Theorem 4.1 will be obvious.

We briefly sketch the construction of the  $E_i$ : The continuous Hermite functions are known to be the unique eigenfunctions of the operator

$$\mathcal{S} := \mathcal{D}^2 + \mathcal{F}\mathcal{D}^2\mathcal{F}^{-1} \quad (4.16)$$

where  $\mathcal{D}$  is the differentiation operator. First  $\mathcal{D}^2$  is approximated by a central difference quotient leading to a matrix approximation  $S$  of  $\mathcal{S}$  which commutes with the DFT matrix  $F$  and thus has a common set of eigenvectors with  $F$ . However the eigenvalues of  $S$  are mutually distinct and the eigenvectors therefore unique. For a thorough treatment we refer to [3]. The algorithm also allows to use higher order differences for the approximation of  $\mathcal{D}^2$  resulting in a better approximation of the  $\psi_j$  by the  $E_j$ .

So we now have a complete orthonormal set  $\{E_j\}_{j=1,\dots,n}$  of eigenvectors for  $F$ . The corresponding eigenvalues  $\{\mu_j\}_{j=1,\dots,n}$  are given by  $\mu_j = (-i)^{j-1}$  for  $j = 1, \dots, n-1$  and  $\mu_n = 1$  if  $n$  is equivalent 0 or 1 modulo 4 and  $\mu_n = -1$  otherwise ([2]). So except for  $\mu_n$  they coincide with the eigenvalues in the continuous case.

We now take look at  $V_\varphi E_j$ . The continuous Hermite functions are known to be concentrated on circles in the TF-plane (see [16]). Figure 7 suggests that this is

approximately true for the  $E_j$ , only if  $j$  is small compared to  $n$ . For larger values of  $j$  the TF-pictures of the  $E_j$  turn into squares which finally fit themselves to the border of the TF-plane. So we can only hope to obtain good approximations for  $\psi_j$  via  $E_j$  if  $j$  is small compared to  $n$ , respectively in the limit  $n \rightarrow \infty$ .

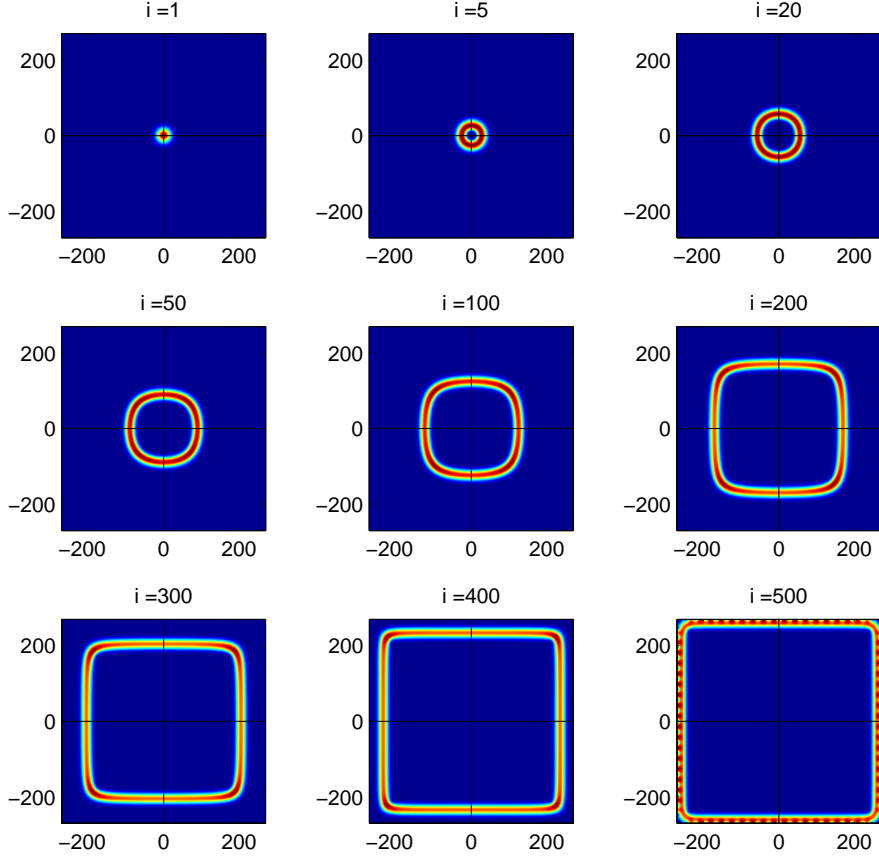


Figure 7: Plots of  $|V_\varphi E_i|$  for  $n = 540$  and different values of  $i$ .

Indeed the following theorem, which is taken from [2], shows that after some rearrangement the  $E_j$  converge to samples of the continuous H-G functions for  $n \rightarrow \infty$ .

**Theorem 4.5.** For  $j, n \in \mathbb{N}$  with  $n > j$  and  $n$  even define

$$e_{j,n} := [E_j(n/2 + 2), \dots, E_j(n), E_j(1), \dots, E_j(n/2 + 2)]^T \quad (4.17)$$

and

$$\Psi_{j,n} := [\psi_{j-1}(x_k) : k = -n/2, \dots, n/2]^T, \quad x_k := k\sqrt{2\pi/(n+1)}. \quad (4.18)$$

Then, after proper normalization,  $e_{j,n}$  converges to  $\Psi_{j,n}$  as  $n \rightarrow \infty$ .

Equipped with the system  $\{E_j\}_{j=1,\dots,n}$  it is not difficult to define an analog to the FrFT. Set  $E := (E_1 | \dots | E_n)$  and for given  $\alpha \in \mathbb{R}$  define the  $n \times n$  diagonal matrix  $D_E^\alpha$  by

$$(D_E^\alpha)_{jj} = e^{-i\alpha(j-1)}, \quad j = 1, \dots, n-1,$$

$$(D_E^\alpha)_{nn} = e^{-i\alpha n} \text{ for } n \text{ even, } (D_E^\alpha)_{nn} = e^{-i\alpha(n-1)} \text{ for } n \text{ odd.}$$

Now we define the discrete fractional Fourier transform with angle  $\alpha$  as

$$R_E^\alpha : \mathbb{C}^n \rightarrow \mathbb{C}^n, \quad f \mapsto ED_E^\alpha E^* f. \quad (4.19)$$

We will investigate  $R_E^\alpha$  further in section 4.3.4.

### 4.3.3 A different approach

A different approach to constructing discrete Hermite-Gauss functions was proposed by Feichtinger. It relies on the fact that the continuous Hermite functions are concentrated on circles in the TF-plane. The corresponding algorithm can be found at [www.nuhag.eu](http://www.nuhag.eu) in form of the MATLAB-file `hermf.m`. We give a brief description and compare the results to the discrete FrFT. Unless stated otherwise all observations made are based on experiments.

Given  $n \in \mathbb{N}$  the algorithm starts by constructing an  $n \times n$  matrix  $W$  that contains samples of a radial symmetric weight which is centered around the origin of the TF-plane and decreases linearly from there (see Figure 8). Next we construct the STFT-multiplier (with Gaussian window) associated to  $W$ , we call it  $M$ . In the continuous case the eigenfunctions of such an operator are known to be the Hermite functions, see [5].

In the finite-dimensional case we find that  $M$  is self-adjoint and commutes with  $F$ . Thus an eigenvalue-decomposition of  $M$  yields an orthonormal set  $\{H_j\}_{j=1,\dots,n}$  of joint eigenvectors of  $M$  and  $F$ . Since every eigenvalue of  $M$  is real and has algebraic multiplicity one (Figure 8), the eigenvectors are unique up to sign and we can reorder them in such a way that the corresponding eigenvalues decrease. Finally the routine checks each  $H_j$  for constant complex factors and removes them, since the continuous Hermite functions are real-valued.

The idea behind the algorithm is that  $H_1$ , the eigenvector corresponding to the largest eigenvalue of  $M$ , should be concentrated around the maximum of  $W$  which

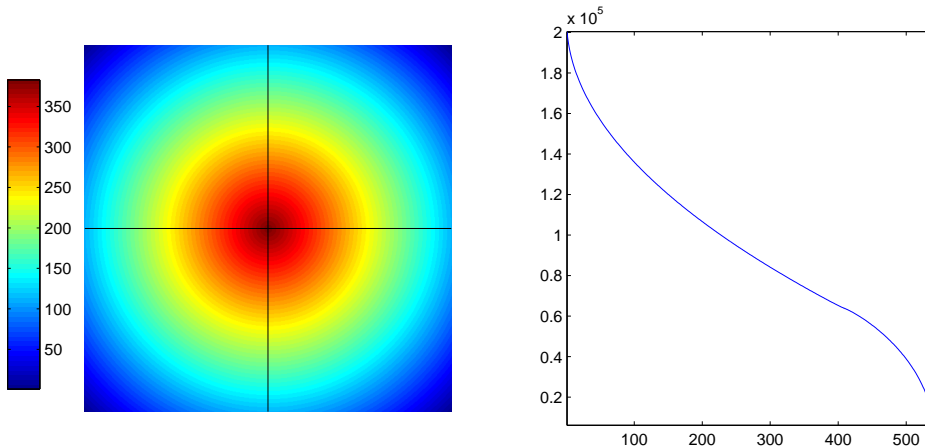


Figure 8: For  $n = 540$ : The weight-matrix  $W$  (left) and the spectrum of the corresponding STFT-multiplier  $M$ .

is obtained at the origin of the TF-plane. And indeed  $H_1$  is equal to the Gaussian (which we used in the construction of  $M$ ). The next of the  $H_j$  we expect to be TF-concentrated on circles of increasing size (corresponding to the level sets of  $W$ ). Figure 9 shows for  $n = 540$  the absolute values of  $V_\varphi H_j$  for different  $j$ . We see that what we expected is mostly the case, but at some point (here around  $i = 380$ ) the circles reach the borders of our finite TF-plane. Then the concentration of the  $H_j$  starts to shift towards the intersection points of the circles with the axes. If we increase  $j$  further the TF-pictures resume the form of circles, but with those parts cut off that would not fit in the picture. After these observations we may hope that, at least for  $j$  not too large, the  $H_j$  give a reasonable discrete approximation to the Hermite-Gauss functions. This will be the topic of the following experiment.

*Experiment 4.1.* We seek experimental verification of a result similar to Theorem 4.5 for the  $H_j$ . It quickly turns out that we cannot adopt the definitions from there unchanged but need to modify them slightly. For  $n, j \in \mathbb{N}$ ,  $n > j$  and  $n$  even we set

$$h_{j,n} := [H_j(n/2 + 2), \dots, H_j(n), H_j(1), \dots, H_j(n/2 + 2)]^T \quad (4.20)$$

and

$$\tilde{\Psi}_{j,n} := [\psi_{j-1}(\tilde{x}_k) : k = -n/2+1, \dots, n/2+1]^T, \quad \tilde{x}_k := (4/5)k\sqrt{2\pi/(n+1)}. \quad (4.21)$$



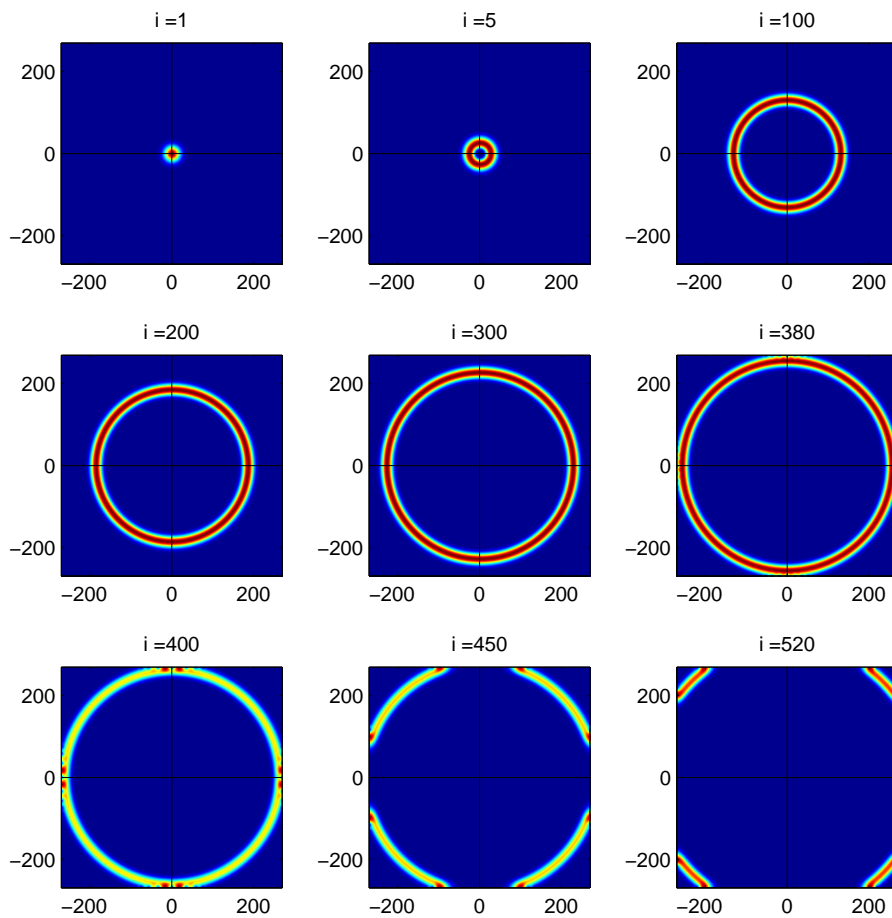


Figure 9: For  $n = 540$ : Plots of  $|V_\varphi H_j|$  for different values of  $j$ .

The factor  $4/5$  in the definition in the definition of  $\tilde{x}_k$  is somewhat mysterious yet numerous experiments suggest that it gives the best results. The evaluation of  $\psi_{j-1}$  via Definition 1.13 is straightforward. We remark that the recursion for the Hermite-polynomials is much faster evaluated when using a loop instead of a purely recursive implementation. For (roughly)  $j > 70$  however the blowup in the coefficients of the  $j$ -th Hermite polynomial causes severe cancellation, making the evaluation of the  $\psi_j$  difficult. Therefore we will restrict our experiments to values  $j < 70$ .

Figure 10 shows that for  $n = 30$  and  $j \in \{2, 5, 10, 20\}$  the  $h_{j,n}$  give good approximations to the  $\tilde{\Psi}_{j,n}$  (of which upsampled versions are plotted). Only for  $j = 20$

there are severe deviations near the borders.

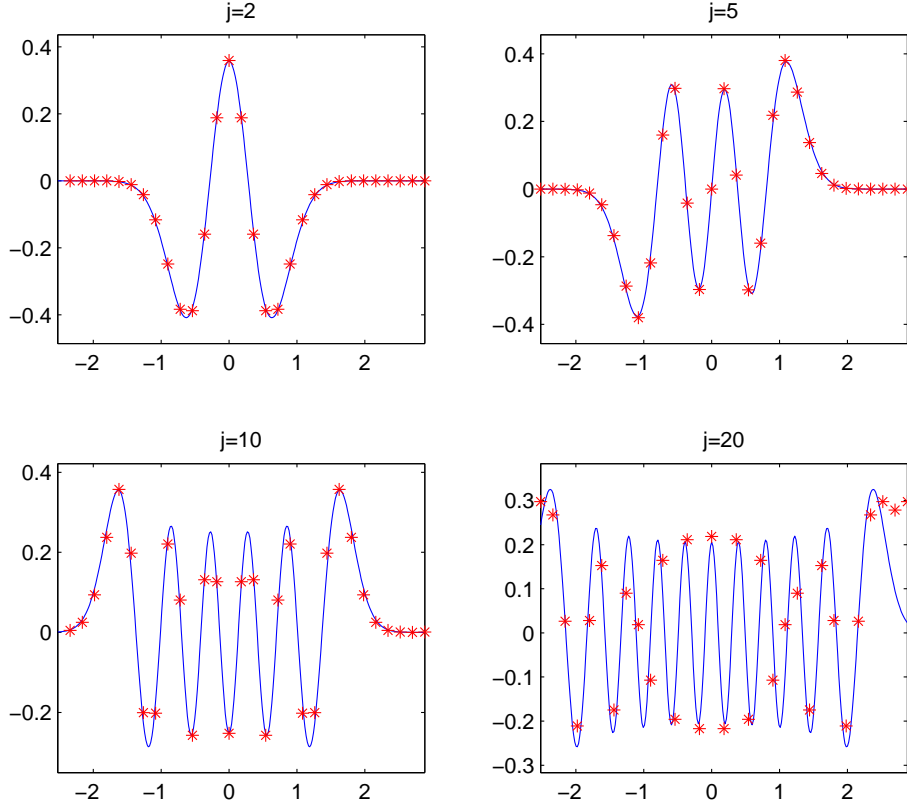


Figure 10: For  $n = 30$  and different values of  $j$ : Comparison of  $h_{j,n}$  (red stars) to the Hermite-Gauss function of order  $j - 1$  (blue)

From Figure 11 we see that, with respect to the  $\infty$ -norm, the  $\tilde{\Psi}_{j,n}$  are indeed very well approximated by the  $h_{j,n}$  as long as  $j < 18$  for  $n = 30$  resp.  $j < 41$  for  $n = 60$ . For higher values of  $j$  the approximation becomes much worse and soon useless. This is not surprising since also the spectrograms of the  $H_j$  no longer resemble circles once they reach the border of the TF-plane. Heuristically one can argue that this happens roughly around  $J_n := n/\sqrt{2}$ , since the ratio of the diagonal of a square to its side is  $\sqrt{2}$ . And indeed  $J_n$  turns out to be a decent estimate for the index up to which the  $h_{j,n}$  resemble the  $\tilde{\Psi}_{j,n}$ .

Finally the data from Figure 12 strongly suggests that for fixed  $j$  we have  $\|h_{j,n} - \tilde{\Psi}_{j,n}\|_\infty \rightarrow 0$  as  $n \rightarrow \infty$  with linear convergence rate and thus an analog

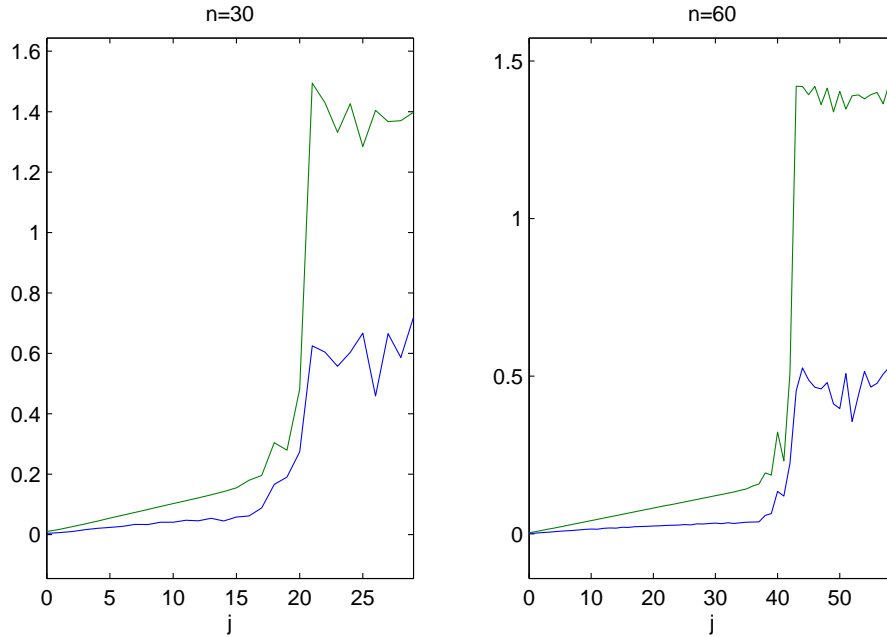


Figure 11: For  $n = 30$  (left) and  $n = 60$  (right):  $\|h_{j,n} - \tilde{\Psi}_{j,n}\|_\infty$  (blue) and  $\|h_{j,n} - \tilde{\Psi}_{j,n}\|_2$  (green) for  $j$  ranging from 0 to  $n$ .

of Theorem 4.5 holds.

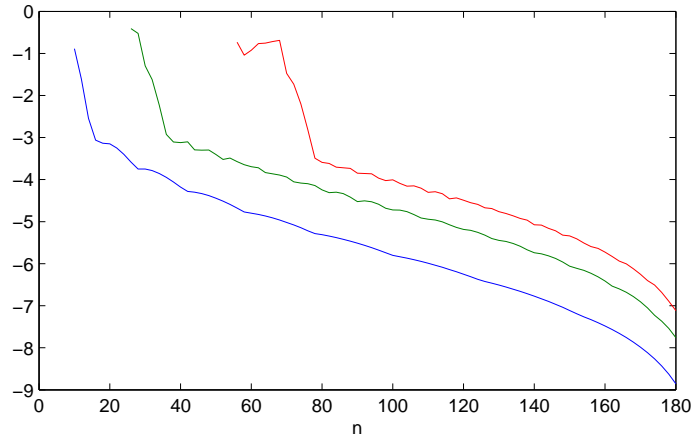


Figure 12: Semi-logarithmic plot of  $\|h_{j,n} - \tilde{\Psi}_{j,n}\|_\infty$  for  $j = 5$  (blue),  $j = 20$  (green) and  $j = 50$  (red) with varying  $n$ .

Next we look at the eigenvalues of the DFT that correspond to the  $H_j$ . From the above it is clear that  $\{H_j\}_{j=1,\dots,n}$  constitutes a complete eigensystem

for the DFT. We denote the eigenvalue corresponding to  $H_j$  by  $\lambda_j$  and set  $\lambda := (\lambda_1, \dots, \lambda_n)$ . The experiments indicate that for each  $n \in \mathbb{N}$  there is an odd index  $j_n$  such that

$$\lambda = ((-i)^0, \dots, (-i)^{j_n-1}, i^{j_n+1}, i^{j_n+2}, \dots, i^n) \quad (4.22)$$

So the eigenvalues start out like in the continuous case but after  $\lambda_{j_n}$  there is a 'jump' (from  $-1$  to  $1$  or  $1$  to  $-1$ ). Afterwards the eigenvalues resume cycling  $\{1, i, -1, -i\}$  but now in the counter-clockwise direction in the complex plane. Figure 13 contains values for  $\frac{j_n}{n}$  for different  $n$ . We see that, at least for  $n$  within a certain range,  $j_n$  depends nearly linearly on  $n$  and in every case we get  $j_n > 0.7 \cdot n$ . For indices this high the  $H_i$  are concentrated outside the 'incircle' of the TF-plane, where the  $H_j$  approximate the Hermite functions (see again Figure 13). So for the  $H_j$ , for which the TF-pictures resemble those of the Hermite functions, the eigenvalues are equal to the ones we get in the continuous case.

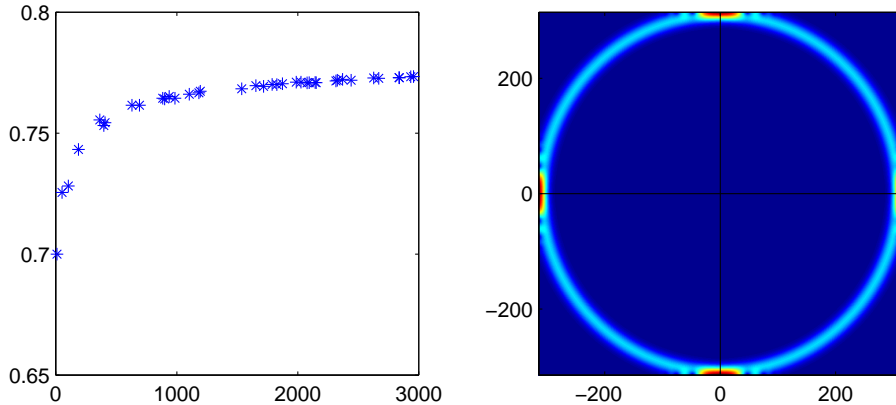


Figure 13: Left: values of  $\frac{j_n}{n}$  for 38 random values of  $n$  between 1 and 3000; Right: for  $n = 397$ , a plot of  $|V_\varphi H_{j_n}|$

We now want to define a FrFT-like operator based on the system  $\{H_j\}_{j=1, \dots, n}$ . Similar to the previous section we set  $H = (H_1 | \dots | H_n)$  and for  $\alpha \in \mathbb{R}$  we define (in light of (4.22)) the  $n \times n$ -diagonal matrix  $D_H^\alpha$  by

$$(D_H^\alpha)_{jj} := e^{-i\alpha(j-1)}, j = 1, \dots, j_n \text{ and } (D_H^\alpha)_{jj} := e^{-i\alpha j}, j = j_n + 1, \dots, n. \quad (4.23)$$

The discrete Hermite-rotation with angle  $\alpha$  is now defined as

$$R_H^\alpha : \mathbb{C}^n \rightarrow \mathbb{C}^n, f \mapsto HD_H^\alpha H^* f. \quad (4.24)$$

*Remark 4.7.* The above definition of  $R_E^\alpha$  requires to know  $j_n$ . The direct way of finding  $j_n$  would be the diagonalization of the DFT-matrix using  $H$ . Here we could use the data from Figure 13 to guess an approximate value and only compute the corresponding part of the diagonalization. However since from the previous results we expect the  $H_j$  to give useful discrete Hermite functions only up to some index  $\hat{j}_n < j_n$  one could argue that  $R_H^\alpha f$  will only be a reasonable substitute for  $R^\alpha f$  if  $\langle f, H_j \rangle \approx 0, \forall j > \hat{j}_n$ . Therefore we could replace (4.23) by  $(D_H^\alpha)_{jj} := e^{-i\alpha(j-1)}, j = 1, \dots, n$  without significant damage. Of course we then no longer have  $R_H^{\pi/2} = F$ .

*Remark 4.8.* We note that the specific choice of the weight  $W$  has only very little effect on the resulting  $H_j$  as long as  $W$  is chosen radial symmetric and strictly decreasing from the origin.

#### 4.3.4 Comparison of $R_E^\alpha$ and $R_H^\alpha$

In this section we want to compare the operators  $R_E^\alpha$  and  $R_H^\alpha$  and look at how well they fulfill properties we know to be true for the continuous FrFT.

It's clear from their definitions that both operators satisfy the analogs of Theorem 4.1. However the distinguishing property of the FrFT is the rotation property from Theorem 4.2. Figure 14 illustrates how a Dirac comb behaves under  $R_H^\alpha$  and  $R_E^\alpha$ . We see that  $R_H^\alpha$ , while showing unclear behavior at the boundaries, acts as a rotation at on the 'in-circle' of the TF-plane. And of course in the finite-dimensional case this circle is the maximum area on which such a rotation property can hold for all  $\alpha$ . When we look at  $R_E^\alpha$  however we see a significantly different behavior: While the results look 'smoother', in the sense that the lines from the pictures for  $\alpha = 0$  are still connected, there is significant distortion towards the corners of the TF-plane and a rotation property is clearly not satisfied.

Based on these observations we will from now on use  $R_H^\alpha f$  as an approximation to the FrFT with angle  $\alpha$ . However before applying the operator we have to make sure that the functions at hand are essentially concentrated on the 'in-circle' of the TF plane, meaning that  $\langle f, H_j \rangle$  is small for (roughly)  $j \geq n/\sqrt{2}$ . Since for

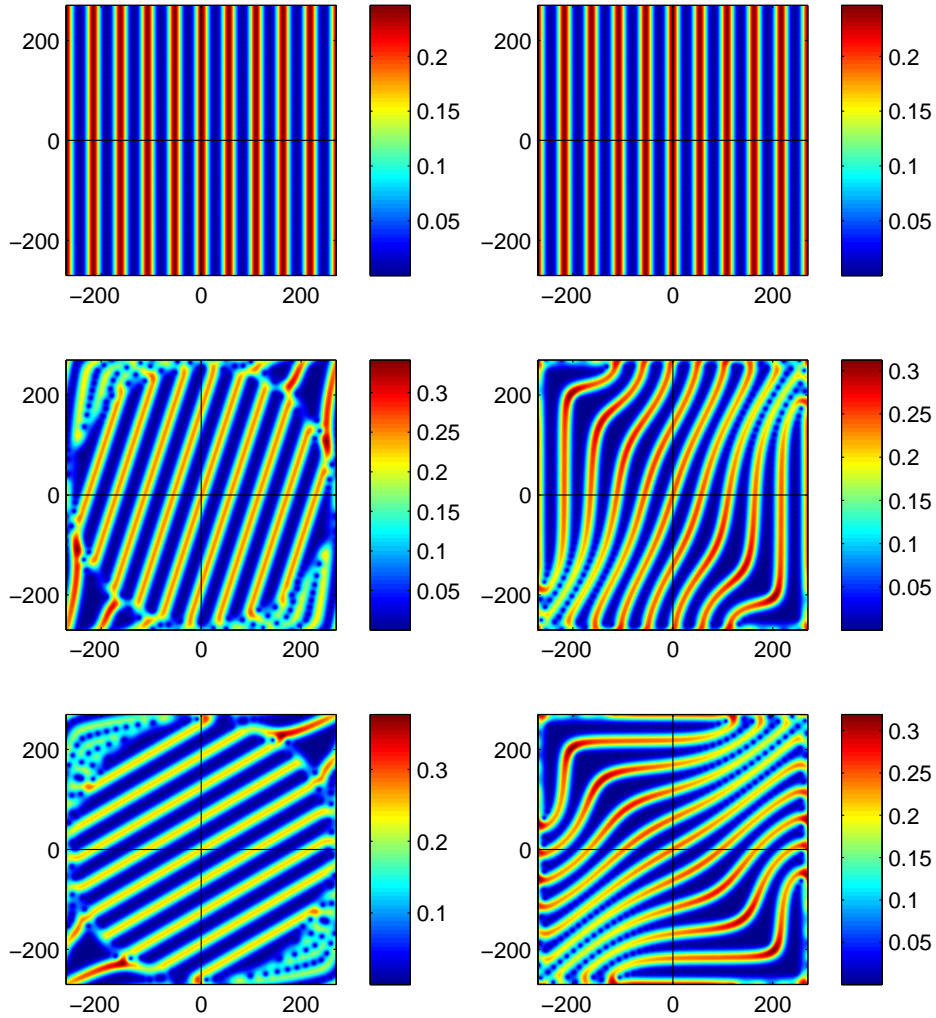


Figure 14: STFTs of a Dirac comb under the action of  $R_H^\alpha$  (left) and  $R_E^\alpha$  (right) for  $\alpha = 0$  (top),  $\alpha = \frac{\pi}{10}$  (middle) and  $\alpha = \frac{\pi}{3}$  (bottom).

us mainly functions of the form  $D_s\varphi$  will be of interest this poses no restriction, as long as  $s$  is not too big.

## 5 Experiments on Rotated Gabor-like Systems

Given  $a, b, s > 0$ ,  $(\alpha_{m,n}) \in \mathbb{R}^{\mathbb{Z} \times \mathbb{Z}}$  we now consider system of the form  $\{g_{m,n}\}_{m,n \in \mathbb{Z}}$  where

$$g_{m,n} := M_{nb} T_{ma} R^{\alpha_{m,n}} D_s \varphi. \quad (5.1)$$

So each function in the system  $\{g_{m,n}\}$  is a dilated Gaussian, which is first rotated in the TF-plane by an angle  $-\alpha_{m,n}$  and then TF-shifted to a point on the lattice  $a\mathbb{Z} \times b\mathbb{Z}$  (see Figure 4). We will refer to systems of this type as rotated Gabor-like systems.

We will look at different choices for the  $\alpha_{m,n}$  and the quality of the resulting systems. Afterwards we will compare these systems to get a feel of how the alignment of these rotated 'ellipses' in the TF-plane is reflected in the frame bounds. Our observations will mostly be based on numerical experiments for which we use finite-dimensional simulations of the  $g_{m,n}$ . In one case however we will compare them to values obtained in the continuous case. For the Matlab file which was used for creating the systems, please see the appendix.

### 5.1 The Gabor case

Given  $a, b$  we set  $\alpha_{m,n} = \alpha \forall m, n$  in (5.1), then the system  $\{g_{m,n}\}$  becomes a regular Gabor system with window  $R^\alpha D_s \varphi$  and lattice-parameters  $a, b$ . We want to investigate these systems, especially their quality as frames, for different values of  $\alpha$  and  $s$ . To make notation easier when comparing different systems we will sometimes write  $g_{m,n}^{\alpha,s}$  for  $g_{m,n}$ . We will denote the optimal frame bounds for the systems  $\{g_{m,n}^{\alpha,s}\}$  by  $A(\alpha, s)$  and  $B(\alpha, s)$ . Since

$$\widehat{g_{m,n}} = T_{nb} M_{-ma} R^\alpha D_{1/s} \varphi$$

the systems for  $s > 1$  and  $s < 1$  are related via an exchange of the lattice parameters and we need only consider  $s > 1$ .

In addition we have

$$\begin{aligned} M_\omega T_x R^{\pi-\alpha} D_s \varphi &= M_\omega T_x R^{-\alpha} D_s \varphi \\ &= \overline{M_{-\omega} T_x R^\alpha D_s \varphi} \end{aligned} \quad (5.2)$$

meaning that  $A(\pi - \alpha, s) = A(\alpha, s)$  and  $B(\pi - \alpha, s) = B(\alpha, s)$ . Since the bounds are obviously  $\pi$ -periodic in  $\alpha$  we will only consider  $\alpha \in [0, \frac{\pi}{2}]$ .

*Remark 5.1.* In the following we will sometimes speak of the time-frequency concentration of a subspace  $V$  of  $\mathbb{C}^n$ . We mean the sum over all spectrograms of some orthonormal basis for  $V$ . Since for any ONB  $(v_1, \dots, v_k)$  for  $V$  and  $x, \omega \in \mathbb{Z}$  we have

$$\sum_{i=1}^k |\langle v_i, M_\omega T_x \varphi \rangle|^2 = \|P_V M_\omega T_x \varphi\|_2^2$$

and the last term is independent of the chosen ONB the time-frequency concentration of  $V$  is well defined.

*Experiment 5.1.* We consider the case  $a = b$ , in which the frame bounds are periodic in  $\alpha$  with period  $\frac{\pi}{2}$ . This follows from

$$M_\omega T_x R^{\alpha+\pi/2} D_s \varphi = \mathcal{F} T_\omega M_{-x} R^\alpha D_s \varphi \quad (5.3)$$

implying that for  $a = b$  the systems  $\{g_{m,n}^{\alpha,s}\}$  for  $\alpha$  and  $\alpha + \frac{\pi}{2}$  are related via the Fourier transform and therefore satisfy the same frame bounds. Together with the observation in (5.2) we get  $A(\alpha, s) = A(\frac{\pi}{2} - \alpha, s)$  and the same for  $B$ .

For signal length 540 and  $a = b = 18$  Figure 15 shows the optimal lower and upper frame bounds for  $s = 3$  and  $\alpha \in [0, \frac{\pi}{2}]$ . We see that the frame bounds (especially the lower one) react very sensitive to changes of  $\alpha$ .  $A$  ranges from 0.0027 to 1.34 varying by a factor 500. Interestingly better lower and upper frame bounds go 'hand in hand' or, to be more precise: The experiment indicates  $\text{sgn}(\frac{d}{d\alpha} A(\alpha, s)) = -\text{sgn}(\frac{d}{d\alpha} B(\alpha, s))$ ,  $\forall \alpha, s$ . So from now on we use  $A(\alpha, s)$  to measure for the quality of the frame. We also see the symmetry over  $\alpha = \frac{\pi}{4}$  mentioned above (it will be missing in the case  $a \neq b$ ).

To understand the effect of  $\alpha$  and  $s$  on  $A$  we extend Figure 15 to an image: Again for signal length 540,  $a = b = 18$  Figure 16 contains the optimal lower frame bounds for  $\alpha$  ranging from 0 to  $\frac{\pi}{2}$  on the horizontal axis and  $s$  varying on a geometric scale from 1.05 to  $1.05^{32}$  on the vertical axis. The vertical black lines mark critical angles which result in low values of  $A$  for large enough  $s$  (see below).

The blue-colored areas correspond to small values of  $A$  indicating frames of poor quality. We'll look at those first and because of the above we can restrict our investigation to  $\alpha \leq \frac{\pi}{4}$ . The largest blue area is on the left border, where  $\alpha$  is close to 0. For  $\alpha = 0$  the functions  $g_{m,n}$  form parallel, horizontal 'lines' in the TF-plane. Along those lines there is high overlap of close-by atoms resulting in a high upper frame bound, whereas in between we have large 'gaps' with low concentration yielding a small lower bound. Increasing  $s$  will only make this worse



since more and more atoms will overlap and the 'gaps' will grow wider.

The second largest blue area is found where  $\alpha$  is close to  $\frac{\pi}{4}$ . Here we have a similar situation, but this time the lines formed by the atoms will be diagonal. Notice that for equally bad frames  $s$  has to be bigger, i.e. the atoms more 'stretched', than for  $\alpha = 0$ . This makes sense since along the diagonal lines the distance between lattice points is greater.

Once we have made these observations it is not difficult to understand the remaining blue areas. For a lattice point  $P$ , Figure 17 shows close-by lattice points. As indicated by the dashed line, we are only interested in those that lie at an angle between  $-\frac{\pi}{4}$  and 0, because for  $s > 1$ ,  $\alpha \in [0, \frac{\pi}{4}]$  these are the directions in which the atoms will be 'pointing' in the TF-plane. Closest to  $P$  is point number 1, which corresponds to  $\alpha = 0$  and we have already seen that this gives the worst frames, even for small  $s$ . If we increase  $s$  the second blue area we find is for  $\alpha = \frac{\pi}{4}$ , corresponding to point no. 2, the second closest to  $P$  among the numbered points. Point no. 3 we find at  $-\arctan(\frac{b}{2a}) = -\arctan(\frac{1}{2}) \approx -0.46$  and  $\alpha = \arctan(\frac{1}{2})$  is exactly where we find the third largest blue area. For  $\alpha = \arctan(\frac{1}{2})$  and  $s$  large enough the atom centered at  $P$  overlaps with the one centered at point no. 3, so in the global picture the atoms are once again 'lined up', resulting in a frame of poor quality. Analogously we find the next largest blue areas at  $\alpha = \arctan(\frac{1}{3})$  (corresponding to point no. 4) and  $\alpha = \arctan(\frac{2}{3})$  (point no. 5).

Interestingly the above reasoning already explains all the blue areas in Figure 16, including the ones we can already guess for larger  $s$ . To get frames of constant good quality, even for large  $s$ , we have to avoid values for  $\alpha$  which cause the rotated atoms to point towards a nearby lattice point (where the meaning of nearby depends on  $s$ ).

*Experiment 5.2.* Using the notation from Experiment 5.1 we want to make the statements from there about areas with high and low concentration more precise by looking at the corresponding frame operators  $S_{\alpha,s}$ . These operators are self-adjoint and positive-semidefinite and hence we can perform an eigenvalue-decomposition. We know from Theorem 2.3 that the optimal frame bounds  $A(\alpha, s)$ ,  $B(\alpha, s)$  are the smallest and largest eigenvalues of  $S_{\alpha,s}$ , so let's look at the corresponding eigenspaces. Again we take signal length 540,  $a = b = 18$ ,  $s = 3$ .

We set  $\alpha = \frac{\pi}{4}$  which, as we have seen in Experiment 5.1, results in a badly con-

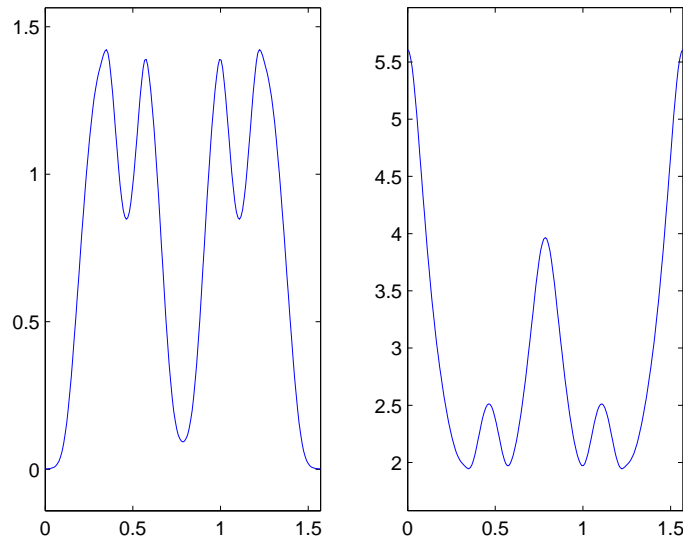


Figure 15: Optimal lower (left) and upper (right) frame bounds for Gabor systems with window  $R^\alpha D_3 \varphi$  for  $\alpha$  varying from 0 to  $\frac{\pi}{2}$

ditioned frame. Figure 18 shows the time-frequency concentration (see Remark 5.1 of the eigenspaces corresponding to  $A(\alpha, s) \approx 0.04$  and  $B(\alpha, s) \approx 3.5$ . The white stars indicate the lattice. The results confirm the heuristic explanations stated in Experiment 5.1: The eigenvectors responsible for the high upper frame bound are concentrated on diagonal lines along the lattice points. In between the vectors corresponding to A are located.

After considering a quadratic lattice in Experiment 5.1 we next look at the case  $a \neq b$ .

*Experiment 5.3.* As in Experiment 5.1 we again compute optimal frame bounds for  $\{g_{m,n}^{\alpha,s}\}$  with signal length 540 but this time for  $a = 27, b = 12$ , which gives the same redundancy as before. Figure 19 shows the results, which are very similar to the quadratic case: Again we find bad frames for angles  $\alpha = \arctan \frac{nb}{ma}$  for small values of  $m$  and  $n$ . They are indicated by the black lines and correspond to neighboring lattice points. Values for  $\alpha$  close to 0 give good frames if  $s$  is not too large since these systems are well fitted to the lattice. On the other hand  $\alpha$  close to  $\frac{\pi}{2}$  results in bad systems, even for small  $s$ , caused by the vertical 'gaps' in between the lattice points. Furthermore we see that good systems exist again for all the considered values of  $s$  and they are of the same quality as those in the quadratic case. And finally the observation from the quadratic case about the connection between upper and lower frame bound also carries over.

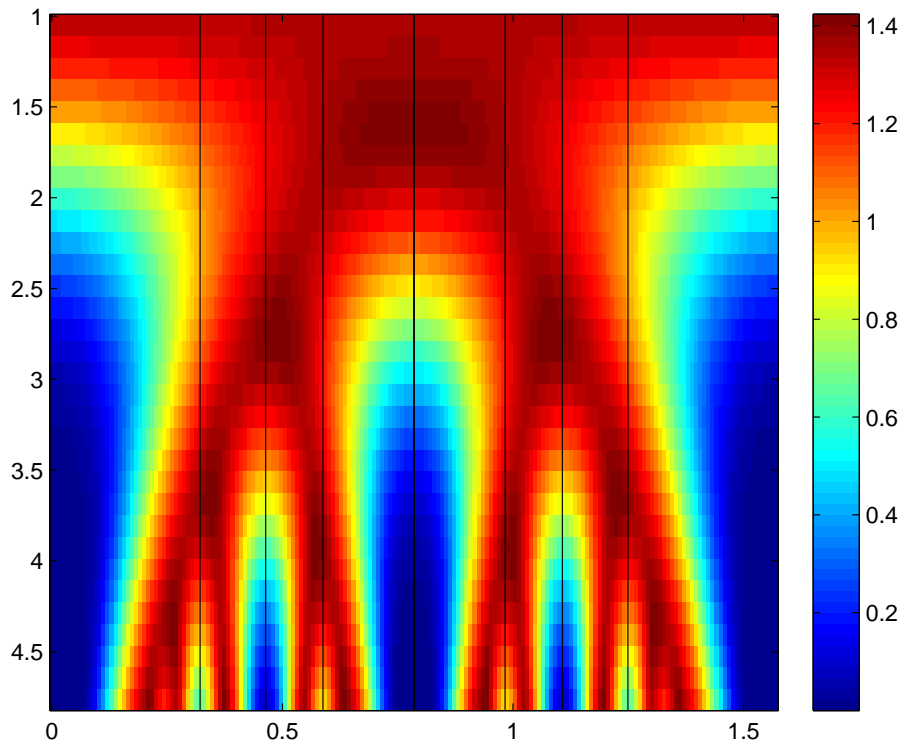


Figure 16: For  $a = b = 18$ : Optimal lower frame bounds for Gabor systems with window  $R^\alpha D_s \varphi$  for  $\alpha$  ranging from 0 to  $\frac{\pi}{2}$  on the horizontal axis and  $s$  varying geometrically from  $1.05^1$  to  $1.05^{32}$ . (See Figure 30 for black and white version)

The same experiment has also been conducted for non-separable lattices, with very similar results.

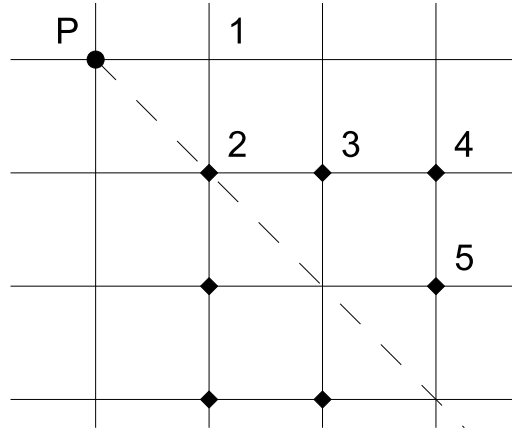


Figure 17: Illustration of the lattice points around a fixed point  $P$ . The diamond-marked points correspond to vertical black lines in figure 16.

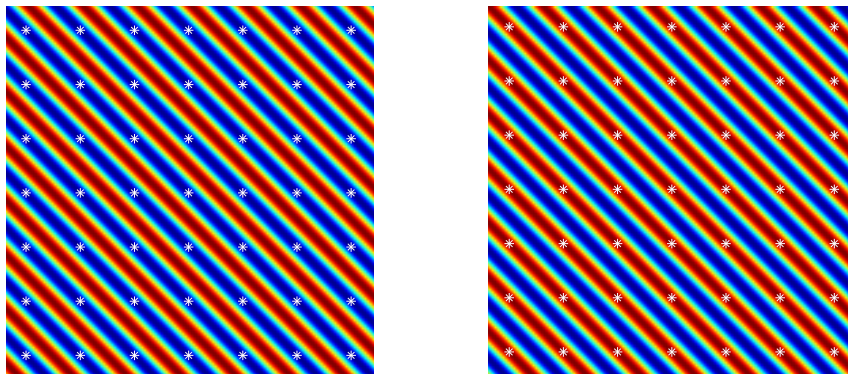


Figure 18: TF-concentration of eigenspaces corresponding to the smallest (left) and largest (right) eigenvalues of  $S_{\pi/4,3}$ .

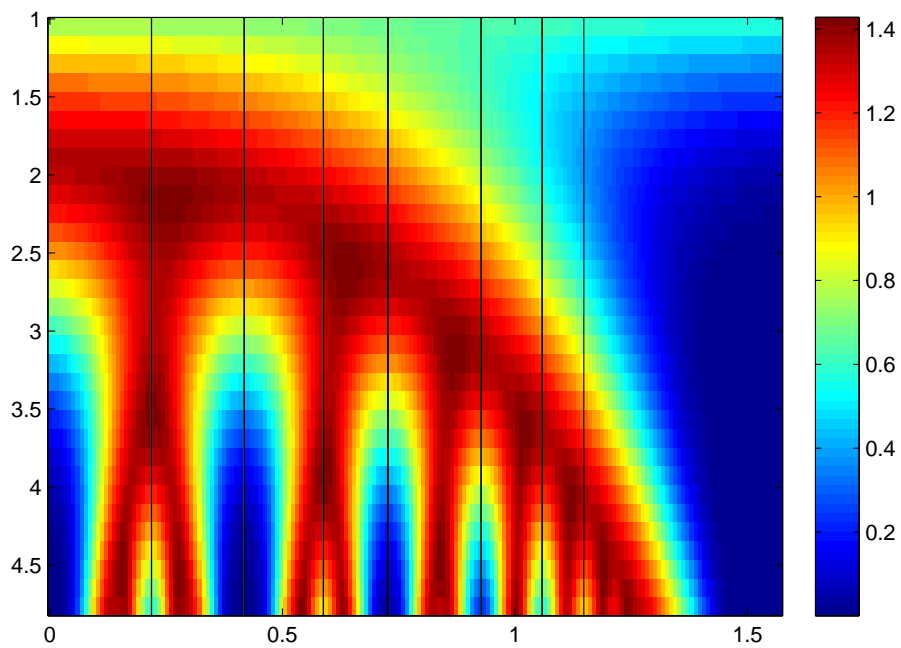


Figure 19: For  $a = 27, b = 12$ : Optimal lower frame bounds for Gabor systems with window  $R^\alpha D_s \varphi$  for  $\alpha$  ranging from 0 to  $\frac{\pi}{2}$  on the horizontal axis and  $s$  varying geometrically from  $1.05^1$  to  $1.05^{32}$  (See Figure 31 for black and white version).

## 5.2 Some special cases

### 5.2.1 Special case 1

After considering the case  $\alpha_{m,n} = \alpha, \forall m, n$  in the previous section and identifying the values for  $\alpha$  and  $s$  which result in bad systems we now want to compare them to a special case: Geometrically we want the atoms  $g_{m,n}$  to be rotated along concentric circles in the TF-plane leaving a 'hole' in the center, i.e. an area with low concentration. Intuitively this should yield a small lower frame bound.

First we make a slight change of notation and set (for  $a, b, s, \alpha_{m,n}$  yet to be defined)

$$\widetilde{g_{m,n}} := \pi((m + \frac{1}{2})a, (n + \frac{1}{2})b)F^{\alpha_{m,n}}D_s\varphi = \pi(\frac{a}{2}, \frac{b}{2})g_{m,n} \quad (5.4)$$

This change to the affine lattice  $a(\mathbb{Z} + \frac{1}{2}) \times b(\mathbb{Z} + \frac{1}{2})$  allows us to center the 'hole' mentioned above at the origin. Its not difficult to see that the choice

$$\alpha_{m,n} := \frac{\pi}{2} - \arctan \frac{(n + 1/2)b}{(m + 1/2)a}, m, n \in \mathbb{Z} \quad (5.5)$$

gives the desired alignment. We first simulate the resulting system numerically.

*Experiment 5.4.* We look at the finite dimensional case with signal length 540,  $a = b = 18$ . Figure 20 illustrates our system for  $s = 3$  and contains the relevant part of the STFT of the eigenvector corresponding to the smallest eigenvalue of the frame operator. It is clearly concentrated at the 'hole' left by the frame elements around the origin of the TF-plane. Thus we might hope to approximate the lower frame bound by looking at the frame coefficients of  $\varphi$ . The double-logarithmic plot in Figure 21 shows that this approximation is not too bad, at least for smaller values of  $s$ , which varies from 1 to 4.6 along the x-axis. The blue line marks the lower frame bounds  $A(s)$  and the green line marks evaluations of the finite-dimensional analog of

$$\sum_{m,n \in \mathbb{Z}} |\langle \varphi, \widetilde{g_{m,n}} \rangle|^2 \quad (5.6)$$

which is obviously an upper bound for  $A(s)$  since  $\|\varphi\|_2 = 1$ .

Now we turn to the continuous case: First observe that by Corollary 4.1 and

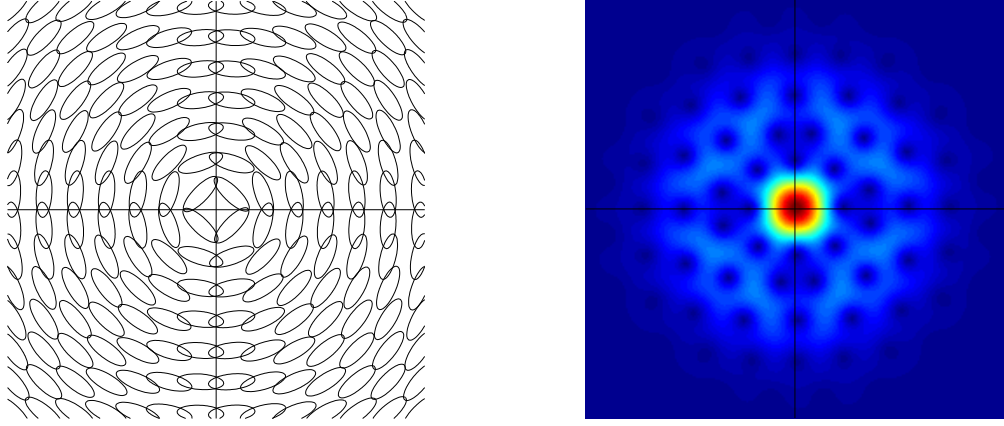


Figure 20: Left: contour plot of (a part of) the system  $\{\widetilde{g_{m,n}}\}$  in the TF-plane. The contour lines are drawn at 90% of the maximal absolute value. Right: STFT of the eigenvector for the smallest eigenvalue of the corresponding frame operator

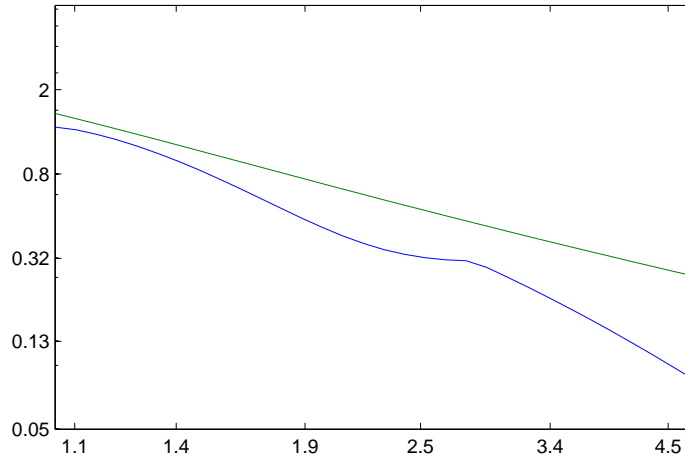


Figure 21: Double-logarithmic plot: Comparison of lower frame bound of  $\{\widetilde{g_{m,n}}\}$  (blue) and (5.6) (green) for varying  $s$ .

Lemmas 1.6 and 4.1 for  $m, n \in \mathbb{Z}$ :

$$\begin{aligned}
|\langle \varphi, \widetilde{g_{m,n}} \rangle|^2 &= |\langle \varphi, M_{(n+1/2)b} T_{(m+1/2)a} F^{\alpha_{m,n}} D_s \varphi \rangle|^2 \\
&= |\langle F^{\alpha_{m,n}} \varphi, F^{\alpha_{m,n}} M_\tau T_y D_s \varphi \rangle|^2 \\
&= |\langle \varphi, M_\tau T_y D_s \varphi \rangle|^2 \\
&= |(V_\varphi D_s \varphi)(-y, -\tau)|^2 \\
&= \varphi_{\frac{s^2+1}{2}}(y) \varphi_{\frac{s^2+1}{2s^2}}(\tau)
\end{aligned} \tag{5.7}$$

Where  $y$  and  $\tau$  are given by

$$\begin{pmatrix} y \\ \tau \end{pmatrix} := \begin{pmatrix} \cos \alpha_{m,n} & -\sin \alpha_{m,n} \\ \sin \alpha_{m,n} & \cos \alpha_{m,n} \end{pmatrix} \cdot \begin{pmatrix} (m + 1/2)a \\ (n + 1/2)b \end{pmatrix}. \quad (5.8)$$

Setting  $x := (m + \frac{1}{2})a$ ,  $\omega := (n + \frac{1}{2})b$  we get

$$\begin{aligned} y &= \cos\left(\frac{\pi}{2} - \arctan \frac{\omega}{x}\right)x - \sin\left(\frac{\pi}{2} - \arctan \frac{\omega}{x}\right)\omega \\ &= \sin\left(\arctan \frac{\omega}{x}\right)x - \cos\left(\arctan \frac{\omega}{x}\right)\omega \\ &= 0 \end{aligned}$$

since

$$\frac{\sin\left(\arctan \frac{\omega}{x}\right)}{\cos\left(\arctan \frac{\omega}{x}\right)} = \tan\left(\arctan \frac{\omega}{x}\right) = \frac{\omega}{x}.$$

And it follows that

$$|\tau| = \sqrt{x^2 + \omega^2}.$$

We now set  $a = b = \sqrt{\frac{3}{5}}$  and assume that  $\{\widetilde{g}_{m,n}\}_{m,n \in \mathbb{Z}}$  is a frame with bounds  $A, B$ . Note that the choice of  $a$  and  $b$  yields the same redundancy as in Experiment 5.4. In order to compare the continuous and finite-dimensional case we want to evaluate the estimate for  $A$  given in (5.6).

$$\begin{aligned} A &\leq \sum_{(m,n) \in \mathbb{Z}^2} |\langle \varphi, \widetilde{g}_{m,n} \rangle|^2 \\ &= \sum_{(m,n) \in \mathbb{Z}^2} \varphi_{\frac{s^2+1}{2s^2}} \left( a \sqrt{\left(m + \frac{1}{2}\right)^2 + \left(n + \frac{1}{2}\right)^2} \right) \end{aligned} \quad (5.9)$$

The points of the affine lattice  $(\mathbb{Z} + \frac{1}{2}) \times (\mathbb{Z} + \frac{1}{2})$  are grouped on squares of increasing size, all centered at the origin. The 4 points on the innermost square all have distance  $\frac{1}{\sqrt{2}}$  from the origin. On the second innermost square we find 4 points with distance  $\sqrt{\frac{9}{2}}$  and 8 points at distance  $\sqrt{\frac{5}{2}}$ . It's easy to see that the  $k$ -th innermost square contains  $4(2k - 1)$  points of the affine lattice, all of which have a distance of more than  $(k - \frac{1}{2})$  from the origin. Using this we can estimate (5.9) by

$$4 \varphi_{\frac{s^2+1}{2s^2}} \left( \sqrt{\frac{1}{2}}a \right) + 8 \varphi_{\frac{s^2+1}{2s^2}} \left( \sqrt{\frac{5}{2}}a \right) + 4 \varphi_{\frac{s^2+1}{2s^2}} \left( \sqrt{\frac{9}{2}}a \right) + \sum_{k \geq 3} 4(2k - 1) \varphi_{\frac{s^2+1}{2s^2}} \left( (k - \frac{1}{2})a \right)$$



And so for  $\lambda := e^{-\pi \frac{2s^2}{s^2+1} a^2}$  we get

$$A \leq 4 \left( \frac{4s^2}{s^2+1} \right)^{1/4} \left( \lambda^{1/2} + 2\lambda^{5/2} + \lambda^{9/2} + \sum_{k=3}^{\infty} (2k-1) \lambda^{(k-1/2)^2} \right). \quad (5.10)$$

Since  $\lambda < 1$  the series in (5.10) converges (very fast) and numerical evaluations suggest that it is sufficiently close to 0 to use (5.10) as an approximation for (5.9). Figure 22 compares evaluations of (5.6) for the finite-dimensional and continuous case. The results are surprising: The value for the continuous case is significantly higher (up to a factor 3.5) and decreases at lower and non-constant rate. In light of this we have to be careful when we draw conclusions about the behavior of frame bounds from numerical simulations.

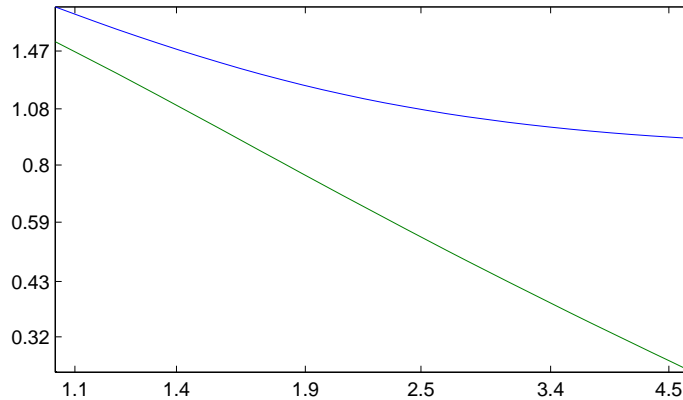


Figure 22: Double logarithmic plotting of the evaluations of (5.6) in the continuous case (blue) and finite-dimensional case (green) for different  $s$ .

*Remark 5.2.* From (5.7) it's not difficult to see that the choice of the  $\alpha_{m,n}$  which we have considered here is the one which minimizes the coefficients of  $\varphi$ , i.e. the expression (5.6).

### 5.2.2 Special case 2

We look at another choice of the  $\alpha_{m,n}$  for which we expect to get bad systems:

$$\alpha_{m,n} = \begin{cases} -\frac{\pi}{4}, & \text{if } m+n \text{ is even} \\ \frac{\pi}{4}, & \text{otherwise.} \end{cases} \quad (5.11)$$

For signal length 540,  $a = b = 18$ ,  $s = 3$  the resulting system is shown in Figure 23, along with the TF-concentration of the eigenspace corresponding to the smallest eigenvalue  $A = 0.0125$  of the frame operator. Clearly there are areas of high concentration where the atoms meet and areas of low concentration in between. We will later see that for growing  $s$  the lower frame bound for this system decreases very fast.

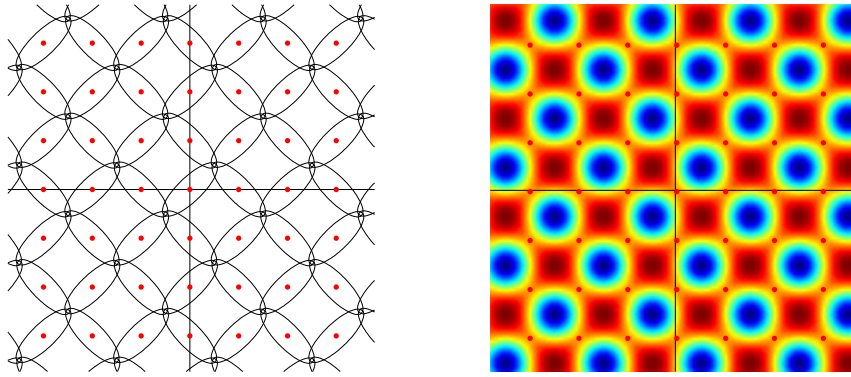


Figure 23: Left: Illustration of the system defined via (5.11), the contour lines are drawn at 90% of the maximal absolute value. Right: TF-concentration of the eigenspace for the smallest eigenvector of the frame operator.

### 5.3 The random case

*Experiment 5.5.* For this experiment we choose the  $\alpha_{m,n}$  in (5.1) randomly (uniformly distributed) between 0 and  $2\pi$ . The histograms in Figure 24 contain the optimal upper and lower frame bounds for 100 rotated Gabor-type systems for signal length 540,  $a = b = 18$  and  $s = 3$ . Both data sets pass a Kolmogorov-Smirnov test for normal distribution at significance level 0.05.

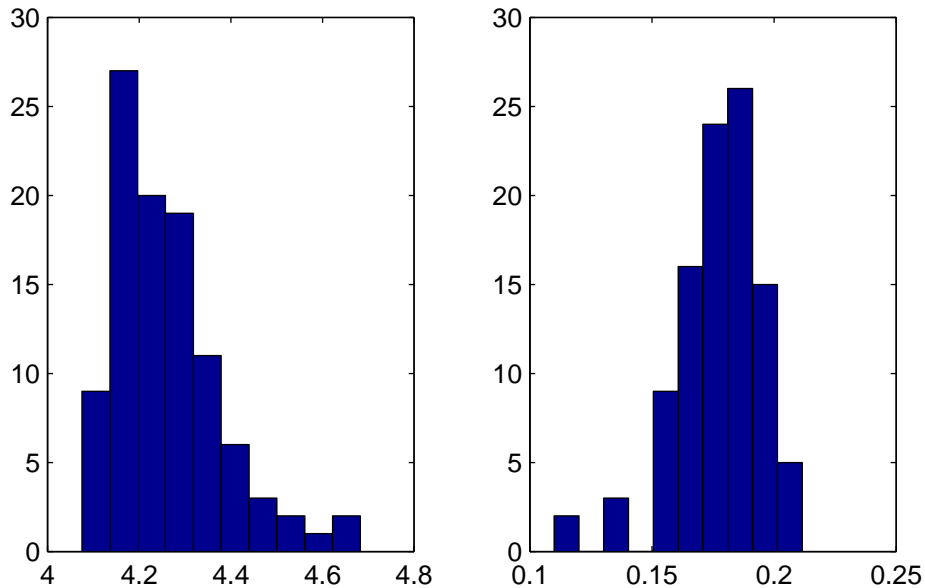


Figure 24: Distribution of the optimal lower (left) and upper (right) frame bounds of 100 random rotated Gabor-type systems

We put  $s$  on a geometric scale ranging, as before, from  $1.05$  to  $1.05^{32}$  and construct for each value 10 random systems. Figure 25 shows the development of the mean of the corresponding optimal bounds, which we will refer to as  $\bar{A}(s)$  and  $\bar{B}(s)$ . Since  $s$  as well as the frame bounds lie naturally on a geometric scale the plots are double-logarithmic. The red lines are the best linear fits for the plots and we see that  $\bar{A}$  is very well approximated, especially for smaller  $s$ , indicating that  $\bar{A}(s) \approx s^k \cdot d$ , for  $k = -1.86$ ,  $d = 1.55$ . We also note that  $\bar{B}$  is best approximated by  $k = 0.52$ ,  $d = 2.34$ .

Finally, for the above range of  $s$  Figure 26 contains the coefficients of variation for the frame bounds (i.e. the standard deviation divided by the mean). For both, upper and lower bounds, the coefficients tend to increase with  $s$ , but there is some oscillation, which might be caused by the rather small sample size (10 for each value of  $s$ ), which is due to high computational effort. The coefficients for the upper bound are remarkably small with a maximum of 0.035.

*Experiment 5.6.* Our goal now is of course to better understand which choices of the  $\alpha_{m,n}$  yield bad systems. Therefore we look at a particular randomly generated system from the previous experiment with lower frame bound  $A = 0.13$ , which is well below average (see Figure 24). Figure 27 contains the relevant part of the

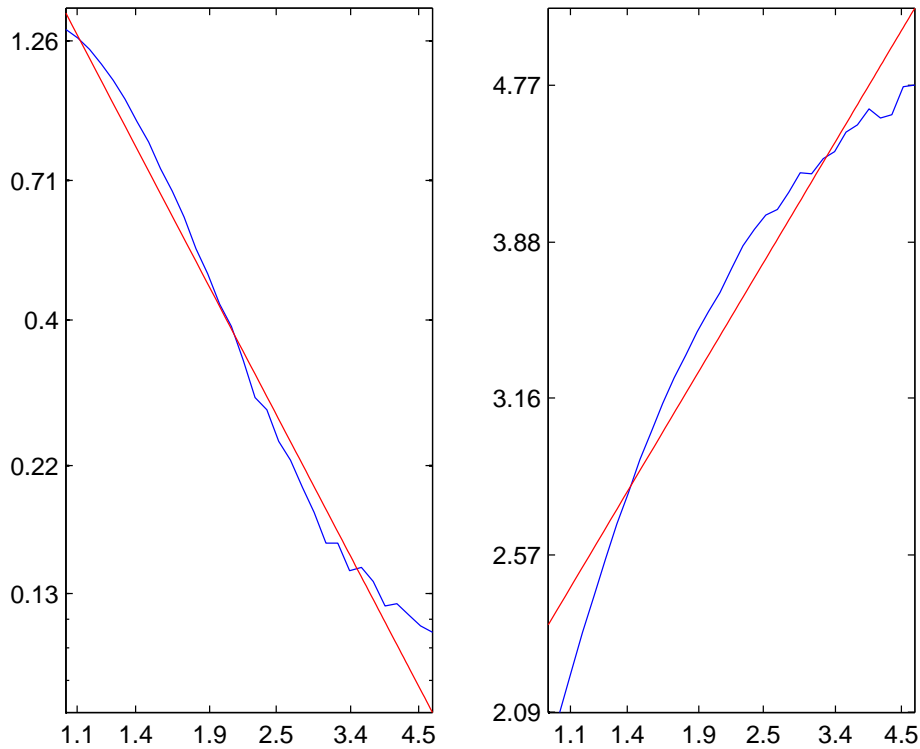


Figure 25: Double-logarithmic plots of the mean of the frame bounds for randomly rotated systems for varying  $s$  (left: lower bound, right: upper bound), together with linear fits (red).

STFT of the eigenvector corresponding to the smallest eigenvalue  $A$  of the frame operator along with an illustration of how the atoms  $g_{m,n}$  are arranged in this part of the TF-plane.

We see four atoms forming an 'x' and thus creating a point of very high concentration between themselves. Furthermore the neighboring atoms, especially those at the left, right and at the top, are aligned in such a way that they do not point towards the 'x'. Apparently the eigenvector responsible for the bad quality of the frame is concentrated around the center of the 'x' except the area on the lower right where some atoms point towards the 'x'. So the arrangement of the atoms in this area is somewhat similar to the above mentioned 'Special Case 2', however not as extreme.

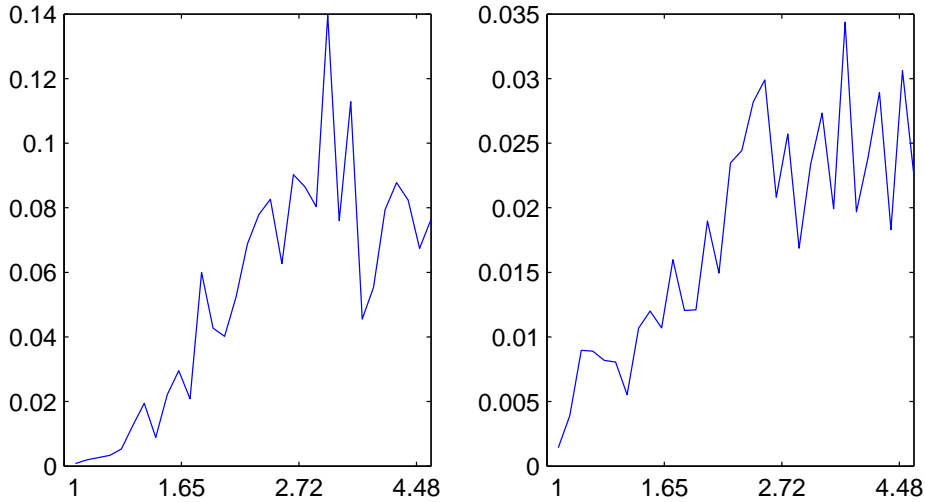


Figure 26: Coefficients of variation for the frame bounds of randomly rotated systems for different  $s$ . (left: lower bound, right: upper bound)

## 5.4 Conclusion

To conclude this section we compare the development of the lower frame bounds of the discussed systems as the dilation parameter  $s$  increases. The experiments have shown that the lower bound is usually the critical one. Compared to it the upper bound does not vary too much.

Figure 28 shows the lower frame bound for the different systems with  $s$  ranging on a geometric scale from 1.05 to  $1.05^{32} = 4.76$ . For large  $s$  by far the worst systems are the Gabor systems obtained with  $\alpha_{m,n} = 0 \forall m, n$  for which  $A(s)$  decreases superexponentially. As we have already mentioned above for the Gabor case there are systems of equally good quality for all of the considered values of  $s$ .

One might expect the special cases 1 and 2 to behave similarly, since the lower frame bound measures the 'worst case' and thus it makes no difference if there are many 'holes' (as in case 2) or just one. This however proves to be absolutely wrong for larger values of  $s$ , for which the bound for case 2 decreases much faster.

The behavior in the random case is well approximated by our special case 1. Concerning the quality of specific random systems some insight could be gained in the above experiments, but in many cases the behavior wasn't clear just from looking at the alignment of the atoms.

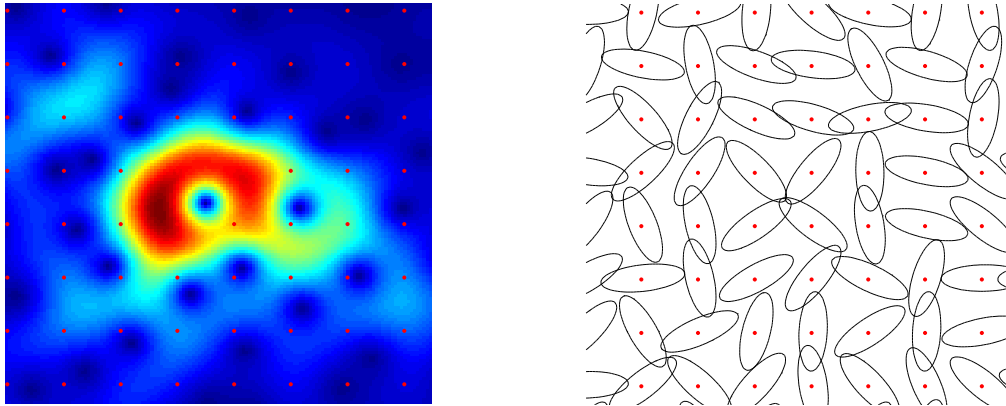


Figure 27: Left: Detail of the STFT of the eigenvector corresponding to the lowest eigenvalue of the frame operator of a badly behaved system. Right: Illustration of the alignment of the frame elements in the corresponding area of the TF-plane. The contour lines are drawn at 90% of the maximal absolute value.

We have also seen that the continuous case can behave very different from our finite-dimensional model raising of course the question how far we can draw conclusions from the performed experiments.

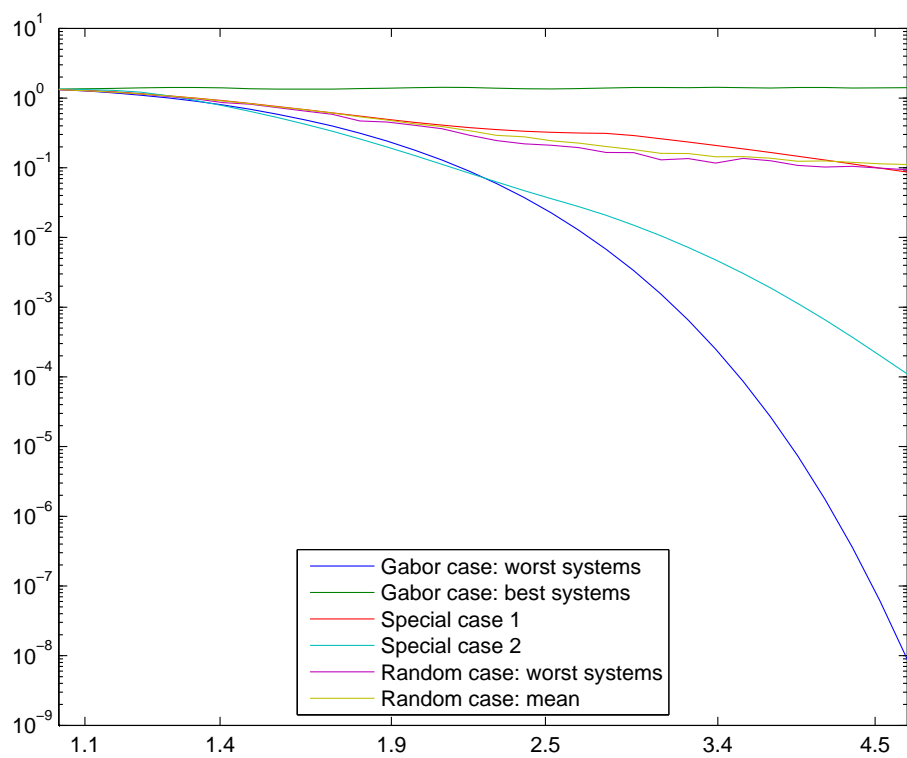


Figure 28: Double-logarithmic plot of the lower frame bounds of different systems for varying  $s$ .

## 6 Stability Results for Rotated Gabor-like Systems

### 6.1 Wiener amalgam spaces

The Wiener amalgam spaces (or Wiener type spaces) were introduced in [7] but we will not define them in the generality found there. The idea is to measure the local and global behavior of function with different norms. In order to separate local and global aspects we first define a special class of partitions of unity.

**Definition 6.1.** (*BUPU*)

Let  $A$  be a Banach space of functions on  $\mathbb{R}^d$ . A family  $\Psi = (\psi_i)_{i \in I}$  of functions in  $A$  is called a bounded uniform partition of unity in  $A$  (or BUPU) if there exists a constant  $M$  and a discrete set of points  $\{y_i\}_{i \in I}$  as well as a neighborhood  $U$  of  $0$  s.t.

- (i)  $\sum_{i \in I} \psi_i(x) = 1, \forall x \in \mathbb{R}^d$
- (ii)  $\sup_{i \in I} \|\psi_i\|_A \leq M$
- (iii)  $\text{supp } \psi_i \subseteq y_i + U, \forall i \in I$
- (iv)  $\sup_{x \in \mathbb{R}^d} |\{i \mid x \in y_i + K\}| \leq C_K < \infty$  for any compact set  $K \subseteq \mathbb{R}^d$ .

**Definition 6.2.** (*Wiener amalgam spaces*)

Given two 'suitable' Banach space  $A$  and  $B$  and  $p \in [1, \infty]$  together with a BUPU  $(\psi_i)_{i \in I}$  for  $A$  we define the space

$$W(B, L^p) := \{f \in B_{loc} : \left( \sum_{i \in I} \|\psi_i f\|_B^p \right)^{1/p} < \infty\}$$

For the explanation of 'suitable' in the above definition and the connection of  $A$  and  $B$  we refer to [7], p.3. We only mention that for  $B = L^q(\mathbb{R}^d)$ ,  $1 \leq q \leq \infty$  or  $B = M(\mathbb{R}^d)$  we can choose  $A = C^0(\mathbb{R}^d)$ . We state some basic facts from [7].

**Theorem 6.1.** (i)  $W(B, L^p)$  is a well-defined Banach space.

- (ii)  $W(L^p, L^p) = L^p$
- (iii) If  $B_1 \subseteq B_2$  and  $p \leq q$  then  $W(B_1, L^p) \subseteq W(B_2, L^q)$ .
- (iv) If  $B_1 * B_2 \subseteq B_3$  and  $L^p * L^q \subseteq L^r$  then  $W(B_1, L^p) * W(B_2, L^q) \subseteq W(B_3, L^r)$ .



## 6.2 Stability results

We now want to show that a system of the form  $\{M_{nb}T_{ma}F^{\alpha_{m,n}}D_s\varphi\}_{m,n\in\mathbb{Z}}$  is a frame, if the lattice allows it and  $s$  is sufficiently close to 1. Our argument will be based on Theorem 2.5. An important part of the strategy for the proof was suggested by H. G. Feichtinger.

**Lemma 6.1.** *Define the weight  $W(x, \omega) := (1 + x^2 + \omega^2)^2$ . Then for  $s \searrow 1$*

$$\|V_\varphi(F^\alpha D_s \varphi - \varphi)\|_{L^\infty_W(\mathbb{R}^2)} \rightarrow 0 \text{ uniformly for } \alpha \in \mathbb{R}$$

*Proof.* First observe that by Lemma 4.2

$$\begin{aligned} |V_\varphi(F^\alpha D_s \varphi - \varphi)(x, \omega)| W(x, \omega) &= |V_\varphi(F^\alpha(D_s \varphi - \varphi))(x, \omega)| W(x, \omega) \\ &= |V_\varphi(D_s \varphi - \varphi)(y, \tau)| W(y, \tau) \end{aligned}$$

where  $y, \tau$  are defined as in 4.8. So w.l.o.g. we set  $\alpha = 0$ . By Lemma 1.6

$$\begin{aligned} \left| V_\varphi(D_s \varphi - \varphi)(x, \omega) \right| &= \left| \varphi_{s^2+1}(x) \varphi_{\frac{s^2+1}{s^2}}(\omega) e^{-2\pi i \frac{s^2}{s^2+1} x \omega} - \varphi_2(x) \varphi_2(\omega) e^{-\pi i x \omega} \right| \\ &= \left| \sqrt{\frac{2s}{s^2+1}} e^{\pi \frac{1}{s^2+1}(x^2+s^2\omega^2)} e^{-\pi i \frac{1-s^2}{1+s^2} x \omega} - e^{-\pi \frac{1}{2}(x^2+\omega^2)} \right| \end{aligned}$$

We first look at the real part:

$$\begin{aligned} |\operatorname{Re}(V_\varphi(\varphi - D_s \varphi)(x, \omega))| &= \left| e^{-\pi \frac{x^2+\omega^2}{2}} - \sqrt{\frac{2s}{s^2+1}} e^{-\pi \frac{1}{s^2+1}(x^2+s^2\omega^2)} \right. \\ &\quad \left. \times \cos\left(\pi \frac{1-s^2}{1+s^2} x \omega\right) \right| \end{aligned}$$

Set

$$\begin{aligned} y_1 &= y_1(x, \omega) := \pi \frac{x^2 + \omega^2}{2}, \\ y_2 &= y_2(x, \omega, s) := \pi \frac{1}{s^2+1}(x^2 + s^2\omega^2) - \frac{1}{2} \log\left(\frac{2s}{s^2+1}\right) \\ z &= z(x, \omega, s) := \pi \frac{1-s^2}{1+s^2} x \omega \end{aligned}$$

$$I_1 := [\min(y_1, y_2), \max(y_1, y_2)], \quad I_2 := [\min(0, z), \max(0, z)]$$

We rewrite the above and use the mean-value Theorem:

$$\begin{aligned}
|Re(V_\varphi(\varphi - D_s\varphi)(x, \omega))| &= |e^{-y_1} - e^{-y_2} \cos(z)| \\
&\leq |e^{-y_1} - e^{-y_2}| + |e^{-y_2} \cos(0) - e^{-y_2} \cos(z)| \\
&\leq \sup_{\xi \in I_1} e^{-\xi} |y_2 - y_1| + e^{-y_2} \sup_{\eta \in I_2} |\sin(\eta)| |z| \\
&\leq e^{-\min(y_1, y_2)} |y_2 - y_1| + e^{-y_2} |z| \\
&=: A(x, \omega, s) + B(x, \omega, s)
\end{aligned}$$

Take  $\epsilon > 0$ . First we look at A: Fix any  $S > 1$ , then  $\forall s \in [1, S]$

$$y_2(x, \omega, s) \geq \pi \frac{1}{S^2 + 1} (x^2 + \omega^2) - \frac{1}{2} \log(S) \leq y_1(x, \omega, s)$$

and also

$$\begin{aligned}
|y_2 - y_1| &\leq \pi \frac{s^2 - 1}{2(s^2 + 1)} (x^2 + \omega^2) + \left| \frac{1}{2} \log\left(\frac{2s}{s^2 + 1}\right) \right| \\
&\leq \pi \frac{S^2 - 1}{2(S^2 + 1)} (x^2 + \omega^2) + \frac{1}{2} \log(S)
\end{aligned}$$

This gives  $\forall s \in [1, S]$

$$\begin{aligned}
A(x, \omega, s)W(x, \omega) &\leq e^{-\pi \frac{1}{S^2 + 1} (x^2 + \omega^2) - \frac{1}{2} \log S} \\
&\times \left( \pi \frac{S^2 - 1}{2(S^2 + 1)} (x^2 + \omega^2) + \frac{1}{2} \log S \right) (1 + |x|^2 + |\omega|^2)^2
\end{aligned}$$

From this we see that  $A(x, \omega, s)W(x, \omega) \rightarrow 0$  for  $x^2 + \omega^2 \rightarrow \infty$  uniformly for  $s \in [1, S]$ . So we can choose  $M_1$  s.t.  $A(x, \omega, s)W(x, \omega) < \epsilon$  for  $x^2 + \omega^2 \geq M_1$ ,  $s \in [1, S]$ .

From the above estimate for  $|y_2 - y_1|$  it's clear that  $|y_2 - y_1| \rightarrow 0$  for  $s \searrow 1$  uniformly on  $\{(x, \omega) : x^2 + \omega^2 \leq M_1\}$ . We can therefore choose  $S_1 \leq S$  such that  $A(x, \omega, s) \leq \epsilon$ ,  $\forall (x, \omega)$ ,  $s \in [1, S_1]$ .

Next we look at  $B(x, \omega, s)$ . For  $s \in [1, S]$

$$B(x, \omega, s)W(x, \omega) \leq \sqrt{S} e^{-\pi \frac{1}{S^2 + 1} (x^2 + \omega^2)} \pi \frac{S^2 - 1}{2} |x\omega| (1 + x^2 + \omega^2)^2$$

So  $B(x, \omega, s) \rightarrow 0$  for  $x^2 + \omega^2 \rightarrow \infty$  uniformly for  $s \in [1, S]$ . So we can choose  $M_2$  s.t.  $B(x, \omega, s)W(x, \omega) < \epsilon$  for  $x^2 + \omega^2 \geq M_2$ ,  $s \in [1, S]$ . And again, since by the above estimate  $B(x, \omega, s)W(x, \omega) \rightarrow 0$  for  $s \searrow 1$  uniformly on  $\{(x, \omega) : x^2 + \omega^2 \leq M_2\}$ , we can choose  $S_2 \leq S$  st.  $B(x, \omega, s) \leq \epsilon$ ,  $\forall (x, \omega)$ ,  $s \in [1, S_2]$ .

We still need to look at the imaginary part:

$$|Im(V_\varphi(\varphi - D_s\varphi)(x, \omega))| = |0 - e^{-y^2} \sin(z)|$$

An argument analogous to that we used for B shows that we can choose  $S_3$  s.t.  $\|Im(V_\varphi(\varphi - D_s\varphi))\|_{L^\infty(\mathbb{R}^2)} < \epsilon$  for  $s \leq S_3$ .

Then for  $1 \leq s \leq \min(S_1, S_2, S_3)$  we have

$$\|V_\varphi(\varphi - D_s\varphi)\|_{L^\infty(\mathbb{R}^2)} < 3\epsilon.$$

□

In [7] was shown that for two 'suitable' Banach-Convolution-Triples  $(B_1, B_2, B_3)$  and  $(C_1, C_2, C_3)$  there is  $C > 0$ , s.t. for  $f_1 \in W(B_1, C_1)$ ,  $f_2 \in W(B_2, C_2)$  we have  $\|f * g\|_{W(B_3, C_3)} \leq C \|f\|_{W(B_1, C_1)} \|f_2\|_{W(B_2, C_2)}$ . In following Lemma we mimic the argument from there to get a concrete value of  $C$  for the BCTs  $(M, C_0, C_0)$  and  $(L^2, L^1, L^2)$ .

**Lemma 6.2.** *Given  $a, b > 0$  define  $\psi := \chi_{[-a/2, a/2] \times [-b/2, b/2]}$  and for  $i = (i_1, i_2) \in \mathbb{R}^2$  set  $\psi_i := T_{(i_1 a, i_2 b)} \psi$ . Denote by  $\|\cdot\|_{W(\cdot, \cdot)}$  the Wiener-Amalgam norms associated with the BUPU  $\Phi := \{\psi_i : i \in \mathbb{Z}^2\}$ .*

Then for  $g \in W(C_0(\mathbb{R}^2), L^1)$ ,  $\mu \in W(M(\mathbb{R}^2), L^2)$ :

$$\|\mu * g\|_{L^2(\mathbb{R}^2)} \leq \sqrt{(3a+1)(3b+1)} \|\mu\|_{W(M, L^2)} \|g\|_{W(C_0, L^1)} < \infty$$

*Proof.* Clearly

$$\|\mu * g\|_2 \leq \left( \int_{\mathbb{R}^2} \|T_z \psi(\mu * g)\|_\infty^2 dz \right)^{1/2}$$

We look at the integrand: for  $z \in \mathbb{R}^2$

$$\|T_z \psi(\mu * g)\|_\infty = \left\| \sum_{(i,j) \in (\mathbb{Z}^2)^2} T_z \psi(\psi_i \mu * \psi_j g) \right\|_\infty$$

In the following denote intervals of the form  $[c-r, c+r]$  by  $[c \pm r]$ . We have for  $x = (x_1, x_2) \in \mathbb{R}^2$

$$\begin{aligned} x \in \text{supp}(\psi_i \mu * \psi_j g) &\Rightarrow \mu(\psi_i T_x((\psi_j g)^\sim)) \neq 0 \\ &\Rightarrow \psi_i T_x((\psi_j g)^\sim) \neq 0 \\ &\Rightarrow ([i_1 a \pm \frac{a}{2}] \times [i_2 b \pm \frac{b}{2}]) \cap \\ &\quad ([-j_1 a + x_1 \pm \frac{a}{2}] \times [-j_2 b + x_2 \pm \frac{b}{2}]) \neq \emptyset \\ &\Rightarrow |(i_1 + j_1)a - x_1| \leq a \wedge |(i_2 + j_2)b - x_2| \leq b \end{aligned}$$

Now for  $z \in \mathbb{R}^2$  define

$$\begin{aligned} I_z &:= \{(i, j) \in (\mathbb{Z}^2)^2 : ([z_1 \pm \frac{a}{2}] \cap [(i_1 + j_1)a \pm a]) \times \\ &\quad ([z_2 \pm \frac{b}{2}] \cap [(i_2 + j_2)b \pm b]) \neq \emptyset\} \\ &= \{(i, j) \in (\mathbb{Z}^2)^2 : |z_1 - a(i_1 + j_1)| < \frac{3}{2}a \wedge |z_2 - b(i_2 + j_2)| < \frac{3}{2}b\} \end{aligned}$$

It's easy to see that

$$\text{supp}(T_z \psi) \cap \text{supp}(\psi_i \mu * \psi_j g) \neq \emptyset \Rightarrow (i, j) \in I_z$$

and that for  $(i, j) \in I_z$  it follows that

$$\begin{aligned} z &\in [a(i_1 + j_1) \pm \frac{3}{2}a] \times [b(i_2 + j_2) \pm \frac{3}{2}b] \\ &\Rightarrow [-j_1 a + z_1 \pm \frac{1}{2}] \times [-j_2 b + z_2 \pm \frac{1}{2}] \subseteq [i_1 a \pm (\frac{3}{2}a + \frac{1}{2})] \times [i_2 b \pm (\frac{3}{2}b + \frac{1}{2})] \end{aligned}$$

and thus, for  $d_1 := \frac{3}{2}a + \frac{1}{2}$ ,  $d_2 := \frac{3}{2}b + \frac{1}{2}$ , we have

$$\chi_{[i_1 a \pm d_1] \times [i_2 a \pm d_2]} * \chi_{[j_1 \pm \frac{1}{2}] \times [j_2 \pm \frac{1}{2}]}(z) = 1, \forall (i, j) \in I_z$$

Using this we obtain

$$\begin{aligned} \|\mu * g\|_2^2 &\leq \int_{\mathbb{R}^2} \sum_{(i, j) \in (\mathbb{Z}^2)^2} \|T_z \psi(\psi_i \mu * \psi_j g)\|_\infty^2 dz \\ &= \int_{\mathbb{R}^2} \sum_{(i, j) \in I_z} \|T_z \psi(\psi_i \mu * \psi_j g)\|_\infty^2 dz \\ &\leq \int_{\mathbb{R}^2} \sum_{(i, j) \in I_z} \|\psi_i \mu\|_M^2 \|\psi_j g\|_\infty^2 (\chi_{[i_1 a \pm d_1] \times [i_2 a \pm d_2]} * \chi_{[j_1 \pm \frac{1}{2}] \times [j_2 \pm \frac{1}{2}]})^2(z) dz \\ &\leq \int_{\mathbb{R}^2} \left( \left( \sum_{i \in \mathbb{Z}^2} \|\psi_i \mu\|_M \chi_{[i_1 a \pm d_1] \times [i_2 a \pm d_2]} \right) * \right. \\ &\quad \left. \left( \sum_{j \in \mathbb{Z}^2} \|\psi_j g\|_\infty \chi_{[j_1 \pm \frac{1}{2}] \times [j_2 \pm \frac{1}{2}]} \right) \right)^2(z) dz \\ &\leq 4d_1 d_2 \|\mu\|_{W(M, L^2)}^2 \|g\|_{W(C_0, L^1)}^2 \end{aligned}$$

And the result follows. In the last step we have used Young's inequality.  $\square$

**Theorem 6.2.** *Take  $a, b \in \mathbb{R}$  and set  $\varphi_{m,n} := M_{nb} T_{ma} \varphi$ . If  $\{\varphi_{m,n}\}_{m,n \in \mathbb{Z}}$  is a frame (this is equivalent to  $ab < 1$ ) then there exists  $S > 1$  and positive numbers  $\tilde{A}, \tilde{B}$  such that for  $s \in [1, S]$  and any sequence  $(\alpha_{m,n})$  the system  $\{\widetilde{\varphi}_{m,n}\}_{m,n \in \mathbb{Z}}$ , where  $\widetilde{\varphi}_{m,n} := M_{nb} T_{ma} F^{\alpha_{m,n}} D_s \varphi$ , is a frame with bounds  $\tilde{A}$  and  $\tilde{B}$ .*

*Proof.* We look at the perturbation operator

$$P : l^2(\mathbb{Z}^2) \rightarrow L^2(\mathbb{R}), \quad (c_{m,n}) \mapsto \sum_{m,n} c_{m,n} (\widetilde{\varphi_{m,n}} - \varphi_{m,n})$$

and show that for  $s \searrow 1$   $\|P\| \rightarrow 0$  independently of the  $\alpha_{m,n}$ . Then the result follows from Corollary 2.1.

Let  $\epsilon > 0$ . By Lemma 6.1  $\exists S > 1$  s.t. for  $W(x, \omega) := (1 + x^2 + \omega^2)^2$  and  $s \in [1, S]$

$$\|V_\varphi(F^a D_s \varphi - \varphi)\|_{L^\infty_W} < \epsilon, \quad \forall a \in \mathbb{R}$$

Then it's easy to see that for any  $m, n \in \mathbb{Z}$  and  $x, \omega \in \mathbb{R}$ ,  $s \in [1, S]$

$$\begin{aligned} |T_{(-ma, -nb)}(V_\varphi(\widetilde{\varphi_{m,n}} - \varphi_{m,n}))(x, \omega)| &= |V_\varphi(F^{\alpha_{m,n}} D_s \varphi - \varphi)(x, \omega)| \\ &\leq \frac{\epsilon}{W(x, \omega)} \end{aligned}$$

Take  $c = (c_{m,n}) \in l^2(\mathbb{Z}^2)$ ,  $s \in [1, S]$ . Using the Wiener-amalgam norms from Lemma 6.2

$$\begin{aligned} \|Pc\|_{L^2(\mathbb{R})} &= \left\| \sum_{m,n} c_{m,n} V_\varphi(\widetilde{\varphi_{m,n}} - \varphi_{m,n}) \right\|_{L^2(\mathbb{R}^2)} \\ &= \left\| \sum_{m,n} c_{m,n} (\delta_{(ma, nb)} * (T_{(-ma, -nb)} V_\varphi(\widetilde{\varphi_{m,n}} - \varphi_{m,n}))) \right\|_{L^2(\mathbb{R}^2)} \\ &\leq \left\| \sum_{m,n} |c_{m,n}| (\delta_{(ma, nb)} * |V_\varphi(F^{\alpha_{m,n}} D_s \varphi - \varphi)|) \right\|_{L^2(\mathbb{R}^2)} \\ &\leq \left\| \left( \sum_{m,n} |c_{m,n}| \delta_{(ma, nb)} \right) * \frac{\epsilon}{W} \right\|_{L^2(\mathbb{R}^2)} \\ &\leq \sqrt{(3a+1)(3b+1)} \left\| \sum_{m,n} |c_{m,n}| \delta_{(ma, nb)} \right\|_{W(M(\mathbb{R}^2), L^2(\mathbb{R}^2))} \left\| \frac{\epsilon}{W} \right\|_{W(C_0(\mathbb{R}^2), L^1(\mathbb{R}^2))} \end{aligned}$$

We have

$$\left\| \frac{\epsilon}{W} \right\|_{W(C_0(\mathbb{R}^2), L^1(\mathbb{R}^2))} \leq \epsilon \underbrace{\sum_{M, N \in \mathbb{Z}} \sup_{(x, \omega) \in C_{M, N}} \frac{1}{(1 + x^2 + \omega^2)^2}}_{:= K, < \infty} \quad (6.1)$$

where  $C_{M, N} := [(M \pm \frac{1}{2})a] \times [(N \pm \frac{1}{2})b]$ .

Furthermore for  $\psi_i$  as in Lemma 6.2

$$\begin{aligned} \left\| \sum_{m,n} |c_{m,n}| \delta_{(ma,nb)} \right\|_{W(M,l^2)}^2 &= \sum_{i \in \mathbb{Z}^2} \left\| \psi_i \left( \sum_{(m,n) \in \mathbb{Z}^2} |c_{m,n}| \delta_{(ma,nb)} \right) \right\|_M^2 \\ &\leq \sum_{i \in \mathbb{Z}^2} \sup_{\|f\|_\infty=1} \left( \sum_{(m,n) \in \mathbb{Z}^2} |c_{m,n}|^2 \underbrace{|f(ma, nb)|^2}_{\leq 1} \underbrace{\psi_i(ma, nb)^2}_{\delta_{i,(m,n)}} \right) \\ &\leq \|c\|_2^2 \end{aligned}$$

It follows that for  $s \in [1, S]$

$$\|Pc\|_{L^2(\mathbb{R})} \leq \epsilon \sqrt{(3a+1)(3b+1)} K \|c\|_{l^2(\mathbb{Z}^2)}$$

and thus  $\|P\| \rightarrow 0$  as  $s \searrow 1$ .  $\square$

*Remark 6.1.* The proof of Theorem 6.2 also works for any other window  $g$  for which an analog of Lemma 6.1 holds.

*Remark 6.2.* Numerical simulations suggest that the frame bounds obtained from Corollary 2.1 are, in our situation, not optimal. Figure 29 shows the result of an experiment for signal length 360,  $a = b = 15$  and randomly chosen  $\alpha_{m,n}$ . The solid lines give the optimal frame bounds for the systems  $\{\widetilde{\varphi}_{m,n}\}$  for  $s$  running from 1 to 3. The dashed lines indicate the bounds coming from Corollary 2.1. (For  $s \geq 2.4$  the condition  $\|P\| < \sqrt{A}$  is not satisfied.)

Nevertheless we want to evaluate the result from Theorem 6.2 in order to obtain concrete frame bounds in the continuous case for different values of  $a$ ,  $b$  and  $s$ .

First we need frame bounds for the standard Gabor system with Gaussian window. As mentioned in [6] the Janssen representation provides an easy way of estimating frame bounds for the frame operator  $S_{g,\Lambda}$  of a Gabor system with window  $g$ , satisfying  $\|g\|_2 = 1$ , and a lattice  $\Lambda$ . Set

$$\gamma := \sum_{\lambda^\circ \in \Lambda^\circ, \lambda^\circ \neq 0} |V_g g(\lambda^\circ)|, \quad (6.2)$$

if  $\gamma < 1$  then

$$A_{opt} = \|S_{g,\Lambda}^{-1}\|^{-1} \geq red_\Lambda (1 - \gamma) \quad (6.3)$$

and

$$B_{opt} = \|S_{g,\Lambda}\| \leq red_\Lambda (1 + \gamma).$$

In our case, for  $g = \varphi$  and  $\Lambda = a\mathbb{Z} \times b\mathbb{Z}$ , we have

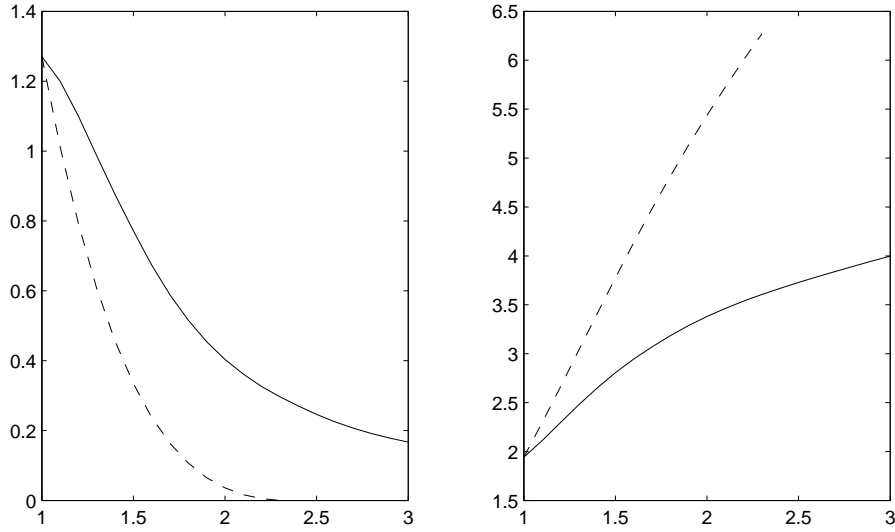


Figure 29: Solid: Optimal lower (left) and upper (right) frame bounds for  $\{\tilde{\varphi}_{m,n}\}$  for different values of  $s$  and a fixed random choice of the  $\alpha_{m,n}$ . Dashed: Lower and upper bounds computed via Corollary 2.1

$$\gamma = \sum_{(m,n) \neq (0,0)} e^{-\pi(\frac{m^2}{2b^2} + \frac{n^2}{2a^2})}.$$

The series converges extremely fast and can be evaluated easily, yielding frame bounds  $A, B$ .

Next we compute  $K$  from (6.1). The series defining  $K$  only converges at a polynomial rate but still allows for sufficiently precise numerical evaluation by restricting the summation to  $\max(|M|, |N|) < K, K \gg 1$ . Then the error is of order

$$\frac{1}{\delta^2} \int_{x^2+y^2 \geq K^2} \frac{1}{(x^2+y^2)^2} dx dy = O\left(\frac{1}{\delta^2 K^2}\right)$$

where  $\delta := \min(a, b)$ .

Following the proof of Theorem 6.2 we now set

$$\epsilon := \frac{\sqrt{A}}{K \sqrt{(3a+1)(3b+1)}}$$

and compute  $s$  as in Lemma 6.1. The easiest way to do this (at least approximately) is to evaluate  $V_\varphi(D_s \varphi - \varphi) \cdot W$  on a grid around 0, find the absolute

maximum and, if this is greater than  $\epsilon$ , reduce  $s$  and repeat until the maximum is smaller than  $\epsilon$ .

Unfortunately for this to happen,  $s$  has to be chosen very close to 1. For  $a = b = 0.75$  we get  $s = 1.025$  and other values for  $a$  and  $b$  yield similar  $s$ . Comparing this with numerical experiments, in which the frame bounds didn't react too sensitive on changes in  $s$ , we conclude that the technique used to proof Theorem 6.2 provides only rather pessimistic estimates and more effort will be required to obtain satisfactory results.

Using the same technique as for Theorem 6.2 we can also easily get result concerning stability in the  $\alpha_{m,n}$ .

**Lemma 6.3.** *For  $s > 0, \alpha, \beta \in \mathbb{R}$  and  $W(x, \omega) := (1 + x^2 + \omega^2)^2$  we have*

$$\|V_\varphi(R^\beta D_s \varphi - R^\alpha D_s \varphi)\|_{L^\infty_W(\mathbb{R}^2)} \rightarrow 0 \text{ as } \beta \rightarrow \alpha.$$

*Sketch of proof:* Since  $W$  is rotationally symmetric and because of Theorem 4.2 we can assume  $\alpha = 0$ . Then the proof is similar to that of Lemma 6.1.

**Theorem 6.3.** *Given  $a, b \in \mathbb{R}, s > 1, \alpha_{m,n} \in \mathbb{R}^{\mathbb{Z} \times \mathbb{Z}}$  set  $\varphi_{m,n} := M_{nb} T_{ma} R^{\alpha_{m,n}} D_s \varphi$  for  $m, n \in \mathbb{Z}$ . If  $\{\varphi_{m,n}\}_{m,n \in \mathbb{Z}}$  is a frame, then there exists  $\delta > 0$  and positive numbers  $\tilde{A}, \tilde{B}$  such that for any sequence  $(\beta_{m,n})$  with  $|\beta_{m,n} - \alpha_{m,n}| < \delta, \forall m, n$  and  $\widetilde{\varphi}_{m,n} := M_{nb} T_{ma} R^{\beta_{m,n}} D_s \varphi$  the system  $\{\widetilde{\varphi}_{m,n}\}_{m,n \in \mathbb{Z}}$  is a frame with bounds  $\tilde{A}$  and  $\tilde{B}$ .*

*Proof.* Like for Theorem 6.2, but using Lemma 6.3 instead of Lemma 6.1. □



# Appendix

## Matlab code

### hermf\_simple.m

```
% HERMF_SIMPLE.M
%
% COPYRIGHT : (c) NUHAG, Dept.Math., University of Vienna, AUSTRIA
%           http://nuhag.eu/
%           Permission is granted to modify and re-distribute this
%           code in any manner as long as this notice is preserved.
%           All standard disclaimers apply.
%
% HERMF(unctions).M   HGFei
% (reduced and simplified for easy readability by A. Missbauer)
%
% generates an orthonormal system of discrete Hermite functions
%
% USAGE:   HERM = hermf(n);
%
% Input:   n       signal length
% Output:  HERM    orthogonal n by n matrix, i-th column approximates the
%               (i-1)-th Hermite function, up to (roughly)  $i=n/\sqrt{2}$ 

function  HERM = hermf_simple(n)

g = gaussc(n,1).';

%construct weight W and corresponding STFT-multiplier,
RW = radwgh(n);
MRW = max(RW(:));
W = 1 + MRW - RW;

GMW = gabmulhf(W,g,1,1);

% perform eigenvalue-decomposition and -sorting on the GMW
HERM = eigsort(GMW);

% eliminate constant complex factors
HERM = twtoreal(HERM,2).';
```

```
%%%%%%%%%%%%%%%%%%%%%%%%%%%%%%%%%%%%%%%%%%%%%%%%%%%%%%%%%%%%%%%%%%%%%%%%
```

```
%weight function:
```

```
function radMat = radwgh(m,n)
if nargin < 2; n = m; end;
dm=min(0:m-1, m:-1:1); % calculating minimum distance along the row
dn=min(0:n-1, n:-1:1); % calculating minimum distance across column
radMat= sqrt((ones(m,1)*dn).^2+((dm(:)*ones(1,n)).^2))+1; %matrix with
% minimum distance of a point from (1,1)
```

### **gabbastfr.m**

```
% GABBASTFR
%
% Andreas Missbauer, 2012
% Uses hermf.m, hermot.m, rotmod.m. which are copyrighted by
% NuHAG, University of Vienna.
%
% Generates a gabor-like system from a window g and a lattice
% xp (given by a 0-1-matrix). For separable lattices use parameters a,b
% instead.
% Each atom is rotated clockwise in the time frequency plane (via the
% routine hermot.m, a discrete analog of the FRFT) according to the values
% in R, which are interpreted in degrees.
% If R==0 the angles are chosen randomly. If R contains nans the
% corresponding functions are left out.
%
% Supports 2 modes:
% 'f': fast: values in R are rounded to degrees (default), fft is
% used for speed-up
% 'p': precise: no rounding, slow
%
% Usage: G=gabbastfr(g,R,xp)
% or G=gabbastfr(g,R,a,b)
% or G=gabbastfr(g,R,xp,'f')
% or G=gabbastfr(g,R,a,b,'f')
%
% Input: g ... window of length n
% R ... nxn matrix containing the angles
% xp ... lattice OR a,b ... lattice parameters
```

```

%           mode ... string specifying mode ('f' or 'p')
%
% Output:   G ... matrix, each row contains an element of the system

function [G]=gabbastfr(g,R,a,b,mode)

n=length(g);

if nargin==4 && ~ischar(b)
    mode='f';
    a=lattp(n,a,b);

elseif nargin==4
    mode=b;

elseif nargin==5
    a=lattp(n,a,b);

end

H=hermf(n);

% In fast-mode: create a dictionary with all the required rotated windows
% use FFT and addition property of the FRFT for speed-up
if strcmp(mode,'f')

    R=round(R);
    R=mod(R,360);

    Rots=nan(360,n);    % dictionary
    ac=zeros(1,360);   % already computed rotations

    for ii=1:n
        for jj=1:n

            if ac(R(ii,jj)+1)==1
                1;
            elseif ac(mod(R(ii,jj)-90,360)+1)==1
                Rots(R(ii,jj)+1,:)= ...
                    fft(Rots(mod(R(ii,jj)-90,360)+1,:))/sqrt(n);
            end
        end
    end
end

```

```

        elseif ac(mod(R(ii,jj)+90,360)+1)==1
            Rots(R(ii,jj)+1,:)= ...
                ifft(Rots(mod(R(ii,jj)+90,360)+1,:))*sqrt(n);

        elseif ac(mod(R(ii,jj)+180,360)+1)==1
            Rots(R(ii,jj)+1,:)= ...
                Rots(mod(R(ii,jj)+180,360)+1,[1,n:-1:2]);

        elseif ac(R(ii,jj)+1)==0
            Rots(R(ii,jj)+1,:)=hermrot(g,H,R(ii,jj));
        end

        ac(R(ii,jj)+1)=1;

    end
end

end

co=a(:); co=find(co>0);
nopoints=length(co);
G=zeros(nopoints,n);

if norm(R)==0
    R=ceil(rand(n)*noang);
end

[rind,cind]=ind2sub([n,n],co);

for jj=1:nopoints

    t=cind(jj)-1;
    f=rind(jj)-1;

    if isnan(R(rind(jj),cind(jj)))
        G(jj,:)=0;

    elseif strcmp(mode,'f')
        G(jj,:)=rotmod(Rots(R(rind(jj),cind(jj))+1,:),t,f);
    end
end

```

```
elseif strcmp(mode,'p')
    G(jj,:)=rotmod(hermrot(g,H,R(rind(jj),cind(jj))),t,f);

end

end
```

## Black and white images

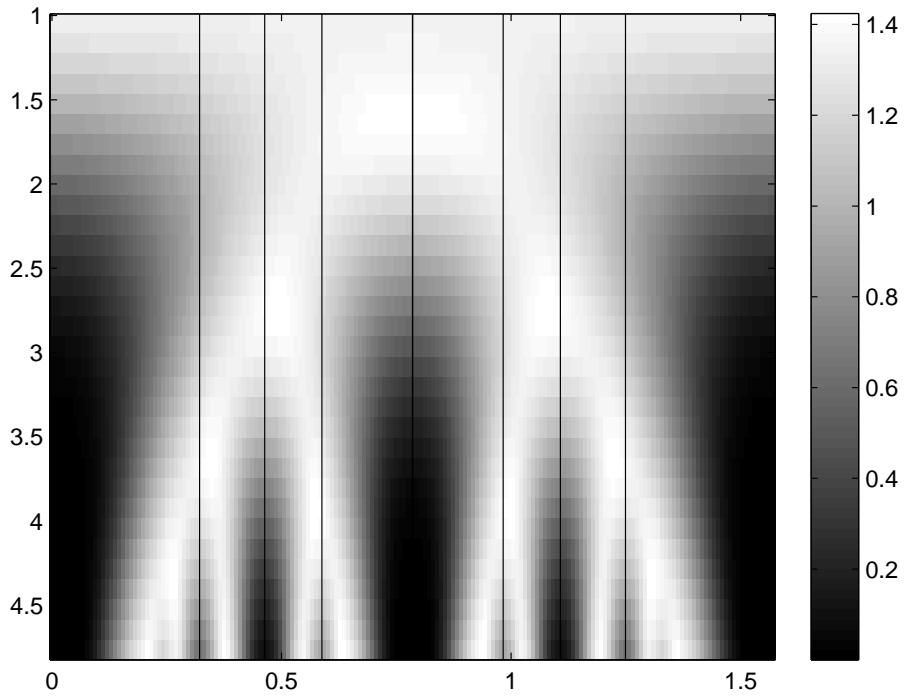


Figure 30: Like Figure 16: For  $a = b = 18$ : Optimal lower frame bounds for Gabor systems with window  $R^\alpha D_s \varphi$  for  $\alpha$  ranging from 0 to  $\frac{\pi}{2}$  on the horizontal axis and  $s$  varying geometrically from  $1.05^1$  to  $1.05^{32}$ .

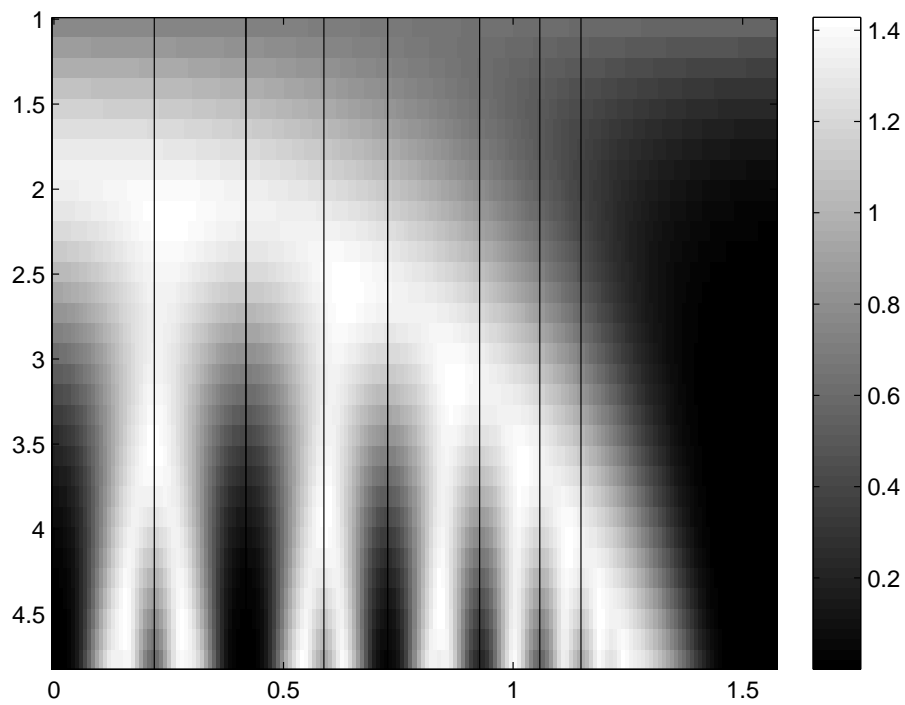


Figure 31: Like Figure 19: For  $a = 27, b = 12$ : Optimal lower frame bounds for Gabor systems with window  $R^\alpha D_s \varphi$  for  $\alpha$  ranging from 0 to  $\frac{\pi}{2}$  on the horizontal axis and  $s$  varying geometrically from  $1.05^1$  to  $1.05^{32}$ .

## References

- [1] L. B. Almeida. The fractional Fourier transform and time-frequency representations. *IEEE Trans. Signal Process.*, 42(11), 1994.
- [2] A. Bultheel and S. Martínez. Computation of the Fractional Fourier Transform. *Appl. Comput. Harmon. Anal.*, 16(3):182–202, 2004.
- [3] C. Candan, M. Kutay, and H. Ozaktas. The discrete fractional Fourier transform. *IEEE Trans. Signal Process.*, 48(5):1329–1337, 2002.
- [4] O. Christensen. *An Introduction to Frames and Riesz Bases*. Applied and Numerical Harmonic Analysis. Birkhäuser, 2003.
- [5] I. Daubechies. Time-frequency localization operators: a geometric phase space approach. *IEEE Trans. Inform. Theory*, 34(4):605–612, July 1988.
- [6] K. Doepfner. Quality of gabor multipliers for operator approximation. Master’s thesis, University of Vienna, Advisor: H. G. Feichtinger, to be published.
- [7] H. G. Feichtinger. Banach convolution algebras of Wiener type. In *Proc. Conf. on Functions, Series, Operators, Budapest 1980*, volume 35 of *Colloq. Math. Soc. Janos Bolyai*, pages 509–524. North-Holland, Eds. B. Sz.-Nagy and J. Szabados. edition, 1983.
- [8] H. G. Feichtinger, F. Luef, and T. Werther. A guided tour from linear algebra to the foundations of Gabor analysis. In *Gabor and Wavelet Frames*, volume 10 of *Lect. Notes Ser. Inst. Math. Sci. Natl. Univ. Singap.*, pages 1–49. World Sci. Publ., Hackensack, 2007.
- [9] H. G. Feichtinger and T. Strohmer. *Gabor Analysis and Algorithms. Theory and Applications*. Birkhäuser, 1998.
- [10] H. G. Feichtinger and W. Sun. Stability of Gabor frames with arbitrary sampling points. *Acta Math. Hungar.*, 113(3):169–195, 2006.
- [11] C. Gasquet and P. Witomski. *Fourier Analysis and Applications Filtering, Numerical Computation, Wavelets Transl From the French by R Ryan*. Springer, 1999.
- [12] L. Grafakos. *Classical Fourier Analysis (Second Edition)*. Springer, 2008.



- [13] K. Gröchenig. *Foundations of Time-Frequency Analysis*. Appl. Numer. Harmon. Anal. Birkhäuser Boston, 2001.
- [14] A. J. E. M. Janssen. From continuous to discrete Weyl-Heisenberg frames through sampling. *J. Fourier Anal. Appl.*, 3(5):583–596, 1997.
- [15] A. J. E. M. Janssen. Classroom Proof of the Density Theorem for Gabor Systems. *ESI preprints*, 2005.
- [16] A. J. E. M. Janssen. Hermite function description of Feichtinger’s space  $S_0$ . *J. Fourier Anal. Appl.*, 11(5):577–588, 2005.
- [17] M. A. Kutay, H. M. Ozaktas, and Z. Zalevsky. *The Fractional Fourier Transform, with Applications in Optics and Signal Processing*. John Wiley and Sons, 2001.
- [18] S. Paukner. Foundations of Gabor Analysis for Image Processing. Master’s thesis, University of Vienna, Advisor: H. G. Feichtinger, 2007.
- [19] S. C. Pei and J. Ding. Relations between Gabor transforms and fractional Fourier transforms and their applications for signal processing. *IEEE Trans. Signal Process.*, 55(10):4839–4850, 2007.
- [20] S. Qiu and H. G. Feichtinger. Discrete Gabor structures and optimal representation. *IEEE Trans. Signal Process.*, 43(10):2258–2268, October 1995.
- [21] P. L. Sondergaard. Gabor frames by sampling and periodization. *Adv. Comput. Math.*, 27(4):355–373, 2007.
- [22] W. Sun and X. Zhou. On the stability of Gabor frames. *Adv. in Appl. Math.*, 26(3):181–191, 2001.
- [23] F. Vrabec. Eigenwerte und Eigenräume allgemeiner diskreter Fouriertransformationen. Master’s thesis, University of Vienna, Advisor: H. G. Feichtinger, August 1995.

## Abstract in English

The intention of this diploma thesis is to examine the effects of the fractional Fourier transform on Gabor frames with Gaussian window. Starting from such a Gabor system we apply some fractional power of the Fourier transform to each element. Geometrically one can think of the resulting family as a collection of (independently) rotated ellipses, positioned along a lattice in the time-frequency plane. We will see how the alignment of the ellipses is reflected in the frame bounds.

While chapters 1 to 3 cover the necessary tools and concepts from Fourier- and Gabor analysis, chapter 4 is dedicated to the fractional Fourier transform and especially its implementation on a computer. We compare two algorithms for computing discrete Hermite functions, one from [3] and one which was developed at NuHAG. We also investigate the convergence behavior of the latter one.

In chapter 5 we conduct numerical experiments for different choices of the rotation-parameters. If the resulting system is a Gabor frame the behavior of the frame bounds is easily understood, yet not unsurprising. We also investigate some special cases and the systems resulting from random choices of the rotation parameters.

Finally chapter 6 contains stability results for the frame bounds of the systems at hand, which we establish via the theory of Wiener amalgam spaces.

## Deutsches Abstract

Ziel der vorliegenden Diplomarbeit ist, den Effekt der fraktionalen Fourier Transformation auf Gabor Frames mit Gaußscher Fensterfunktion zu untersuchen. Ausgehend von solch einem Gabor-System wird auf jedes Element eine Wurzel der Fourier Transformation angewandt. Die entstehenden Systeme kann man sich geometrisch als eine Familie rotierter Ellipsen vorstellen, die entlang eines Gitters in der Zeit-Frequenz Ebene positioniert sind. Es wird ersichtlich, wie sich die Anordnung dieser Ellipsen in den Frame-Schranken widerspiegelt.

Nachdem in den Kapiteln 1 bis 3 die Grundlagen der Fourier- und Gabor Analysis beschrieben werden, widmet sich Kapitel 4 der fraktionalen Fourier Transformation und ihrer Implementation. Hierzu wird ein etablierter Algorithmus (siehe [3]) mit einem in der NuHAG entwickelten Verfahren verglichen, für das auch eine Konvergenzanalyse durchgeführt wird.

Kapitel 5 beschreibt die Ergebnisse numerischer Experimente zu den oben genannten Systemen. Es zeigt sich, dass falls das resultierende System ein Gabor Frame ist, das Verhalten der Frameschranken leicht verständlich, aber durchaus erstaunlich ist. Außerdem werden einige Spezialfälle betrachtet, sowie jene Systeme, die durch eine zufällige Wahl der Rotationsparameter entstehen.

In Kapitel 6 schließlich finden sich Stabilitätsresultate für die Frame-Schranken der untersuchten Systeme. Diese werden mit Hilfe der Theorie der Wiener-Amalgam Räumen bewiesen.

## Author's curriculum vitae

Full name: Andreas Rudolf Missbauer  
Date of birth: November 21, 1986  
Place of birth: Linz, Austria  
Citizenship: Austria  
E-mail address: andreas.missbauer@gmx.at

## Education

2006-2012 University of Vienna  
Diploma study in mathematics  
Performance scholarships awarded in 2008 and 2010

2008-2009 University of Vienna  
Physics, discontinued

2005-2006 Civil service at AKH Linz

1997-2005 Khevenhüller Gymnasium Linz  
High school graduation with distinction